INFORMATION TO USERS

This manuscript has been reproduced from the microfilm master. UMI films the text directly from the original or copy submitted. Thus, some thesis and dissertation copies are in typewriter face, while others may be from any type of computer printer.

The quality of this reproduction is dependent upon the quality of the copy submitted. Broken or indistinct print, colored or poor quality illustrations and photographs, print bleedthrough, substandard margins, and improper alignment can adversely affect reproduction.

In the unlikely event that the author did not send UMI a complete manuscript and there are missing pages, these will be noted. Also, if unauthorized copyright material had to be removed, a note will indicate the deletion.

Oversize materials (e.g., maps, drawings, charts) are reproduced by sectioning the original, beginning at the upper left-hand corner and continuing from left to right in equal sections with small overlaps.

Photographs included in the original manuscript have been reproduced xerographically in this copy. Higher quality 6" x 9" black and white photographic prints are available for any photographs or illustrations appearing in this copy for an additional charge. Contact UMI directly to order.

ProQuest Information and Learning
300 North Zeeb Road, Ann Arbor, MI 48106-1346 USA
800-521-0600

UMI®

Design Optimization Techniques for Printed Antennas and Periodic Structures

by

Zhifang Li

A dissertation submitted in partial fulfillment
of the requirements for the degree of
Doctor of Philosophy
(Electrical Engineering)
in The University of Michigan
2001

Doctoral Committee:

Professor John L. Volakis, Co-Chair
Professor Panos Y. Papalambros, Co-Chair
Professor Anthony W. England
Professor Noboru Kikuchi

UMI Number: 3029375

UMI Microform 3029375

Bell & Howell Information and Learning Company
300 North Zeeb Road
P.O. Box 1346
Ann Arbor, MI 48106-1346

To My Grandparents and Parents

ACKNOWLEDGEMENTS

I would like to express my deepest gratitude to my advisors, Professor Volakis and Professor Papalambros, who directed me to the University of Michigan and have given me invaluable opportunity to study under their guidance. Their kindness and attitude to life and research have influenced me considerably.

I would also like to sincerely thank each of my committee members, Professor Volakis, Professor Papalambros, Professor England and Professor Kikuchi for the time they spent reading and evaluating my thesis.

I would like to thank all my friends in the University of Michigan, especially those at the Radiation Laboratory and the Optimal Design Laboratory: Dr. Tao Jiang, Dr. Tayfun Özdemir, Dr. Jong-Gwan Yook, Dr. Paul Siqueira, Dr. Stephane Legault, Dr. Mark Casciato, Mr. Mike Nurnberger, Dr. Arik Brown, Dr. Lars Andersen, Dr. Erdem Topsakal, Mr. Yunus Erdemli, Mr. Dejan Filipovic, Mr. Kubilay Sertel, Mr. Michael Carr, Ms. Gullu Kiziltas, and Dr. Hasnain Syed. I would also like to thank the department and laboratory staff for their kind help in graduate school.

Finally and most importantly, I want to thank my family members: my grandma and late grandpa for bringing me up and nourishing my interests in science and literature; my father and mother for their endless love and support, their view of life, and being role models for me; and Yifei, without whose encouragement, patience and understanding, I would not have finished this thesis.

TABLE OF CONTENTS

LIST OF FIGURES

Figure

LIST OF TABLES

CHAPTER I

INTRODUCTION

Growing applications in wireless communications present us with continuing demands for new antenna designs. Various antenna features and performance metrics are desired, including miniaturization, pattern control, new composites and artificial dielectrics, and multi-function capabilities. Antenna design is therefore a topic of great importance to electromagnetics (EM). It involves the selection of antenna physical parameters to achieve optimal gain, pattern performance, voltage standing wave ratio (VSWR), bandwidth and so on, subject to some specified constraints. Trial and error process is typically used for antenna design and consequently the designer is required to have great experience and intuition.

Optimization is the act to either "minimize the effort required" or "maximize the desired benefit" [93]. It can be defined as the process of finding the conditions of design variables that give the minimum or maximum value of an objective function. Optimization methods have matured mathematically and have been applied extensively in many engineering branches [1, 37, 83, 93] such as mechanical engineering, operations research, and artificial intelligence.

In the past ten years, design optimization methods started to be applied in antenna applications to either improve the current design or speed up the design pro-

cess. Various types of antennas have been designed and optimized, such as wire type (dipoles, loops, helices, etc.), aperture type (horns, reflectors, lenses, etc.), and microstrip antennas. These antennas can be used either as single elements or in arrays [10]. In this thesis, a variety of optimization techniques will be combined with numerical antenna analysis simulators to design microstrip antennas, periodic structures, and related EM devices. To our knowledge, this is the first ever integration of optimization and rigorous electromagnetic analysis tools. This is made possible as a result of the new fast algorithms recently introduced in EM.

1.1 Motivation

1.1.1 Microstrip Antennas

Microstrip antennas form one of the most active and innovative research areas among current antenna work. They were introduced in the early 1950's by Deschamps [31], became very popular in the 1970's, and have since been extensively investigated experimentally, analytically and numerically [8, 18, 49, 50, 87]. Microstrip antennas consist of very thin metallic patches printed on a grounded dielectric substrate. The patch can be fed with either a coaxial probe through the bottom of the substrate, as shown in Figure 1.1, or a coplanar microstrip line. Microstrip antennas have very low profile that is conformable to planar and non-planar surfaces. They are also easy and inexpensive to fabricate using printed circuit technology, and compatible with monolithic microwave integrated circuits (MMICs). Thus they have found a wide range of applications in both the military and civilian sectors, from communication systems in aircrafts and satellites to cellular phones and other mobile communication devices.

Disadvantages of microstrip antennas include narrow bandwidth, low efficiency,

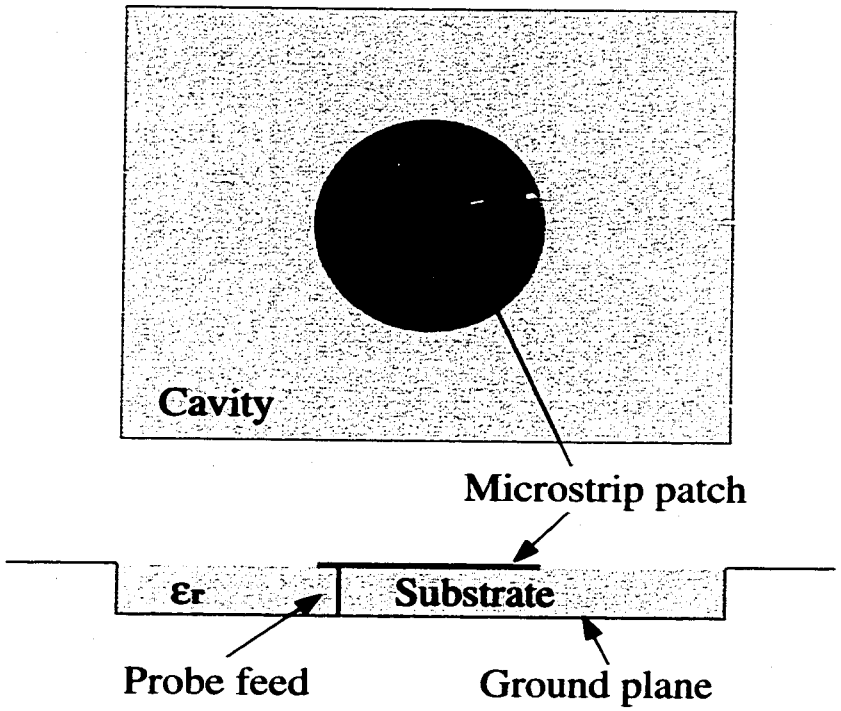

Figure 1.1: A circular patch antenna with probe feed: top and side view.

limited power capacity, poor polarization purity, and spurious feed radiation. Therefore, much research work has been put into efforts to overcome these problems.

1.1.2 Numerical Techniques for Antenna Analysis

The goal of antenna analysis is to compute the electric and magnetic fields radiated by the system components subject to some sources / excitation. Once this is accomplished, many parameters and figures-of-merit that characterize the performance of an antenna system can be found. Some of the commonly used performance metrics include radiation pattern, power density, radiation intensity, directivity, gain, radiation efficiency, input impedance, beamwidth, bandwidth, and polarization.

Most antennas exhibit intricate structures, and consequently computational techniques are necessary for their analysis. Over the past decade, computational methods have been developed for fast and accurate antenna analysis. Integral equation (IE)

methods and partial differential equation (PDE) methods are computationally effective for antennas with small electrical sizes as compared to the wavelength and are classified as the *low-frequency methods*. When the dimensions of antennas are large as compared to the wavelength, then radiation, propagation, scattering and diffraction phenomena exhibit a highly localized behavior. This is exploited in the context of *high-frequency methods* such as geometrical theory of diffraction (GTD) and physical theory of diffraction (PTD) for an approximate but fast computation of the radiated fields. Figure 1.2 shows the major computational methods for antenna analysis. In this thesis, we are mainly concentrated on low frequency methods, since these are the techniques to be used in conjunction with our optimization process. It should also be remarked that the term "low frequency methods" does not imply that the techniques are only applicable to small structures. This term has been used because the initial use of the methods was limited to small geometries due to their large memory and CPU requirements. However, the recent introduction of fast $O(N\log N)$ and low memory algorithms has allowed use of these rigorous methods for large scale computations.

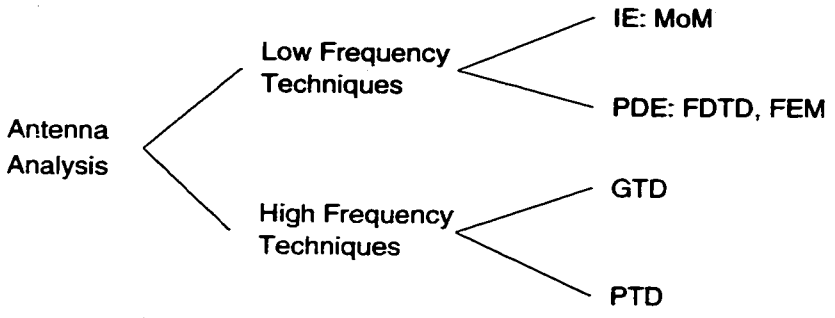

Figure 1.2: Computational methods for antenna analysis.

IE methods cast the solution of an antenna problem in the form of an integral where the unknown quantity, usually the induced current density, is under the in-

tegral. Numerical techniques, such as the method of moments (MoM) [9, 80] are therefore required to solve for the unknown quantity. MoM is a rigorous approach for solving IE and has been widely used in the analysis of conformal antennas since the 1960's. However, IE techniques are usually formulated under the assumption of an infinite substrate, which deviates from the practical patch antenna configuration employing finite substrates. Furthermore, IE methods are not able to represent antenna excitations exactly, and additional complexities arise with substrate anisotropies or inhomogeneities in the antenna structure. In recent years, PDE such as the finite-difference time-domain (FDTD) [61, 71] and finite element methods (FEM) [51, 100, 106] methods have been substantially developed as well.

The increasing reliance on PDE methods stems from their inherent geometrical adaptability, low $O(N)$ memory demand, and capability to model heterogeneous (isotropic or anisotropic) geometries. These attributes are essential in developing general-purpose analysis codes for EM scattering, antennas and other applications. Without placing restrictions on the geometry and material composition for the structure, PDE methods and their hybrid versions with IE and high-frequency techniques show a great promise for larger scale simulations.

The key advantage of the FEM is its ability to handle geometrical details and material variations within the computational domain. In addition, while the MoM requires use of Green's function and storage of a fully populated matrix, the FEM can be implemented via approximate boundary conditions and result in a 99% sparse matrix with large storage savings.

When Green's function is available, a hybridization of the MoM and the FEM is an ideal approach to combine the rigor of the MoM and the geometrical fidelity of the FEM. This method was pioneered at the University of Michigan [51, 106], and

several algorithms and programs exist for antenna analysis. Throughout this thesis, the analysis of patch antennas and other electromagnetic structures encountered is carried out by an edge-based hybrid finite element - boundary integral (FE-BI) technique [52, 53, 107, 108]. The FEM is used for modeling the inhomogeneous cavity without any compromise in geometry, feed structure or material loading. The mesh truncation of FEM, however, is a challenging task and must be accurately performed for input impedance calculations. The use of BI for mesh truncation yields robust formulation at the expense of higher computational requirements. Details of the FE-BI formulation is outlined in Chapter II.

1.1.3 Antenna Design Optimization

Over the past several years, a variety of sophisticated computer programs have been developed for antenna analysis based on the popular IE and PDE methods outlined in Section 1.1.2. However, the utility of these programs can be greatly enhanced if they can be used for design, a situation that typically involves iterative optimization algorithms.

The process of antenna design optimization typically consists of two modules linked together with a loop, as shown in Figure 1.3. Starting with some initial designs, the analysis module computes the antenna performance using numerical techniques, such as the IE and PDE methods. On the other hand, the synthesis module using some optimization algorithm allows for the estimation of the design. This process is repeated iteratively until some a priori convergence criteria are met.

Most antenna analysis techniques to date have not been extended to include design capabilities primarily because of their complexity and non-linearity with respect to the physical properties of the antenna (e.g. material constants, dimensions, feed

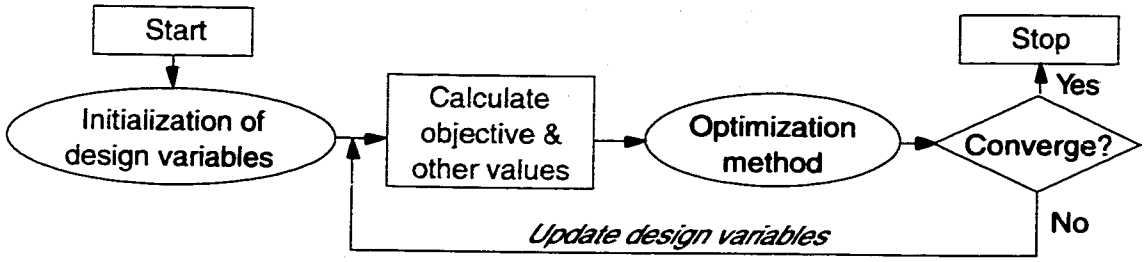

Figure 1.3: Antenna design process.

location and type). In most applications where optimization methods have been employed for antenna design, the objective function has been either available in closed form or has required little computational time. Since microstrip antenna simulations rely on relatively more complex and computationally expensive IE and PDE methods, they are not practical for use in an optimization loop. The geometrical and material adaptability of the methods is another matter.

The major requirements for antenna analysis and synthesis that make antenna design a challenging task and which limit the applications in antenna optimization are:

- *Full geometrical adaptability.* The simulation module must be capable of handling complex antenna geometries, such as irregular patch shapes and various feeding structures. Automatic re-meshing of the geometry is also necessary during the optimization iterations.

- *Full material adaptability.* The algorithms should have the capability of handling composite or artificial materials for antenna substrates and/or superstrates, resistive loading, and conducting pins (wires).

- *Wide range of performance requirements.* The relationship between design variables and system performance is very complicated. Examples of desired per-

formance include maximum bandwidth, minimum size, bandpass or bandstop frequency response, pre-specified scan angles, etc. Many of these objectives are in conflict with each other and trade-offs have to be made to find a design satisfying all system requirements.

- *Speed.* Many antenna problems involve a discretization scheme with hundreds of thousands of unknowns. This would be unrealistic for a design unless very fast algorithms are available.

Some of the above difficulties can be alleviated by the combination of design optimization algorithms with an FE-BI simulator. The availability of recent fast and accurate numerical techniques for antenna simulation can bring antenna design to realization. Automated antenna design optimization is no longer unrealistic.

In this thesis, a comprehensive study of optimization algorithms for designing patch antennas, periodic arrays, and other EM devices is shown. Superior antenna designs are generated by optimizing the antenna geometrical parameters, such as patch size, substrate thickness, stacked patch spacing, and element shape.

The goals of this thesis are: (1) show the effectiveness of combining the numerical computational methods such as FEM with design optimization methods for the synthesis of microstrip antennas and periodic structures; (2) use optimization algorithms for generating new antenna designs systematically; (3) compare different optimization methods on certain antenna designs, and (4) provide insight on practical issues when designing and analyzing these radiating structures.

1.2 Previous Work

In this section, optimization work on EM devices and antennas is reviewed, especially patch antenna and layered EM device designs using gradient-based methods,

genetic algorithm (GA), and simulated annealing (SA). The methods involved in this thesis are discussed in more details in Chapter II.

1.2.1 Antenna Array Optimization

Early antenna optimization work concentrated on array synthesis. An array is an assembly of antenna elements in an electrical and geometrical configuration. Arrays can produce very high gains to meet the demands of long distance communication. Because the computation on array patterns is analytically tractable, there have been tremendous interest and development for array optimization. Two broadly investigated topics of array synthesis are summarized below:

Array pattern synthesis with null constraints. The problem of finding optimal complex weight vector norm subject to a "look direction" and null constraints has been studied extensively. Commonly used objective functions are the antenna directive gains [20, 69], the signal-to-noise ratio (SNR) [19, 35, 62], and the mean square error between a desired pattern and the null constrained pattern [72, 81]. In most cases, the problem is formulated as a constrained optimization problem. Various optimization techniques were employed to solve this problem. Gradient-based methods used for the adaptive nulling problem include the gradient search algorithm [39], conjugate gradient method [97], or quadratic programming [43, 81]. Gradient-free methods, such as GA [5, 41] and neural networks (NN) [19], have also been widely applied to this problem.

Reduction of sidelobes. A large amount of research work has been devoted to the reduction of sidelobes of an array using various optimization techniques. For example, by thinning an array, some elements in a uniformly spaced or periodic array are turned off to create a desired amplitude density across the aperture. The

conjugate gradient method [84], GA [40] and SA [95] were used for this problem. Another way to reduce the sidelobes is by amplitude or phase tapering using GA [4] and SA [4, 103].

1.2.2 Single Antenna Optimization

GA, evolutionary programming (EP) and evolutionary strategies (ES) form the family of evolutionary algorithms, which have been applied to single antenna optimization and proved very efficient. Wire antennas loaded with passive resonant circuits have been designed with GA to broaden their frequency response [14]. Yagi antennas and reflector antennas have also been optimized with GA [58, 68, 96] or EP [45].

Patch antennas are computationally expensive with no closed-form solution available although their structures are simple and easy for fabrication. Therefore, numerical techniques such as MoM and FEM are needed for objective function evaluations during the optimization process. In [2], a steepest descent method with MoM simulation was employed to obtain impedance matching for an inset-fed patch. In [64], we combined sequential quadratic programming (SQP) with FE-BI simulation to optimize sizes of stacked patches with probe and slot feed to obtain broadband performance. In [66], we applied the same method to ferrite antenna design for resonant frequency tuning and beam steering applications by adjusting the direction and strength of biased external magnetic field. Creation of irregular patch shapes has also been investigated for various purposes. They include Q factor improvement using a combination of FDTD and GA [30], bandwidth improvement using a combination of MoM and GA [21, 56], dual band performance with MoM and GA [56], and maximum axial ratio for a circularly polarized patch using MoM and GA [2]. Ex-

perimental optimization with a response surface methodology [79] was conducted to obtain broadband performance of two-layer patches by optimizing the patch lengths and spacing between substrate layers [78].

1.2.3 Layered EM Device Optimization

Multi-layered filters have been designed with GA by minimizing the difference between the observed and the desired filter characteristics. In [74], the design variable was real-valued and real-encoded layer thicknesses. The layering materials for the filter were preselected. Another layered structure requiring a similar design approach is the case of microwave absorbers [76, 102]. In [76], GA was used to choose materials from a finite database.

Frequency selective surfaces (FSSs) are layered planar periodic structures consisting of perfectly electrically conducting (PEC) patches or apertures that are either free standing or backed by a dielectric substrate. They exhibit total reflection (for patches) or transmission (for apertures) in the neighborhood of the FSS element resonance. Unlike filters and absorbers, analysis of FSSs requires numerical techniques instead of closed-form formulae, making the computation of the objective functions more expensive task. Recent efforts have nevertheless already been made to design optimal FSSs. FSS characteristics depend on the element shape and dimensions. With a fixed element type, the element size was optimized using NN [28] and gradient-based method [111] to obtain desired frequency responses. For greater design flexibility to further determine the types of elements in a multi-layer FSS design, element blocks were selected by GA from a database of pre-defined regular element shapes and then dielectric layer thicknesses were adjusted to achieve the design goals [75]. Elements with irregular shapes have been investigated by dividing an

FSS unit cell into binary sub-cells. Each sub-cell is denoted as 1 when it is inside the conductor region, or as 0 when it is outside the conductor region. Both NN [48] and GA [65, 67] have been employed to achieve the desired frequency response. In [67], we employed the fast spectral domain algorithm (FSDA) to speed up the FSS analysis and thus obtain a design with greater geometrical flexibility. Also in [67], the design emphasized a constant phase (rather than amplitude) design to improve the the impedance bandwidth of a dipole array when the FSS is used as a substrate.

1.3 Contributions and Overview of Thesis

This thesis demonstrates a comprehensive study of optimization algorithms combined with FE-BI simulations used on microstrip antennas and periodic structures. Among the various optimization methods considered, the sequential quadratic programming (a class of gradient-based algorithms) is applied to several size optimization problems; and two gradient-free methods (genetic algorithms and simulated annealing) are employed on shape and topology optimization problems. We begin our work by verifying the optimization algorithms by solving problems that have been analytically investigated yet without optimization study. Subsequently, new antenna designs and periodic structures are developed by utilizing optimization methods. The methodology of optimization with FE-BI simulations is shown to not only reduce the effort of antenna design, but also enable the design of complicated novel structures that are beyond the capability of conventional antenna design approaches.

This thesis is structured as follows:

In Chapter II, numerical techniques for antenna synthesis and analysis are reviewed. For the synthesis part, specific optimization algorithms are chosen based on each antenna design problem's requirements and characteristics. Gradient-based

methods are fast in convergence yet depends on the initial point, and can usually find only local optima. Sequential quadratic programming, one of the most efficient gradient-based methods, is summarized. Gradient-free methods, on the other hand, are able to find global optima and are independent of starting points, yet such methods need a lot of function evaluations. Two stochastic search techniques, genetic algorithms (GA) and simulated annealing (SA), are introduced. The reviewed analysis methods for antenna design are based on the hybrid FE-BI method [106, 108].

In Chapter III, several patch antenna design problems are proposed and solved. Most of these antenna designs have been previously studied and are well understood. These designs serve to validate the optimization algorithms. Furthermore, optimization can produce better designs in addition to saving time and effort.

In the first part of Chapter III, optimization of ferrite antennas is presented. Ferrite materials are attractive for microwave circuit devices and patch antennas because of their non-reciprocal properties. FE-BI analysis for anisotropic materials is discussed and shown to be consistent with the moment method by examining a ferrite-loaded cavity. Two ferrite antenna designs are presented: resonant frequency tuning and beam steering. For the frequency tuning design, both normal biasing and parallel biasing are investigated. The relationship between resonant frequency, bias field H_0 and saturation magnetization $4\pi M_s$ is revealed. It is also shown that circular polarization can be achieved with even a single feed point for ferrite antennas. An optimization model is established to find the resonant frequency for fixed values of H_0 and $4\pi M_s$. For the beam steering design, a ferrite cover is put on top of a patch antenna, and its thickness h_{sup} along with H_0 and $4\pi M_s$ are optimized to obtain several desired beam angles. The SQP optimizer is used for both designs.

Microstrip antennas have narrow bandwidth due to their high Q factor. Band-

width enhancement with various configurations and feeding structures is one of the most active research areas for microstrip antennas. In the second part of Chapter III, several bandwidth enhancement configurations are reviewed, with the focus on stacked patches. Two different stacked patch schemes are then investigated. First, stacked rectangular patches with probe feed are studied. The thickness of the driven patch substrate is chosen as the design variable to maximize the bandwidth. Again, an SQP optimizer is employed to solve the optimization problem. Then a new scheme based on a stacked rectangular patch with a folded-slot is proposed. Several widths associated with the folded-slot are used as design variables, and a simplified discrete optimization is carried out by GA. Measured data are also compared with the simulated optimal design. Both stacked patch configurations produce more than 20% bandwidth. Although the stacked patches have a significantly larger bandwidth (than the single patch), they occupy too much space and are not ideal if the design space is limited.

To obtain a good bandwidth while still maintaining a compact profile, the third part of Chapter III continues to investigate broadband antennas by generating a single-layer irregular-shaped patch. The aperture is discretized into small cells with each cell allowed to be either in an "on" state (i.e., metal filled inside) or "off" state (i.e., without metal inside). Then, optimizers are developed to operate on a binary sequence that corresponds to the shape of the broadband patch. In a similar design with different objective functions, an irregular-shaped dual-frequency patch is also obtained for resonating at two GPS frequencies. Both GA and SA are applied to these two problems, and the obtained designs from the two methods are compared and discussed.

In Chapter IV, frequency selective surfaces (FSSs) are investigated. FSSs are

composed of several layers of infinite periodic patches or apertures that exhibit total reflection or transmission near the element resonance. By controlling the transmission and reflection coefficients, we can construct high-pass, low-pass, bandpass or bandstop filters. The first design presented in Chapter IV is free-standing high-pass filter with a stopband below 3 GHz. The optimization model is established by taking sample frequency points in a certain frequency range and by having the frequency responses as near to the desired values as possible. Numerical results for both single-layer and two-layer filters are shown to have good high-pass performance. A second design carried out in Chapter IV is a flat-phase FSS element. Such a design can be used as a "substrate" to printed antennas and may serve to emulate a magnetic ground plane. With a flat-phase element below, a patch antenna can exhibit broadband performance. However, the magnitude of the reflection coefficients must be compromised to obtain smooth phase performance. Resistive loading is needed in place of metal elements. GA is used for both filter and flat-phase element designs. Optimization models for the two element shape design problems are similar to the irregular-shaped patch designs conducted in Chapter III. Furthermore, a dipole array is put on top of a flat-phase FSS, and is shown to achieve a considerably larger bandwidth than that without FSS.

In Chapter V, 3-D frequency selective volumes (FSVs) and photonic bandgap (PBG) structures are studied. FSVs/PBGs consist of periodic implants within another contrast medium. Such structures can produce a frequency region where propagation of EM waves is forbidden, therefore having the capability of improving efficiency, gain and bandwidth of the patch antennas atop. Two approaches of manipulating the antenna substrates are discussed. When the size of periodic holes in the substrate is small compared to the wavelength, the substrate can be viewed

as a uniform one with an effective ϵ_{reff} which is lower than the one without holes. When the implant size is comparable to the wavelength, effective medium theory is no longer valid. The corresponding structure needs to be modeled exactly. Substrates using both approaches are simulated with patch antennas on top and shown to obtain larger bandwidth than those without PBG substrates.

In Chapter VI, we summarize the contributions and discuss future topics.

CHAPTER II

FORMULATION OF DESIGN OPTIMIZATION PROBLEMS

Optimization is the process of maximizing or minimizing a desired objective function while satisfying a set of constraints. As discussed in Chapter I, an optimization cycle typically consists of a synthesis module and an analysis module. The synthesis module contains a specific optimization algorithm and the analysis module computes the objective function and its derivatives, if necessary. Most optimization algorithms are iterative methods and have their own way of searching towards the optimum solution.

Specifically for antenna design optimization problems, the desired performance characteristics are described and formulated in terms of an objective function, such as bandwidth, beam angle, frequency response, or efficiency. The analysis part usually resorts to numerical techniques, since the antenna structure is rather complicated for deriving a closed-form solution.

Mathematically, an optimization problem can be defined as follows:

$$\begin{aligned} \underset{\mathbf{x}}{\text{Minimize}} \quad & f(\mathbf{x}, \mathbf{p}) \\ \text{subject to} \quad & \mathbf{g}(\mathbf{x}, \mathbf{p}) \leq \mathbf{0} \\ & \mathbf{h}(\mathbf{x}, \mathbf{p}) = \mathbf{0} \end{aligned} \tag{2.1}$$

where $\mathbf{x} \in \chi \subseteq \Re^{\mathbf{n}}$, $f : \Re^{n} \rightarrow \Re, \mathbf{h} : \Re^{\mathbf{n}} \rightarrow \Re^{\mathbf{m}}$, and $\mathbf{g} : \Re^{\mathbf{n}} \rightarrow \Re^{\mathbf{s}}$. Here $\mathbf{x}$ are called *design variables* with χ as the *design space*; the $\mathbf{p}$ vector contains certain *parameters* with values fixed during optimization. $f(\mathbf{x}, \mathbf{p})$ is the *objective function*, the $\mathbf{g}(\mathbf{x}, \mathbf{p})$ vector is a set of *inequality constraints* and $\mathbf{h}(\mathbf{x}, \mathbf{p})$ denotes the *equality constraints*. The set of $\mathbf{x}$ values satisfying all constraints, i.e., $\Omega = \{\mathbf{x} : \mathbf{g} \leq \mathbf{0}, \mathbf{h} = \mathbf{0}\}$, is called the *feasible region*.

In the most general form, (2.1) is a constrained nonlinear programming (NLP) problem. Optimization problems can be classified in several ways such as constrained or unconstrained problems, integer- or real-valued programming problems [93], and component or system design optimization problems, etc. [83]. In this thesis, all optimization problems encountered are component problems. Traditionally, component-level optimization problems can be classified into size, shape, and topology optimization, where the design variables are proportions, boundaries, and topology of a component, respectively. In this thesis, all three kinds of optimization problems are investigated.

Optimization methods can also be classified in various ways. In this chapter, two broad classes of optimization methods, gradient-based and gradient-free methods, are discussed.

The organization of the chapter is as follows. In Section 2.1, gradient-based techniques are summarized, followed by a detailed formulation of sequential quadratic programming (SQP), which is one of the most successful gradient-based methods. In Section 2.2, gradient-free methods are introduced, and two methods that belong to this category are outlined, namely, genetic algorithms (GA) and simulated annealing (SA). Finally, in Section 2.3, we present the general formulation of the finite element - boundary integral (FE-BI) method, the numerical technique used for antenna

analysis in this thesis.

2.1 Gradient-Based Techniques

The iterative gradient based methods use information of the first and possibly second order derivatives of the given function to obtain search directions towards the optimum. They guarantee descent in successive iterations and usually have fast convergence. A disadvantage of gradient based methods is that they can be sensitive to the initial estimates of the design variables, although proper scaling usually addresses this problem effectively. If the objective function has more than one local optima, the algorithm may converge to a local optimum instead of the desired global one.

A typical gradient-based method works as follows. Starting with an arbitrary initial point $\mathbf{x}_0$, a new estimate is generated at each iteration till convergence towards a local optimum of the objective function is achieved. At the beginning of the k-th iteration, the estimate $\mathbf{x}_k$ is available. Two steps are performed during the k-th iteration:

1. A *direction finding* step to compute a search direction $\mathbf{s}_k$ towards the next iteration point;

2. A *line search* step to compute the step size α_k along the search direction.

Using these steps, the next iteration point $\mathbf{x}_{k+1}$ is given by

$$\mathbf{x}_{k+1} = \mathbf{x}_k + \alpha_k \mathbf{s}_k. \tag{2.2}$$

Convergence criteria to terminate the algorithm is given by, for example,

$$|f_k - f_{k+1}| \leq \epsilon, \tag{2.3}$$

where f_k is the value of the objective function at the k-th iteration. A common termination criterion for constrained problems is the Karush-Kuhn-Tucker (KKT) norm

$$||\nabla f_k + \lambda_k^T \nabla \mathbf{h}_k + \mu_k^T \nabla \mathbf{g}_k|| \leq \epsilon. \tag{2.4}$$

Some methods, known as trust region methods [83], do not use a line search. Instead they impose bounds on how large the step can be in each iteration.

Classical gradient-based methods for unconstrained NLP problems include: steepest descent (Cauchy) method, conjugate gradient (Fletcher-Reeves) method, and quasi-Newton methods such as the Davidon-Fletcher-Powell (DFP) method and the Broydon-Fletcher-Goldfarb-Shanno (BFGS) method [93]. Since the late 1970's, SQP [83, 86, 98], a class of gradient-based methods, has become prominent due to its capability to solve problems with nonlinear constraints. In the remainder of this section, details of the SQP algorithm are presented.

2.1.1 Sequential Quadratic Programming (SQP)

The basic idea of SQP is to replace a given nonlinear problem by a sequence of quadratic subproblems that are easier to solve. That is, at a given approximate solution, say $\mathbf{x}_k$, we replace the problem by a quadratic programming subproblem, then use the solution of the subproblem to construct a better approximation $\mathbf{x}_{k+1}$. This process is repeated to create a sequence of approximations that converge to the optimal solution $\mathbf{x}_*$.

SQP has several advantages besides its rapid convergence: the initial point and subsequent iterates are allowed to be infeasible (a feasible point satisfies all constraints of (2.1)); gradients of only active constraints are needed; both equality and inequality constraints can be handled; and the method is mathematically proved to

converge under certain assumptions.

Like most optimization methods, SQP is not a single algorithm, but rather a conceptual method from which specific algorithms have evolved. In this section, a basic SQP method will be summarized briefly for a simplified NLP problem with equality constraints only.

Consider the equality constrained problem:

$$\begin{aligned} \min \quad & f(\mathbf{x}) \\ \text{subject to} \quad & \mathbf{h}(\mathbf{x}) = \mathbf{0}, \end{aligned} \tag{2.5}$$

where $\mathbf{x}$ is the design variable vector, $f(\mathbf{x})$ is the objective function, and $\mathbf{h}(\mathbf{x})$ is the vector of equality constraints. Using the Lagrange-Newton method to solve the first order necessary condition of this problem, at the k-th iteration, we have [83]

$$\begin{bmatrix} \mathbf{W}_k & \mathbf{A}_k^T \\ \mathbf{A}_k & \mathbf{0} \end{bmatrix} \begin{bmatrix} \mathbf{s}_k \\ \lambda_{k+1} \end{bmatrix} = \begin{bmatrix} -\nabla f_k^T \\ -\mathbf{h}_k \end{bmatrix}, \tag{2.6}$$

where $\mathbf{W} = \nabla^2 f + \lambda^T \nabla^2 \mathbf{h}$, $\mathbf{A} = \nabla \mathbf{h}$, and λ is the vector of Lagrange multipliers. Solving the above equations iteratively, we obtain the new estimate $\mathbf{x}_{k+1} = \mathbf{x}_k + \mathbf{s}_k$ and λ_{k+1} which should eventually approach $\mathbf{x}_*$ and λ_*, the local optima.

Alternatively, we observe that equation (2.6) can be viewed as the first order optimality (KKT) conditions for the quadratic model:

$$\begin{aligned} \min_{\mathbf{s}_k} \quad & q(\mathbf{s}_k) = f_k + \nabla_{\mathbf{x}} L_k \mathbf{s}_k + \tfrac{1}{2} \mathbf{s}_k^T \mathbf{W}_k \mathbf{s}_k \\ \text{subject to} \quad & \mathbf{A}_k \mathbf{s}_k + \mathbf{h}_k = \mathbf{0}, \end{aligned} \tag{2.7}$$

where $\nabla_{\mathbf{x}} L_k = \nabla f_k + \lambda_k^T \nabla \mathbf{h}_k$. Solving the quadratic programming subproblem (2.7) gives the same $\mathbf{s}_k$ and λ_{k+1} as solving equation (2.6) and thus the two formulations are equivalent. In the second formulation, the optima $\mathbf{x}_*$ and λ_* can be obtained

by solving a sequence of quadratic programming (QP) subproblems, hence the name SQP for relevant algorithms. The QP subproblem can be solved efficiently by well-developed QP solvers, for example, based on projection or augmented Lagrangian methods. Using an active set strategy [83], problems with both equality and inequality constraints can be solved.

Local convergence is the rate at which the iterates converge to a solution, given that the initial point is sufficiently close to the solution and the problem converges. The local convergence of the SQP can be shown to be quadratic. On the other hand, an algorithm is globally convergent if, under suitable conditions, it converges to some local solution from any remote starting point. To establish the global convergence for the SQP algorithm, a way of measuring progress towards a solution is needed. For SQP, this is done by constructing a *merit function*, a reduction in which implies that an acceptable step has been taken. To do this, we view $\mathbf{s}_k$ as a search direction and define the iteration as $\mathbf{x}_{k+1} = \mathbf{x}_k + \alpha_k \mathbf{s}_k$, where the step size α_k is introduced and computed by minimizing an appropriate merit function along the search direction. An example merit function can be written as (the l_1 exact penalty function) [86]

$$\phi(\mathbf{x}, \lambda) = f(\mathbf{x}) + \sum_{j=1}^{m} \lambda_j |h_j|. \tag{2.8}$$

In summary, SQP algorithms have the following steps:

1. Initialize;

2. Solve the QP subproblem (2.7) to determine a search direction $\mathbf{s}_k$;

3. Minimize a merit function along $\mathbf{s}_k$ by performing a line search to determine the step length α_k;

4. Set $\mathbf{x}_{k+1} = \mathbf{x}_k + \alpha_k \mathbf{s}_k$;

5. Check for termination, go to step 2 if not satisfied.

Two other aspects of SQP algorithms that need to be noted in the implementation are listed as follows:

- Inexact Line Search. The line search determines a value of α_k that ensures an acceptable objective function decrease from $\mathbf{x}_k$ to $\mathbf{x}_{k+1}$. It is usually unnecessary and computationally expensive to perform a line search with perfect accuracy. Therefore, an inexact line search is typically used, where a suitable step size rather than the optimal one is found. With a suitable step size, a sufficient decrease in f_k is realized. The most common conditions for inexact line search are the Armijo-Goldstein criteria [6, 38]. The importance of using an inexact line search is that the number of function evaluations needed in step 3 is substantially reduced.

- Finite Differences. Finite differences can be used when the derivatives of a function must be approximated using information only from function values. Forward difference ($f' = (f_{j+1} - f_j)/\Delta h$) or central difference ($f' = (f_{j+1} - f_{j-1})/2\Delta h$) can be used for this purpose. However, in antenna problems where the objective function evaluations are high, it is usually recommended to use forward differences.

2.2 Gradient-Free Methods

Gradient-based methods typically find local optima instead of global optima. As a result, they must be used with care to avoid getting trapped in local optima. A method that always yields the global optimum would imply an exhaustive search method, in which the optimum is selected by checking all feasible points. Obviously,

this method is terribly slow and not practical when there are many design variable values.

For the past several decades, gradient-free methods, a class of optimization methods which do not use derivative information but utilize only function values, have been introduced to search for global optima.

Gradient-free methods [46], or direct-search methods, are generally robust and particularly effective for problems with a small number of design variables, but typically require fast objective function evaluations for their practical implementation. They are largely independent of the initial designs and solution domain. Therefore, global optima are more likely to be found. As can be understood, the gradient-free methods work very well when many local optima exist, whereas gradient-based methods break down in these cases. On the other hand, gradient-free methods are generally slow with no guidance from gradient information, and require a large number of objective function evaluations to achieve convergence. Hence, they have limited use in problems involving complicated electromagnetic structures where field distributions cannot be solved in closed-form and traditional numerical simulations must be used for the objective function computation. Recent fast integral algorithms and their integration with finite element methods make the use of such gradient-free optimizations more practical.

Below we discuss the ideas behind two gradient-free methods, GA and SA, Genetic algorithms and simulated annealing are two types of (gradient-free) stochastic search techniques. Both methods bear the characteristics of the global optimization methods, are modeled on natural processes (evolution and thermodynamics), and have been applied in a variety of engineering areas such as operations research, image processing, chemical engineering, and VLSI design. GA and SA are likely to avoid

trapping themselves in a local optimum. Although a rigorous proof is not known, practical applications almost always produce the global optimum. Both methods can be hybridized with conventional optimizations.

2.2.1 Genetic Algorithm

Proposed by Holland [44], GAs are robust, stochastic-based search methods modeled on the concepts of natural selection and evolution.

There are several essential components in an GA process:

- A chromosomal encoding (usually binary strings) of solutions to the problem (see Figure 2.1);
- A way to create an initial population of solutions;
- An evaluation function (i.e. objective function) that rates solutions in terms of fitness;
- Genetic operators to generate successive generations of solutions (reproduction);
- Parameter settings: population size, probability of applying genetic operators, etc.

There are two basic types of operators for GAs. The *crossover* operator, as illustrated in Figure 2.2, swaps parts of two solutions to generate two new solutions. The *mutation* operator, shown in Figure 2.3, randomly changes a small percentage of bits in chromosomes, from 1 to 0 or vice versa.

The flowchart of a GA process is shown in Figure 2.4. In the beginning, a desired performance is described and formulated as a fitness function $f(\mathbf{x})$ to be minimized

by the GA optimizer, where $\mathbf{x}$ is a vector of design variables. If the optimization model contains constraints, they can be included as penalties in the fitness function or encoded directly into the solution strings. Several initial designs coded into binary strings are produced for the first generation either by the user or randomly. For each design, the fitness values are computed using the FE-BI solver and rated. Good solutions survive and have off-springs, while bad solutions are discontinued. Pairs of good solutions are selected using certain strategies to perform crossover. Mutation is usually allowed with a very small probability to flip some bits from 0 to 1 in the binary string and vice versa, thus providing a way to introduce new designs. This process is repeated until the termination criteria are met. Then the optimal binary string is decoded back into the corresponding design. In GA, local optima are avoided by hyperplane sampling in the Hamming space (i.e., crossovers) plus random perturbations (i.e., mutations) [37].

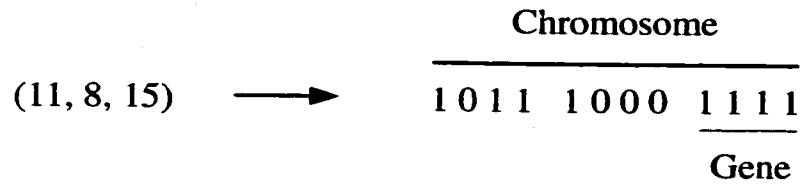

Figure 2.1: Illustration of binary encoding in GA.

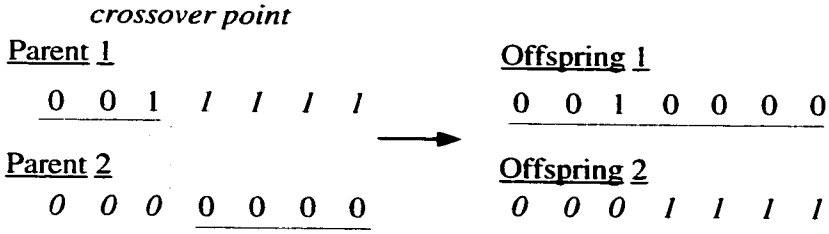

Figure 2.2: Illustration of a single-point crossover in GA.

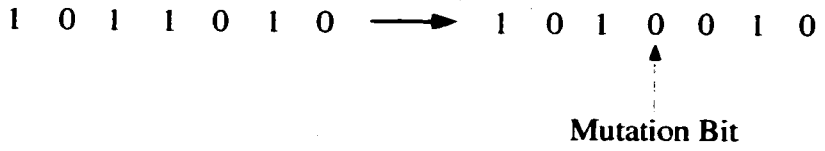

Figure 2.3: Illustration of mutation in GA.

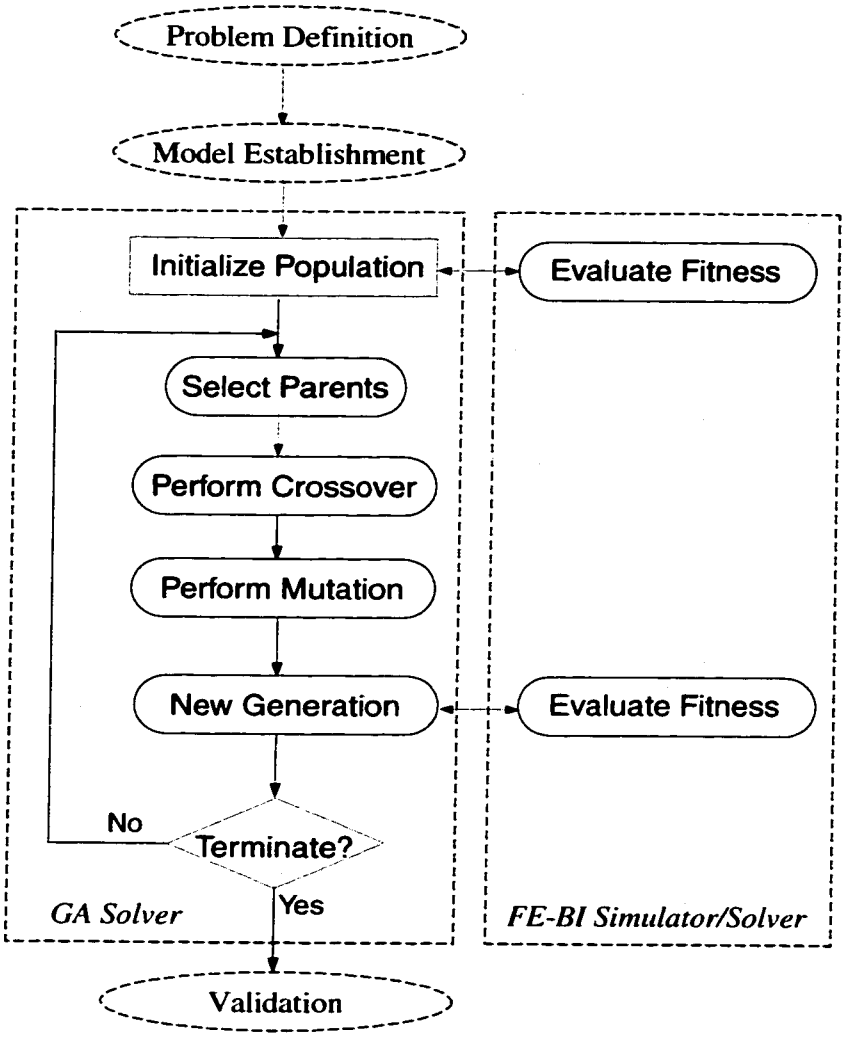

Figure 2.4: General optimization process using GA and an FEM solver.

2.2.2 Simulated Annealing

Simulated annealing [1, 29] was proposed by Kirkpatrick *et al.* in 1983 [59]. SA is a stochastic hill-climbing algorithm based on an analogy with the physical process of annealing. In physics of condensed matter, annealing is known as "a thermal process for obtaining low energy states of a solid in a heat bath" [1]. The process contains two steps:

- Increase the temperature to a value at which the solid starts to melt. In this liquid state, all particles arrange themselves randomly.
- Decrease the temperature slowly until the particles arrange themselves in the ground state of the solid. In this ground state, the particles are arranged in a highly structured lattice and the system energy is minimal.

To achieve the ground state, the melting temperature must be sufficiently high and the cooling is done sufficiently slowly. One must use an annealing process, where the temperature of the system is elevated, and then gradually lowered, spending enough time at each temperature to reach thermal equilibrium. If insufficient time is spent at any temperature, especially near the freezing point, the solid will be frozen into a meta-stable state called *quenching*.

To apply SA to optimization problems, proper analogues must be identified between the SA and physical annealing: the energy equation becomes the objective function, the current state of the thermodynamic system becomes the iterate solution, ground state becomes the global minimum, and temperature becomes the control parameter for the process.

Briefly, SA works in the following manner to minimize an objective function $f(\mathbf{x})$ (see Figure 2.5 for the flow chart):

1. Start with a feasible initial point $\mathbf{x}_0$ and temperature $T = T_0$.

2. Generate a new point $\mathbf{x}_{k+1} = \mathbf{x}_k + \mathbf{s}_k$, where $\mathbf{s}_k$ is the step size.

3. Apply the Metropolis criterion [73] to judge $f(\mathbf{x}_{k+1})$:

   If $f(\mathbf{x}_{k+1}) \leq f(\mathbf{x}_k)$, accept $\mathbf{x}_{k+1}$;

   Otherwise, accept $\mathbf{x}_{k+1}$ with probability $P = e^{-\frac{f(\mathbf{x}_k) - f(\mathbf{x}_{k+1})}{T}}$, or reject with probability $(1 - P)$.

4. Decrease temperature T according to some heuristic cooling schedule (for example, $T_{k+1} = 0.9T_k$).

5. Goto Step 2.

SA is similar to a GA (of single-size population) when crossovers are disabled and only mutations are used. Of course SA has its unique characteristics, as described below, and cannot be seen simply as equivalent to GA.

The essence in SA is that the optimization process is not required to go always downhill, but is allowed to make uphill moves occasionally. The probabilities of accepting an uphill move and step size are determined by the value of temperature T, both of which are reduced as the temperature becomes lower. At the beginning of the SA process, T is relatively large, making the step size large and the accepting probability high. Thus, more designs can be explored within the domain. As SA progresses, T is lowered. Therefore the step size is decreased and uphill moves are more likely to be rejected, constraining the search to a more 'local' area. Eventually, the process settles by only accepting downhill moves. In this maneuver, SA prevents itself from getting stuck in inferior local optima, and is more likely to settle in areas of global quality, especially if the objective function has an overall trend to it.

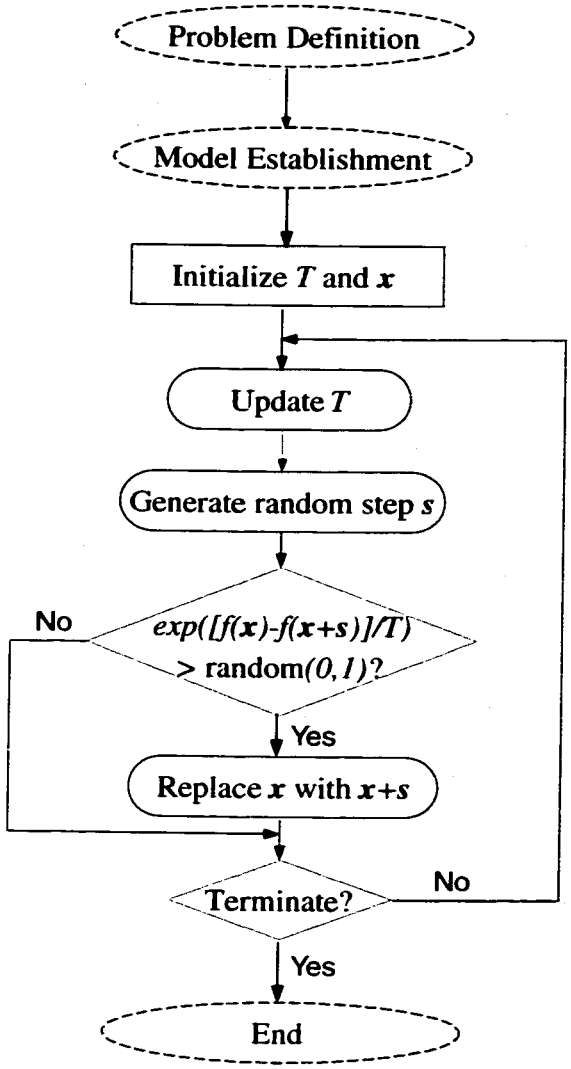

Figure 2.5: General optimization process using SA.

The disadvantage of SA is that the parameter settings for the cooling schedules are very complicated and not well understood. Such parameters are the initial temperature, the relationship between step size and temperature, number of iterations at each temperature, and the temperature decrease rate at each step as cooling proceeds. Determining appropriate values for all these parameters is often accomplished through trial and error, which can become prohibitively expensive for all but the simplest problems. Recently, an adaptive simulated annealing (ASA) algorithm [57] was introduced to improve the basic SA algorithm, but its study is beyond the scope of this thesis.

2.3 Finite Element - Boundary Integral Method Formulation

Here we present the FE-BI formulation. Specialization towards the need of the particular problems in later chapters will be qualitatively outlined accordingly.

Consider a patch antenna configuration shown in Figure 2.6, where the cavity housing the radiating elements and feeding structures is recessed in a ground plane. The goal is to seek the solution of the vector wave equation

$$\nabla \times \{\mu_r^{-1} \cdot (\nabla \times \mathbf{E})\} - k_0^2 \epsilon_r \cdot \mathbf{E} = -jk_0 Z_0 \mathbf{J}^{\text{int}} - \nabla \times (\mu_r^{-1} \cdot \mathbf{M}^{\text{int}}) \qquad (2.9)$$

where $\mathbf{E}$ is the total electric field, (ϵ_r, μ_r) denote the relative permittivity and permeability of the domain, k_0 is the free space wave number and Z_0 the free space intrinsic impedance. $\mathbf{J}^{\text{int}}$ and $\mathbf{M}^{\text{int}}$ are internal electric and magnetic sources due to the antenna feeds.

To obtain the unknown field using FEM, the variational equation

$$\delta F(\mathbf{E}) = \mathbf{0} \qquad (2.10)$$

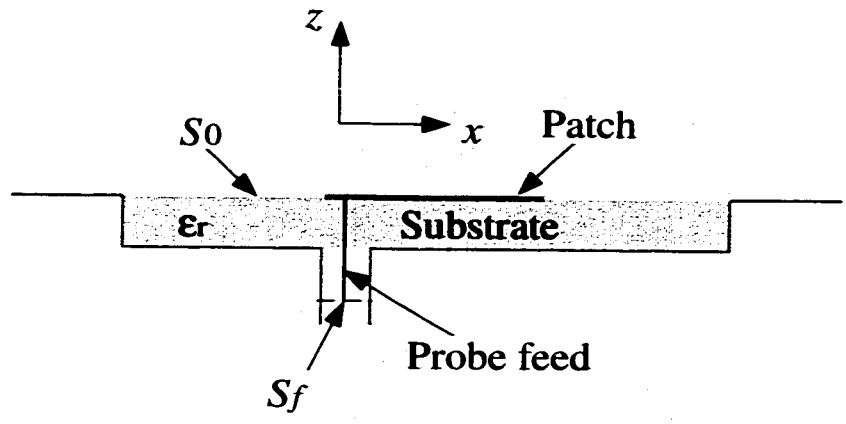

Figure 2.6: Geometry of a cavity-backed microstrip antenna.

is solved, where [108]

$$\begin{aligned} F(\mathbf{E}) &= \frac{1}{2}\iiint_V [\mu_r^{-1}(\nabla\times\mathbf{E})\cdot(\nabla\times\mathbf{E}) - k_0^2\epsilon_r\mathbf{E}\cdot\mathbf{E}]dV \\ &+ \iiint_V [jk_0Z_0\mathbf{J}^{\text{int}}\cdot\mathbf{E} - \mu_r^{-1}\mathbf{M}^{\text{int}}\cdot(\nabla\times\mathbf{E})]dV \\ &+ jk_0Z_0\iint_{S_0+S_f}(\mathbf{E}\times\mathbf{H})\cdot\hat{z}dS \end{aligned} \tag{2.11}$$

Here V denotes the cavity volume, S_0 is the cavity aperture excluding the metallic portions, S_f represents the junction opening to possible guided feeding structures, and $\mathbf{H}$ is the magnetic field on S_0 and S_f whose outer normal is given by $\hat{z}$. The last term in (2.11) is the BI term.

For cavity-backed patch antennas, the cavity is first discretized into a number of finite elements (typically prismatic or tetrahedral elements for regular shaped patches and nonuniform elements for arbitrarily shaped patches) that naturally reduce to triangular elements on the cavity's aperture. Edge-based basis functions are used to expand the field within each volume element. Compared with node-based ones, edge-based functions are better suited for simulating 3-D EM fields at corners and edges, and they overcome difficulties associated with spurious solutions. Although

edge-based elements increase the unknown count, this is balanced by the increased sparsity of the resulting stiffness matrix. Using Galerkin's method, after the element matrices are assembled altogether, the resulting matrix system can be written as [108]

$$[\mathcal{A}]\begin{Bmatrix}\{E^V\}\\ \{E^B\}\end{Bmatrix}+\begin{bmatrix}[0] & [0]\\ [0] & [\mathcal{G}]\end{bmatrix}\begin{Bmatrix}\{E^V\}\\ \{E^B\}\end{Bmatrix}=\begin{Bmatrix}\{b^V\}\\ \{b^B\}\end{Bmatrix}. \tag{2.12}$$

Here, E^V denotes the field unknowns within the volume enclosed by $S_0 + S_f$, E^B is the corresponding unknowns on the boundaries S_0 and/or S_f. The matrix $[\mathcal{A}]$ is very sparse and the boundary matrix $[\mathcal{G}]$ is fully populated. Figure 2.7 gives an example matrix system generated by the FE-BI method [106]. The full BI system, although only a small part of the overall system, still has high computational demands, which can be further alleviated by absorbing boundary conditions (ABCs) or artificial absorbers (AAs) [106].

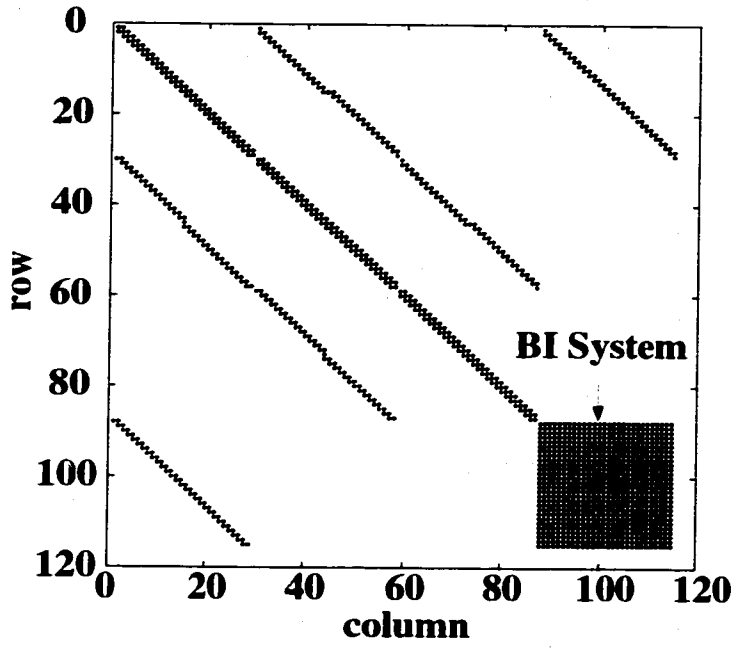

Figure 2.7: Examples of matrix systems generated by the FE-BI methods.

2.4 Conclusions

In this chapter, the formulation for optimization problems was presented. Design optimization methods were classified and summarized in general. Gradient-based techniques utilize derivative information for fast convergence. However, they usually only find local optima. On the other hand, gradient-free techniques are largely independent of initial points and work well for problems with discontinuities and many local optima. However, a considerable amount of function evaluations are needed due to a lack of gradient information use. The principles of several optimization methods, i.e., the SQP gradient-based method, and GA and SA gradient-free methods, were outlined. At the end of the chapter we presented the FE-BI formulation for antenna analysis.

CHAPTER III

VERIFICATION OF DESIGN PRACTICE

Antenna design is a topic of great importance in electromagnetics and involves the selection of antenna physical parameters to achieve optimal gain, pattern performance, bandwidth, VSWR, and so on, subject to specified constraints. Trial and error design methods are inefficient and depend mainly on the engineer's intuition and experience. Even with the availability of numerical methods and sophisticated computer programs, such as the method of moment (MoM) and the finite element method (FEM), design of antennas and arrays with complicated geometry and feeding structures is still a demanding and time-consuming task, sometimes even intractable. To speed up the design process of antenna systems and reduce cost, a more attractive approach is to combine the numerical antenna analysis with various optimization algorithms. Optimization methods are not only able to refine or redesign existing designs faster, but also to obtain novel designs that are not easily found otherwise.

In this chapter, three different antenna design problems are proposed and solved using various optimization techniques. Although these problems have not been solved with optimization methods before, extensive research has been conducted on these problems. Therefore, we treat them as a verification of design optimization practice.

In section 3.1, ferrite materials are introduced and their applications for patch

antennas are demonstrated when they are used as substrates or superstrates to provide extra freedom in tuning resonant frequencies or steering beams. The sequential quadratic programming (SQP) algorithm is used for both frequency tuning and pattern control problems. In section 3.2, stacked patch antennas are investigated and broadband performance is obtained, again with SQP used for continuous variable optimization. Finally, in section 3.3, two irregular-shaped single patch antennas are designed for broadband and dual frequency performance, respectively, using both genetic algorithm and simulated annealing.

3.1 Ferrite Antennas: Proportional Design

Ferromagnetic materials are inherently anisotropic and exhibit non-reciprocal behavior. The non-reciprocal properties of ferrites are very attractive for microwave circuit devices [3] as well as for microstrip antennas [15] because of the high permittivity and tensor permeability of ferrite materials. The material properties of ferrites are mainly controlled by the direction and strength of an externally applied magnetic bias field, thus enabling control of various antenna radiation and scattering characteristics. These unique properties of ferrite materials provide many desirable features such as tunability, polarization diversity, beam steering and radar cross section control. Furthermore, because of additional variables such as bias field strength, bias direction and saturation magnetization, optimization methods are very suitable for ferrite antennas.

Ferrite substrates and superstrates have been used in several applications of microstrip antennas. In their unbiased state, the high effective permittivity of ferrite substrates allows smaller antenna sizes at low frequencies. This miniaturization is shown to produce antennas with larger bandwidth and efficiency than antennas on

dielectrics [26, 27].

When a DC bias field is applied to the ferrite material, antenna performance can be further enhanced. Specifically, several applications have been proposed and studied for ferrite patch antennas:

- Resonant frequency tuning. By changing the bias field H_0, multiple resonant frequencies can be achieved using a single patch antenna that increases functionality compared with traditional narrow-bandwidth patch antennas [92].

- Radar cross section (RCS) reduction. It is shown in [89] that by changing H_0, a patch antenna can be switched between 'on' and 'off' states. When the antenna is in an 'off' state, the RCS can be significantly reduced within certain frequency range. Ferrite cover layer can also be used to reduce RCS [112].

- Beam steering. The main beam can be scanned using single element antennas as phase shifters [101]. Biased ferrite superstrate has also been used to achieve pattern control [42]. On the other hand, a microstrip line printed on a ferrite changes its phase significantly when a normal directed bias is applied [11].

- Generation of circular polarization. This can be obtained over a large bandwidth with a single probe feed under a rectangular or circular patch antenna [88].

- Gain improvement. At the cost of bandwidth, gain can be improved by placing a dielectric and/or magnetic overlay on top of an infinite ground plane [113].

As can be seen above, ferrite materials are widely used in electromagnetic applications, especially in microstrip antennas. In the rest of this section, we consider the effect of biased ferrite substrate and superstrate on resonant frequency tuning [88] and beam steering [42]. Because of the additional variables from ferrite materials

such as bias field strength, bias direction and saturation magnetization, optimization methods are suitable for finding optimal designs that satisfy prescribed performance. The tools used will be gradient-based optimization in conjunction with finite element - boundary integral (FE-BI) models [64]. The FE-BI simulator allows the modeling of finite and inhomogeneous layers. The Bi-Conjugate (BiCG) solver is used to solve the resulting general matrix system, but the general minimal residual (GMRES) may be necessary in case BiCG experiences convergence difficulties [16]. For the optimizer, the SQP method is used.

In the rest of this section, basic concepts of ferromagnetic materials and the FEM formulation are presented first. Some validation of the FEM codes is then presented on a ferrite loaded cavity. Subsequently, two optimization problems relating to resonant frequency tracking and pattern control are established. We conclude this section with a discussion of numerical results.

3.1.1 Basic Properties of Ferromagnetic Materials

The magnetic anisotropy of a ferromagnetic material is caused by the interaction between an applied DC bias field and a microwave signal. The DC field causes the magnetic moments in the material to align themselves with the field producing a net magnetization. Depending on the polarization of the field, a microwave signal will propagate through a ferrite medium differently in different directions [91]. Thus, a tensor is needed to characterize the ferrite medium. A biased ferrite slab can support two different types of waves: ordinary and extraordinary [91, 112]. The ordinary wave is polarized perpendicular to the direction of the bias field, possesses the same characteristics as that inside a dielectric material, and is not affected by the magnetization. On the other hand, the extraordinary wave is polarized along

the direction of the bias field. Therefore, it is strongly affected by the biasing. The propagation constant of this extraordinary wave is given by [63, 91]

$$\beta_e = \omega\sqrt{\epsilon\mu_{eff}} \tag{3.1}$$

where

$$\mu_{eff} = \frac{\mu^2 - \kappa^2}{\mu} \tag{3.2}$$

$$\mu = \mu_0(1 + \frac{\omega_0\omega_m}{\omega_0^2 - \omega^2}) \tag{3.3}$$

$$\kappa = \mu_0\frac{\omega\omega_m}{\omega_0^2 - \omega^2}. \tag{3.4}$$

Here $\omega_0 = \mu_0\gamma(H_0 + j\frac{\Delta H}{2})$ is the Larmor or precession frequency, at which the electron precesses about the external bias field H_e [91]; and $\omega_m = \mu_0\gamma(4\pi M_s)$. In these expressions, H_0 is the internal bias field; ΔH is the linewidth, a quantity related to loss; $4\pi M_s$ is saturation magnetization, a physical property of ferrite materials which typically ranges between 300 to 5000 Gauss; and γ is the gyromagnetic ratio, which is the ratio of the spin magnetic moment to the spin angular momentum [91]. Throughout this section, the ferrite materials are assumed to be in saturated state.

The permeability is modeled in tensor form and depends on the direction of the bias field. For example, if the ferrite is biased in the $\hat{z}$ direction, as shown in Figure 3.1(a), the permeability tensor is given by

$$[\mu] = \begin{bmatrix} \mu & j\kappa & 0 \\ -j\kappa & \mu & 0 \\ 0 & 0 & \mu_0 \end{bmatrix} \tag{3.5}$$

where μ and κ are given in (3.3) and (3.4)

For bias along the tangential ($\hat{x}$ or $\hat{y}$) direction (see Figure 3.1(b)), the tensor needs to be rotated 90 degrees. For an arbitrary bias, the expression for $[\mu]$ becomes more complex.

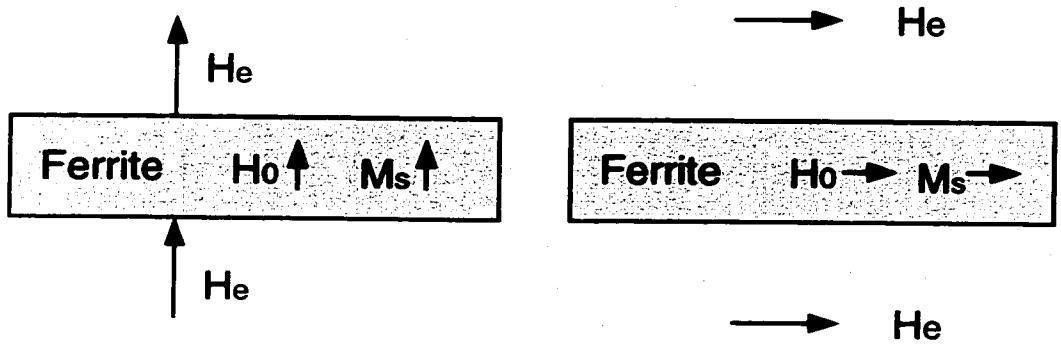

(a) Normal bias (b) Tangential bias

Figure 3.1: Biasing directions for ferrite materials.

The external and internal magnetic fields are related by

$$H_0 = H_e - N(4\pi M_s) \tag{3.6}$$

where $N = N_x$, N_y or N_z is called the demagnetization factor. The demagnetization factors satisfy $N_x + N_y + N_z = 1$.

Traditionally, the CGS unit system (the system of units based on measuring lengths in centimeters, mass in grams, and time in seconds) is used for magnetic quantities. Hence for the rest of this section, CGS units will be used. That is, the magnetization (measured in Gauss) and field strength (measured in Oersteds) can be converted using the following relations

$$1\ [\mathrm{G}] = 10^{-4}\ [\mathrm{W/m^2}] \tag{3.7}$$

$$4\pi \times 10^{-3}\ [\mathrm{Oe}] = 1\ [\mathrm{A/m}]. \tag{3.8}$$

3.1.2 FEM Analysis for Ferrite Antennas

The FEM provides a computational tool that is needed to solve the vector unknowns (electric and magnetic fields). It is used to discretize the problem domain,

which is characterized by a differential equation. For reference purposes let us consider a perfect electric conductor (PEC) cavity with a patch residing on the cavity aperture. The finite element formulation for anisotropic materials begins with Maxwell's equations

$$\nabla \times \mathbf{E} = -jk_0 Z_0 \bar{\bar{\mu}}_r \mathbf{H} \tag{3.9}$$

$$\nabla \times \mathbf{H} = +jk_0 Z_0 \bar{\bar{\epsilon}}_r \mathbf{E} \tag{3.10}$$

where $\mathbf{E}$ and $\mathbf{H}$ are the electric and magnetic fields, respectively. The permittivity $\bar{\bar{\epsilon}}_r$ and permeability $\bar{\bar{\mu}}_r$ are in tensor form. The free-space wavenumber and impedance are denoted by $k_0 = \omega\sqrt{\mu_0\epsilon_0}$ and $Z_0 = \sqrt{\frac{\mu_0}{\epsilon_0}}$, respectively. Using the above two equations, the second-order partial differential equation (PDE) derived from (3.9) and (3.10) is

$$\nabla \times (\bar{\bar{\mu}}_r^{-1} \cdot \nabla \times \mathbf{E}) - k_0^2 \bar{\bar{\epsilon}}_r \cdot \mathbf{E} = -jk_0 Z_0 \mathbf{J} - \nabla \times (\bar{\bar{\mu}}_r^{-1} \cdot \mathbf{M}) \tag{3.11}$$

This is the vector wave equation for solving $\mathbf{E}$ (i.e. a single unknown) with $\mathbf{J}$ and $\mathbf{M}$ being the impressed electric and magnetic current densities within the computational domain, respectively.

The functional for the FEM has been shown in equation (2.11) in Chapter II. However, this equation must be modified to incorporate the anisotropy of the ferrite material. Specifically, we have

$$\begin{aligned} F(\mathbf{E}) = & \frac{1}{2}\iiint_V [\bar{\bar{\mu}}_r^{-1} \cdot (\nabla \times \mathbf{E}) \cdot (\nabla \times \mathbf{E}) - k_0^2 \bar{\bar{\epsilon}}_r \cdot \mathbf{E} \cdot \mathbf{E}] dV \\ & + \iiint_V [jk_0 Z_0 \mathbf{J}^{\text{int}} \cdot \mathbf{E} - \bar{\bar{\mu}}_r \cdot \mathbf{M}^{\text{int}} \cdot (\nabla \times \mathbf{E})] dV \\ & + jk_0 Z_0 \iint_S (\mathbf{E} \times \mathbf{H}) \cdot \hat{z} dS. \end{aligned} \tag{3.12}$$

The detailed FE-BI formulation for anisotropic materials can be found in [15].

3.1.3 Validation: Ferrite-Loaded Cavity

In this subsection, we compare results based on our FE-BI code with published data in the literature. The RCS and resonant frequency of a ferrite-tuned cavity-backed slot antenna are shown to be consistent with [60].

Consider a multi-layer ferrite loaded cavity-backed slot (CBS) antenna shown in Figure 3.2. This geometry was analyzed in [60] with cavity dimensions of 5.08cm $\times$ 5.08cm. Layers 2 and 4 are magnetized in the $\hat{y}$ direction. There are 6776 unknowns for this problem and 420 BI unknowns. The RCS of this layered ferrite cavity for two different bias values of $H_0 = 500$ Oe and 700 Oe is given in Figure 3.3. Our results are shown to be in agreement to those in [60] for both cases.

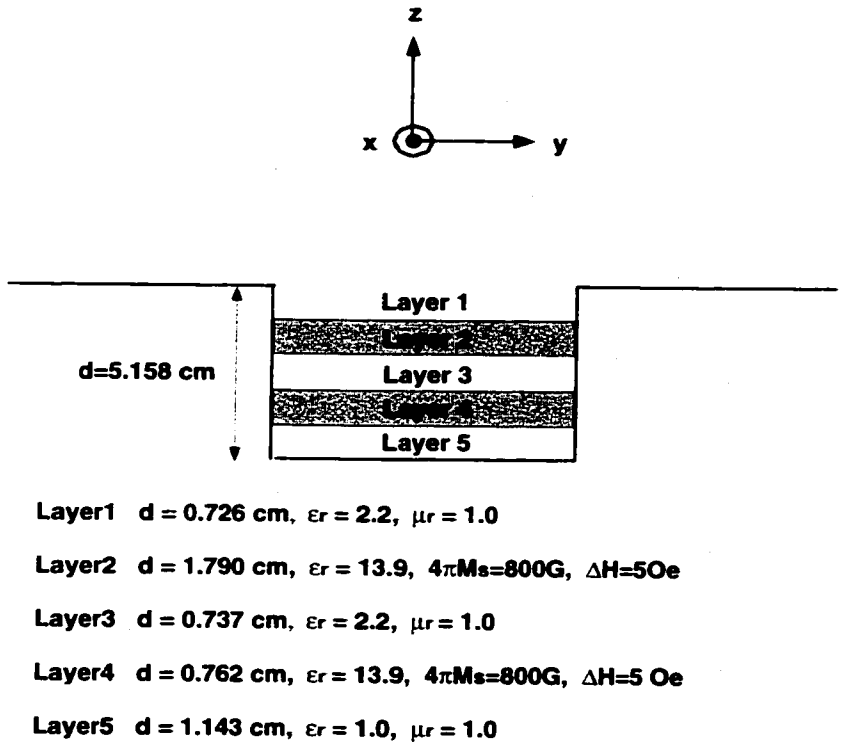

Figure 3.2: Geometry of the multilayer ferrite-loaded CBS antenna.

This example validates the FE-BI method and also demonstrates the frequency shifting capability of ferrite materials when biased.

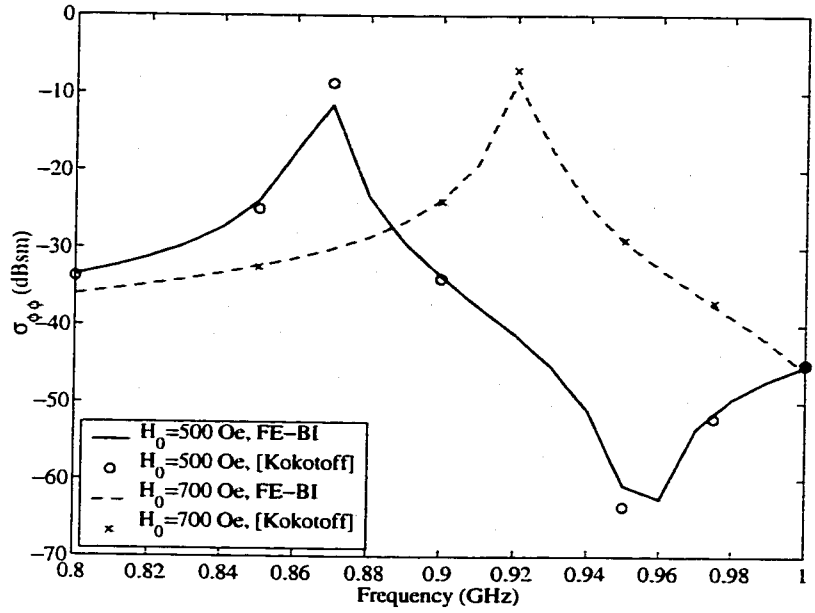

Figure 3.3: RCS of the ferrite biased cavity in Figure 3.2.

3.1.4 Resonant Frequency Tracking

Resonant frequency tracking and tuning are two of the most important features for ferrite patch antennas. Biased ferrite substrates offer extra degrees of freedom for resonant frequency tuning. Also, circular polarization can be achieved with a single feed using a ferrite substrate (dielectric substrates cannot achieve this). We will first verify that our results are in agreement with those in [88]. We will then formulate the resonant frequency tracking as an optimization problem.

The antenna we study is similar to the one in [88], with a patch of size $L = W =$ 0.61 cm. This patch is placed at the aperture of a 1.22 cm $\times$ 1.22 cm $\times$ 0.127 cm cavity filled with a dielectric of $\epsilon_r = 15$, and a probe feed located in the middle of the edge, as shown in Figure 3.4. For the isotropic case, the resonance occurs at about 5.5 GHz.

First, a normal biasing field is applied. The results are shown in Figure 3.5, and compared to those of Pozar [88], who used the moment method (MoM). Our results

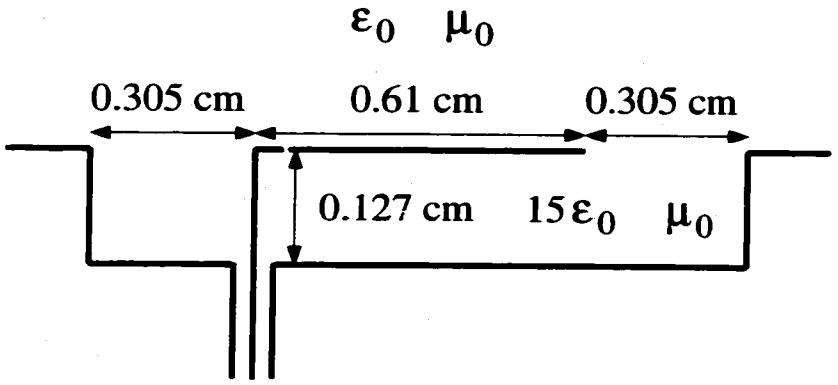

Figure 3.4: A cavity-backed patch antenna.

are consistent with the MoM data except for a slight shift in frequency. It is observed that the resonant frequency increases with increased normal biasing strength and saturation magnetization. Left-hand circular polarization (LHCP) and right-hand circular polarization (RHCP) have also been achieved using just a single feed point. For this configuration, the LHCP frequency is higher than the RHCP one at any specific value of biasing and magnetization.

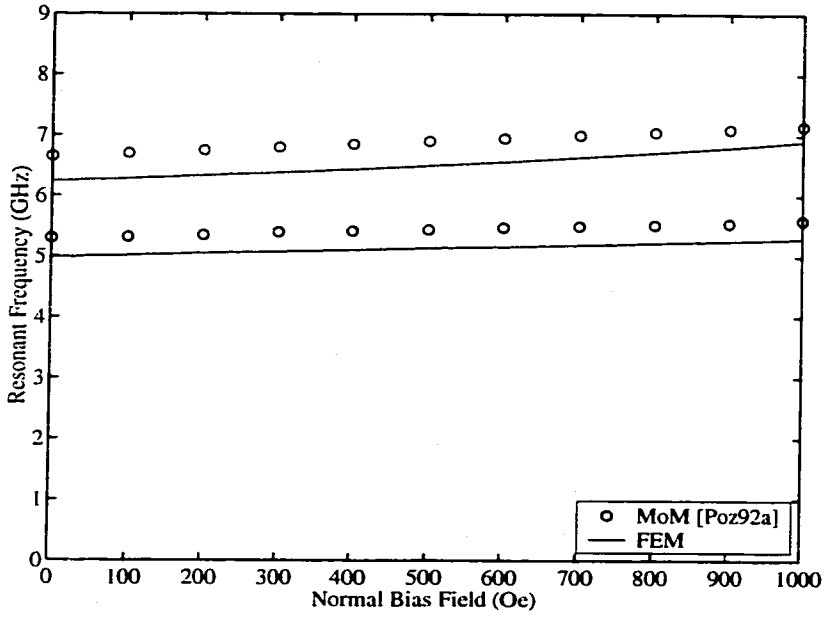

Figure 3.5: Resonant frequency for the patch in Figure 3.4 as a function of the bias field and saturation magnetization (normal bias).

Because of the multitude of parameters that control the resonance of a ferrite patch, it is advantageous to use an optimizer to predict the resonant frequency of the ferrite patch instead of locating the resonance by frequency sweep. The optimization problem statement can be formulated as follows:

$$\begin{aligned} &\text{Find } f_* \quad \text{that minimizes } |\text{Imag}(Z_{in}(f))| \\ &\text{subject to} \qquad f_L \leq f \leq f_U \end{aligned} \tag{3.13}$$

where Z_{in} is the frequency-dependent input impedance, and f_L and f_U are lower and upper bounds of the frequency. Here we use the definition that the antenna reaches resonance when the imaginary part of the input impedance is zero.

Next, we use the above optimization model to find the resonant frequencies of the antenna when the substrate is biased parallel to one of the edges of the patch, which was not explored in [88]. We solve the optimization problem (3.13) for various values of the bias field strength H_0 and saturation magnetization $4\pi M_s$. For each fixed H_0 and $4\pi M_s$, a gradient-based optimization method SQP is employed and the optimal f_* (i.e., resonant frequency) is obtained within 3 iterations that require less than 30 FEM calls. The results are plotted in Figure 3.6 (a) and (b) for $\hat{x}$-bias (bias field perpendicular to the edge where the feed is located) and $\hat{y}$-bias (bias field parallel to the edge where the feed is located), respectively. Again, the resonant frequency of the antenna shifts higher as H_0 or $4\pi M_s$ increases. However, $\hat{x}$ and $\hat{y}$ biasing provides linear polarization and greater dynamic range for frequency tuning. Also, the resonant frequencies for $\hat{y}$-bias are higher than those for $\hat{x}$-bias. This provides more tuning flexibility. Other ferrite parameters may also play a role in resonant frequency tuning.

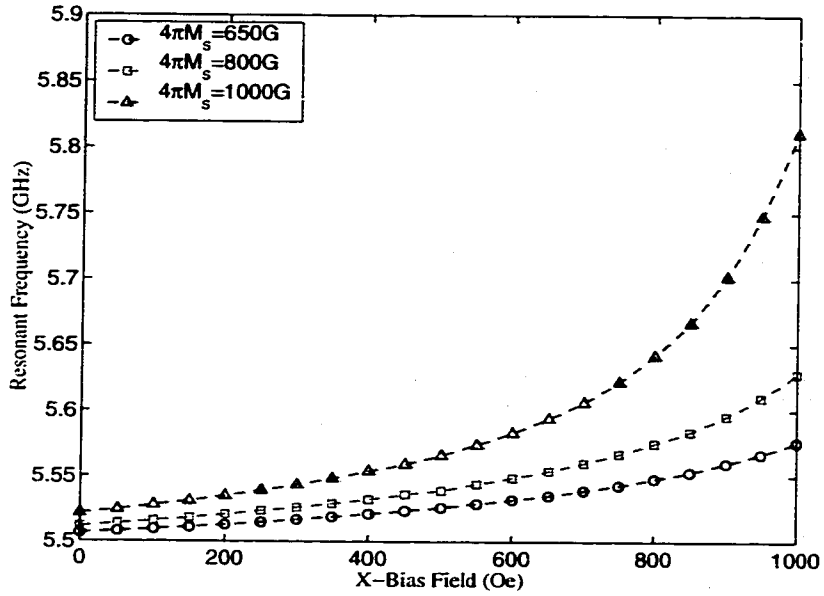

(a) $\hat{x}$-bias

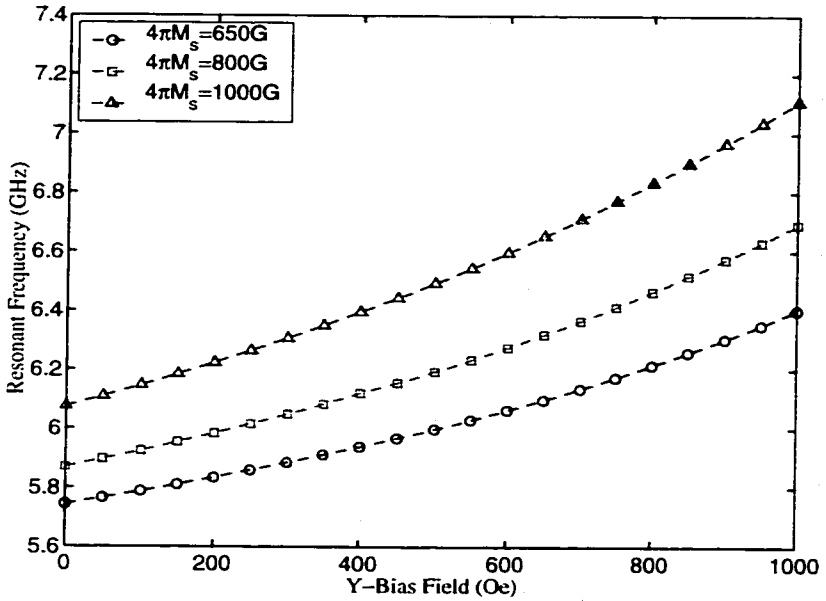

(b) $\hat{y}$-bias

Figure 3.6: Resonant frequency for the cavity-backed patch antenna in Figure 3.4 as a function of the bias field and saturation magnetization.

3.1.5 Beam Scanning with a Ferrite Cover Layer

Traditional antenna array pattern control uses delay lines / phase shifters to achieve a beam shift. However, achieving such control becomes more expensive as the number of array elements increases. Severe conflicts of element spacing might also happen for packaging. Recently, the introduction of low-profile, ferrite-loaded microstrip antennas with beam scanning capability offers unique design flexibilities because beam steering can be achieved by simply changing H_0. The use of ferrites for phase shifting has been investigated under various configurations, such as: placing a uniform ferrite substrate under the patch antenna [47], placing a uniform ferrite superstrate above the patch antenna [42], or placing ferrite only underneath the microstrip feeds [11]. In this section, we will employ the second configuration to establish an optimization model.

For this configuration, a single antenna patch is sandwiched between an upper ferrite layer and a lower dielectric substrate layer, as shown in Figure 3.7. With zero bias, the main beam of the H-plane pattern is normal to the antenna patch. When a bias field is applied, the main beam can be shifted with appropriate choices of ferrite material, layer thickness, and bias field. The thickness of the superstrate h_{sup}, the strength of externally applied magnetic field H_0, and the saturation magnetization $4\pi M_s$ can be adjusted to obtain different beam angles.

In the first example, all of the above three design variables (h_{sup}, H_0, and $4\pi M_s$) are allowed to change to obtain the desired beam angles (such as 10°, 20°, or 30°, etc.). Design optimization methods can be used in conjunction with FE-BI simulation [64] to find the appropriate values for them. Therefore, this optimization problem can

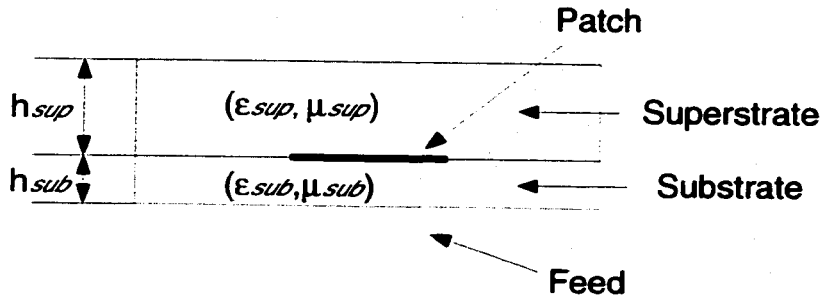

Figure 3.7: Patch between ferrite cover layer and dielectric substrate layer: side view.

be formulated as follows:

$$\text{Find } h_{sup}, H_0 \text{ and } 4\pi M_s \text{ that minimize } |\theta_* - \theta_0| \tag{3.14}$$

where $\theta_* = \arg\max_{\theta} \{\text{Relative Power}\}$, and θ_0 is the desired beam direction.

Consider a rectangular patch with fixed size $L = W = 0.4$ cm. The antenna is placed in a 3.2 cm $\times$ 3.2 cm $\times$ 0.1 cm cavity with a dielectric substrate of $\epsilon_{rsub} = 10$, and a ferrite cover layer with $\epsilon_{rsup} = 13.8$ is placed above the patch. A probe feed is located at the mid point of an edge for excitation. This configuration is shown in Figure 3.8. The antenna is biased parallel to one of the edges of the patch. We solve the optimization problem three times for $\theta_0 = 10°$, $20°$, and $30°$, respectively. These scanning angles are achieved when the values of h_{sup}, H_0, and $4\pi M_s$ given in Table 3.1 are applied at $f = 6.18$ GHz. A 5×2 array with the same ferrite cover layer and dielectric substrate layer is used to narrow the beam, as shown in Figure 3.9. This pattern is obtained by multiplying the pattern of the single patch with the appropriate array factor.

The above design is not as practical since the thickness of the superstrate is allowed to vary, which shifts resonant frequencies. A more practical design, where only the externally applied magnetic field H_0 is allowed to vary, is investigated next. For this optimization problem, the geometry is the same as in Figure 3.8 except that

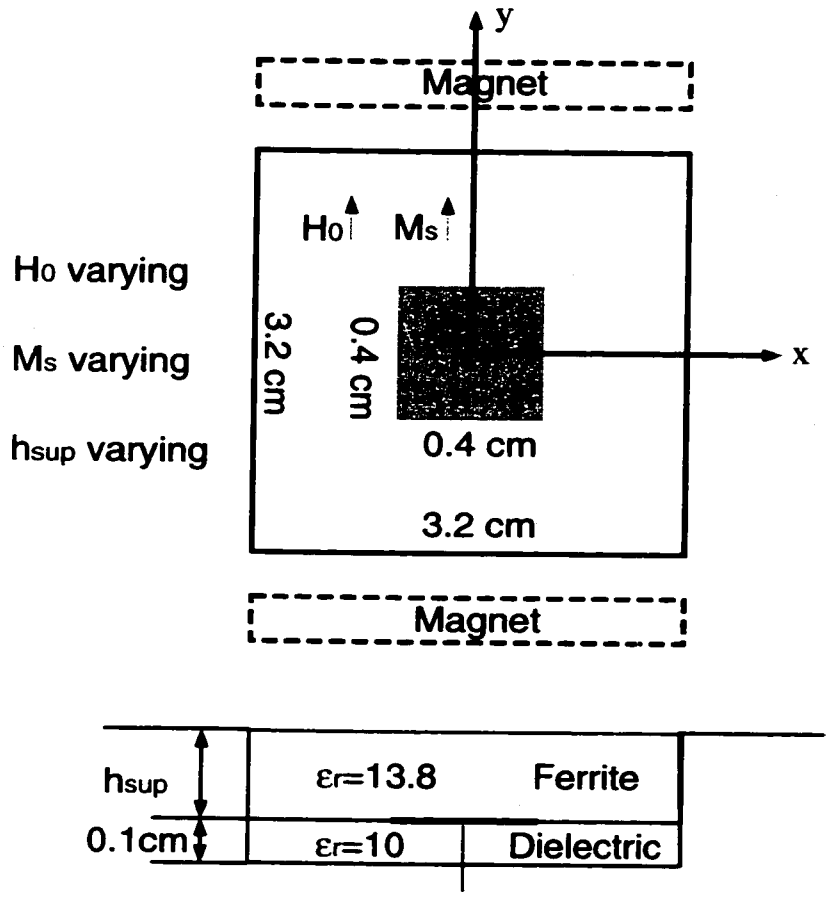

Figure 3.8: Geometry of a single patch under a ferrite cover layer: top view and side view.

Scan angle (°)	h_{sup} (cm)	H_0 (Oe)	$4\pi M_s$ (G)
0	0.3	0	0
10	0.25	800	1040
20	0.332	1000	800
30	0.1	800	2050

Table 3.1: Optimal h_{sup}, H_0 and $4\pi M_s$ to achieve specified beam angles.

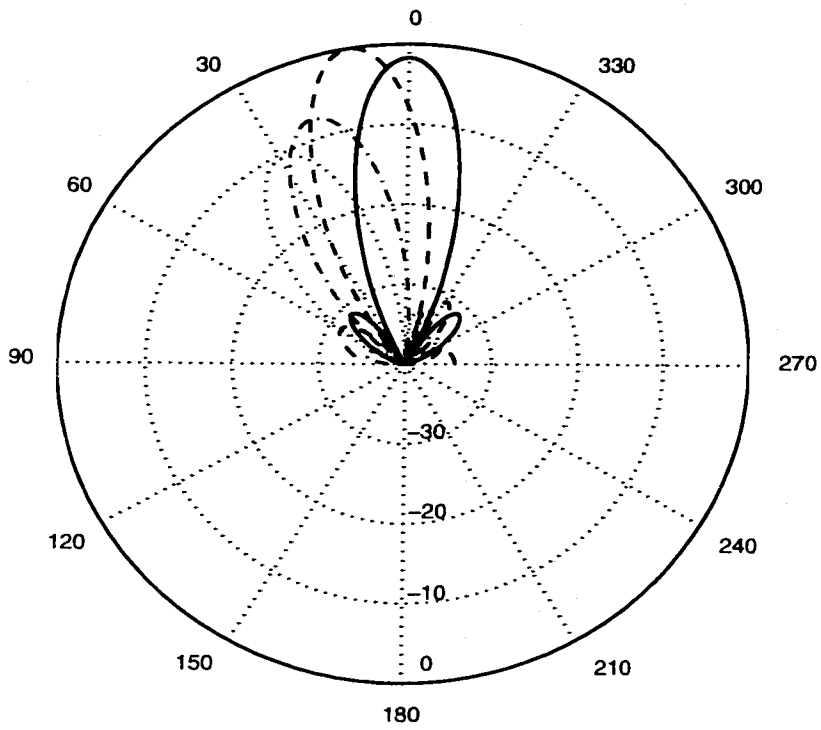

Figure 3.9: Scanning of the 5 × 2 sandwiched array to achieve beam angles of 10°, 20° and 30°, respectively, at 6.180 GHz: Y-bias, $\phi = 0$ cut. Optimal values of h_{sup}, H_0 and $4\pi M_s$ for each specified scan angle are shown in Table 3.1.

$h_{sup} = 0.2$ cm and $4\pi M_s = 1300$ G are fixed here. Figure 3.10 shows the results of H_0 to get specific beam angles. As seen, the resulting pattern has the prescribed beam direction of $\theta_0 = 10, 20$ and 30 degrees corresponding to $H_0 = 800, 2000$ and 2050 Oe. These values of H_0 were predicted by the optimizer after just a few iterations. On average, 30-60 FEM calls are needed for the computation of objective function and gradients during the optimization process. The patterns are broad because only a single antenna element is used. Narrow beams can again be achieved by using an array configuration.

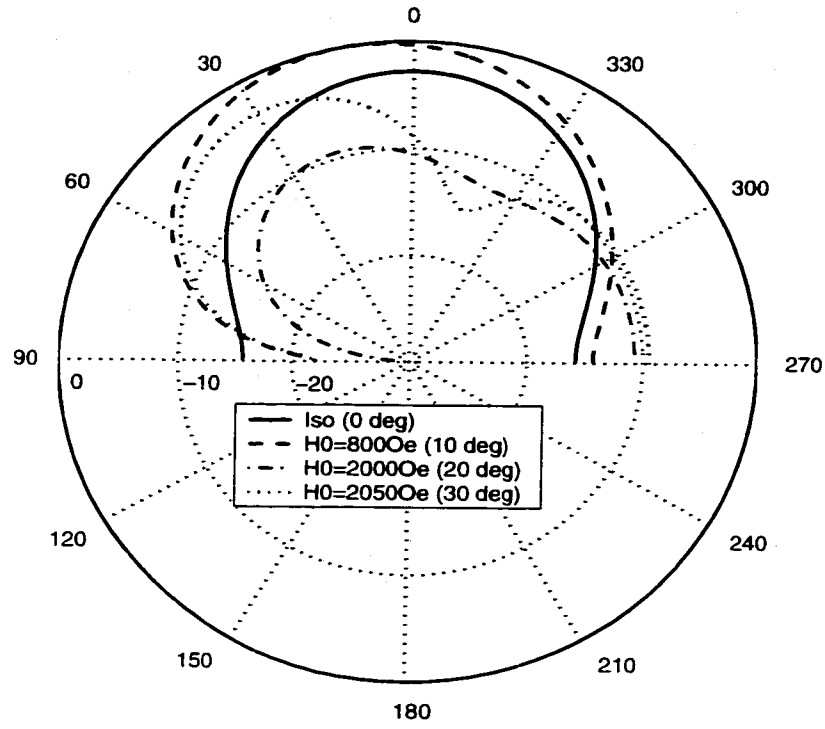

Figure 3.10: Scanning of single patch at 6.9 GHz: Y-bias, $\phi = 0$ cut. Only H_0 is varied, $h_{sup} = 0.2$ cm, and $4\pi M_s = 1300$G.

The above two examples sufficiently demonstrate the frequency tuning and beam steering capability of ferrite antennas. Tuning and steering are achieved by adjusting the external magnetic field without modifying the antenna configuration.

3.2 Broadband Antennas: Proportional Design

3.2.1 Introduction

In this section, two broadband antenna configurations will be proposed and optimized. The design variables involved are sizes, hence we are dealing with proportional patch design optimization problems.

One of the principal limitations of patch antennas is their narrow bandwidth (usually on the order of a few percent). A number of techniques have been suggested and implemented to improve the bandwidth of microstrip patch antennas. In this section, we first review the basic relationship between bandwidth and microstrip patch parameters, then summarize traditional techniques for bandwidth enhancement. Subsequently, stacked patch configurations are considered and optimized with regards to bandwidth.

There are basically two kinds of bandwidth for microstrip antennas: *impedance* bandwidth and *pattern* bandwidth [10]. Impedance bandwidth is usually associated with input impedance and radiation efficiency, and is specified in terms of return loss or maximum VSWR (typically less than 2.0 or 1.5) over a frequency range. Pattern bandwidth is related to gain, side lobe level, beamwidth, and polarization. For a single antenna element, the impedance bandwidth is usually the limiting factor, while the pattern bandwidth does not vary much with frequency. In the rest of this section, bandwidth refers to the impedance bandwidth.

The quality factor Q, bandwidth, and efficiency are figures-of-merit of an antenna. However, they are not independent and there are always tradeoffs among them. The relationship between bandwidth BW and Q is [18]

$$\mathrm{BW} = \frac{\mathrm{VSWR} - 1}{Q\sqrt{\mathrm{VSWR}}} \tag{3.15}$$

The above formulae implies that higher Q leads to narrower bandwidth. On the other hand, bandwidth increases with increasing substrate thickness, and decreases with increasing substrate dielectric constant. However, thicker substrate makes impedance matching difficult, because surface waves are excited, which lowers efficiency rapidly [90].

Most bandwidth enhancement approaches can be put into one of three categories [90]: 1) improved impedance matching, 2) reduced efficiency, 3) introduction of multiple resonances. Among them, (3) is the most popular approach. The idea of using multiple resonances is to stack two or more patches resonating at nearby frequencies. Usually only one patch (referred to as the *driven patch*) is fed directly with a probe feed or slot feed, and the other patches (as *parasitic patches*) are coupled by proximity effects. In practice, dual stacked patches are typically used for broadband or dual-resonance performance. The two patches are usually similar in size, with the top one slightly larger than the bottom one. Buy using a dual patch configuration, bandwidth can be increased to about 10% - 20%.

There are many possible design variables associated with dual patches. Among them are: (1) patch sizes; (2) thicknesses; (3) dielectric constants of the substrates; and (4) feed position, etc. In the rest of this section, we will discuss two stacked patch configuration designs: one of these involves a pair of rectangular patches with a probe feed, and the other is a rectangular patch coupled to folded-slot (slot-patch configuration). Bandwidths of up to 21% and 22% are observed from the simulated results. Measured results are also shown for the folded-slot design.

3.2.2 Probe-Fed Dual Patches

The geometry of the probe-fed dual patches is shown in Figure 3.11. The two patches use a high-low dielectric constant material combination, and this is done to facilitate the integration of the antenna with applicable photonic and microwave devices [110]. The driven patch has a size of 0.96 cm × 0.88 cm with a probe feed located below the middle point of its width edge, and a substrate of $\epsilon_{r1} = 10.4$ and $\tan\delta_1 = 0.001$. The parasitic patch is 2.16 cm × 1.98 cm in size, with a substrate of $\epsilon_{r2} = 1.07$, $\tan\delta_2 = 0.001$, and thickness $d_2 = 0.45$ cm. The two patches along with substrates are enclosed within a 4.32 cm × 3.96 cm cavity. The driven and parasitic patches are separately designed to resonate at 4.2 GHz and 4.3 GHz, respectively.

To achieve optimal bandwidth for this dual patch antenna, we proceed to find the optimal thickness of the bottom substrate layer d_1. That is, d_1 is the design variable. We also need an objective function for the optimization problem. To construct our objective function, we note that bandwidth is related to the ratio of the maximum and minimum input resistances $R_{\max}$ and $R_{\min}$. Also we note that the input impedance needs to vary smoothly around resonance. Therefore, the objective function can be defined as minimizing the ratio of $R_{\max}$ to $R_{\min}$. For this problem, we define $R_{\max}$ to be the maximum of the input resistance at 4.0, 4.1, ..., 4.8 GHz, and $R_{\min}$ the minimum. The optimization model can now be set to read:

$$\begin{aligned} &\text{minimize} && R_{\max}/R_{\min} \\ &\text{subject to:} && 0.1 \text{ cm} \leq d_2 \leq 0.18 \text{ cm} \end{aligned} \tag{3.16}$$

This is a one-variable optimization problem with simple inequality constraints. As in the previous chapter, an SQP optimizer combined with the FE-BI simulator is utilized to generate the optimal design. After 10 iterations involving 20 FEM calls

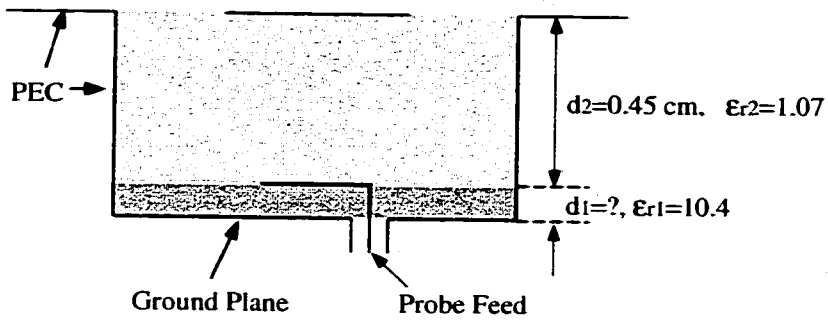

Figure 3.11: Geometry of the dual patch antenna.

and 160 frequency response computations, a value of $d_2 = 0.1295$ cm is obtained to deliver a 10 dB return loss bandwidth of 21%. The FEM discretization produces 6662 non-zero edge unknowns and the whole optimization run takes about 200 minutes on an HP 9000/785 workstation. Figure 3.12 gives the iteration history for this optimization problem, and Figure 3.13 shows the input impedance and return loss of the optimal patch configuration.

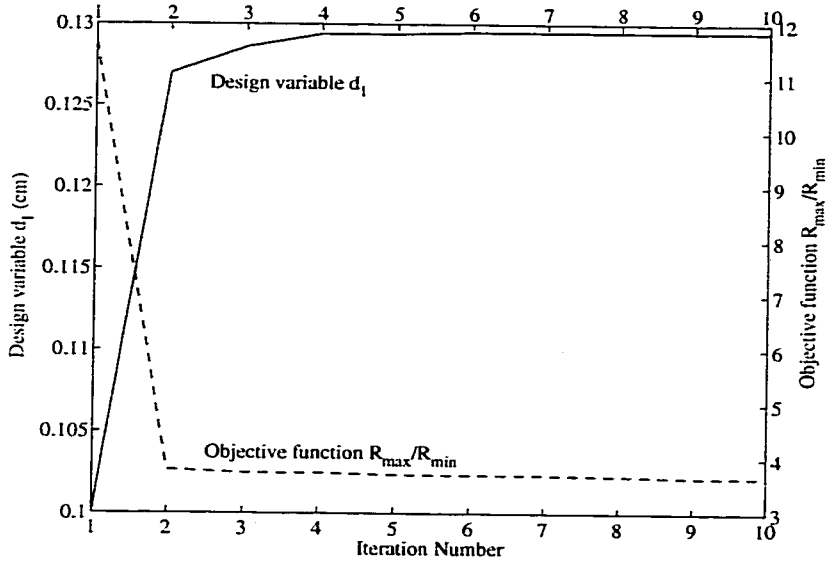

Figure 3.12: Iteration history for the optimization of the dual patch antenna.

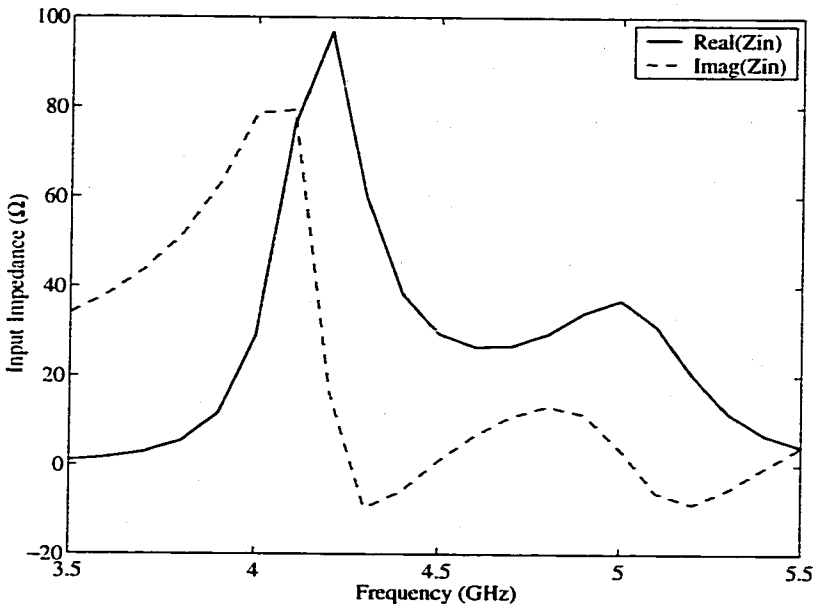

(a) Impedance

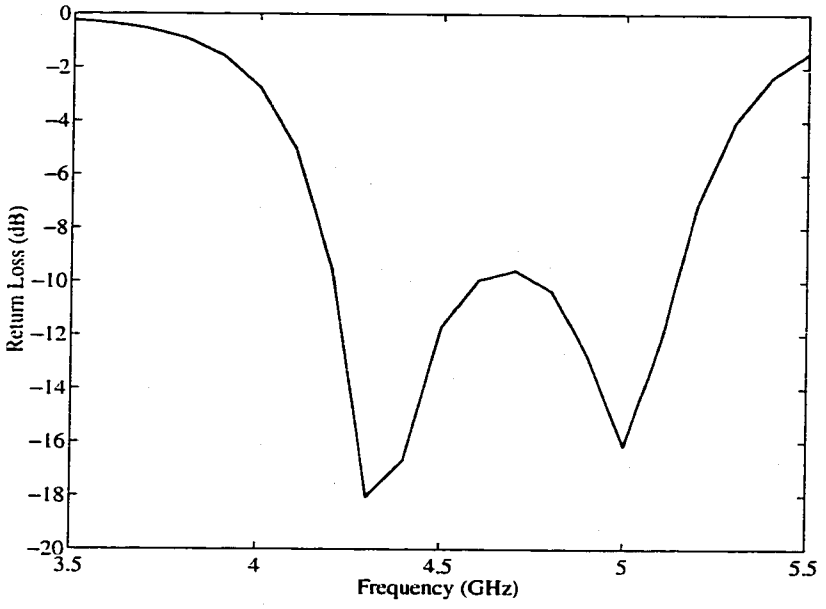

(b) Return loss

Figure 3.13: Performance of the optimal dual patch antenna.

3.2.3 Stacked Rectangular Patch and Folded-Slot

It was shown in the previous example that a pair of stacked rectangular patches can be used to increase bandwidth. Other resonators in different configurations and combinations, especially slots, have also been used for this purpose. For example, a U-shaped slot antenna stacked with a rectangular patch has shown substantial bandwidth improvement [22, 82]; and a crossed slot in the ground plane with stacked patches has also been proposed [94]. In this section, a novel configuration of a folded-slot below a rectangular patch is designed and a 22% bandwidth is achieved. A fast hybrid FE-BI code having $O(N\log N)$ CPU requirements [33] is used to compute the input impedance and integrate with an GA optimizer. Finally, measured data are presented to validate the design.

One reason for considering folded-slot feeds is because they provide greater bandwidth [104] than traditional coupled slot feeds. In addition, when compared with a simple slot, folded-slot has lower input impedance while retaining the same physical size. Here we propose the use of a rectangular patch stacked with a folded-slot to further increase the antenna bandwidth.

The proposed configuration is displayed in Figure 3.14 and the goal is to find the optimal values for the various slot and strip widths of the folded-slot feed to achieve a 10 dB return loss over the 134-175 MHz (VHF frequencies) bandwidth with reference to a 50 Ω input impedance. The actual antenna resides in a cavity of size 116 cm $\times$ 56 cm, and the folded-slot is separated from a patch by a foam substrate with $\epsilon_r = 1.07$ and thickness $h = 9$ cm. The rectangular patch on the top is fixed at length $L_a = 60.0$ cm and width $W_a = 24.0$ cm. There is an extra metal bar of length 64 cm and width 8 cm inside the folded-slot which serves to reduce the input impedance value [105].

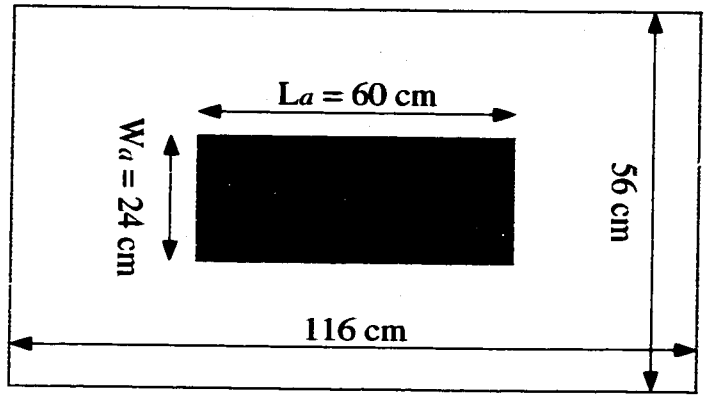

(a) Top layer

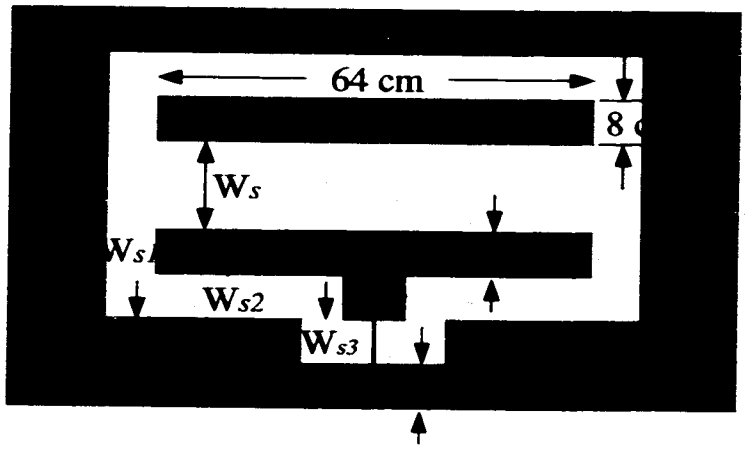

(b) Bottom layer

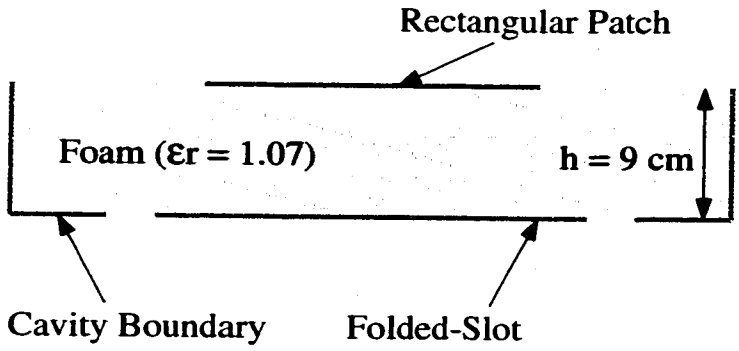

(c) Side view

Figure 3.14: Geometry of the stacked rectangular patch and folded-slot: top, bottom, and side view.

The geometrical complexity of the folded-slot allows us to choose among the slot widths W_s, W_{s1}, W_{s2} and W_{s3}, and/or the metal bar widths W_{b1}, W_{b2}, W_{b3} and W_{b4} (see Figure 3.14). For this optimization problem, we choose the following design variables: W_s, W_{s2}, W_{s3}, W_{b2} and W_{b4}. During the analysis process, the whole antenna volume is discretized using the finite elements (using prism elements for the volume and triangles for the surface integral) involving 44000 edge unknowns with 7000 surface unknowns at the top boundary integral aperture. For this system size the per frequency CPU time is about 45 - 60 minutes on a SUN Ultra-10 workstation. However, since the computation time per frequency is rather large, a continuous 5-variable gradient-based optimization is not realistic. To simplify the design process, the sizes of the design variables are not allowed to change continuously, but only discretely within the fixed discretization grid of $\Delta x = 4.0$ cm and $\Delta y = 2.0$ cm. A GA optimizer is used for this discrete variable optimization and the resulting FEM discretization of the optimal folded slot is plotted in Figure 3.15. The values of the design variables for the initial and optimal designs are shown in Table 3.2, and their performance is illustrated in Figure 3.16. The optimal design has an improved 10 dB bandwidth of 22.2% (from 136 MHz to 170 MHz), as compared to the 15.9% bandwidth of the initial design. Both the initial and optimal designs were fabricated and measured. Figure 3.17 shows the measured data of the optimal design. As seen, they are in excellent agreement with our simulations, thus verifying the analysis and design methods.

In the next section, the shape and topology of a single layer patch antenna are optimized to obtain broadband performance again, followed by a patch with dual-frequency performance.

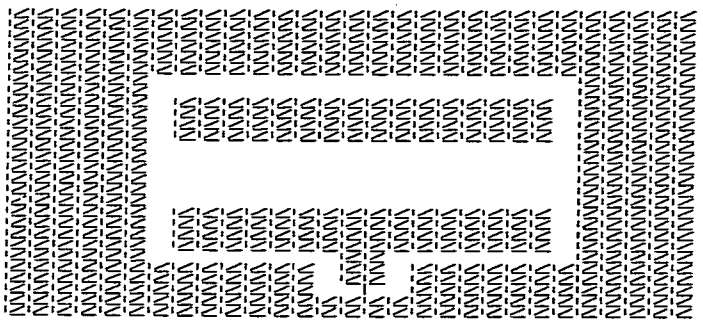

Figure 3.15: FEM discretization of the optimal folded-slot.

	W_s (cm)	W_{s2} (cm)	W_{s3} (cm)	W_{b2} (cm)	W_{b4} (cm)
Initial design	8.0	4.0	4.0	8.0	6.0
Optimal design	12.0	2.0	2.0	6.0	8.0

Table 3.2: Values of the four design variables of the initial and optimal folded-slot antennas.

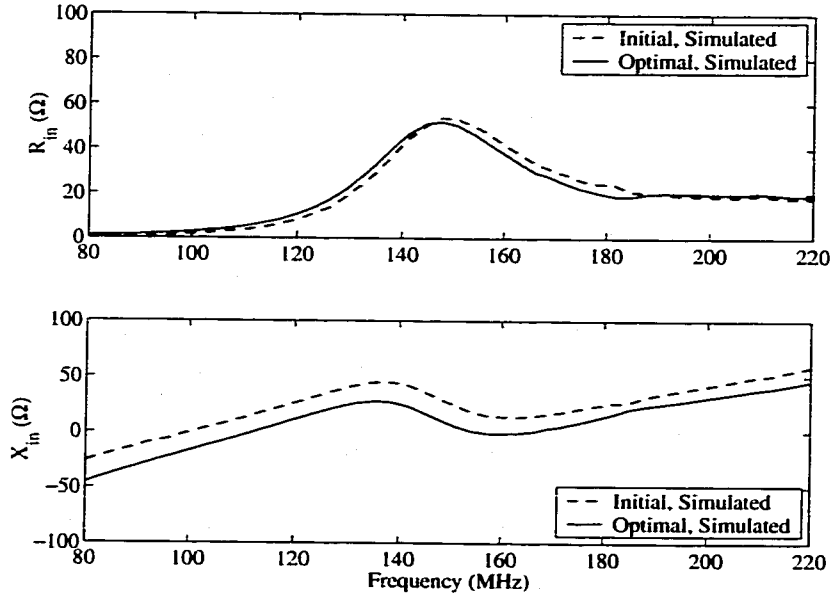

(a) Impedance

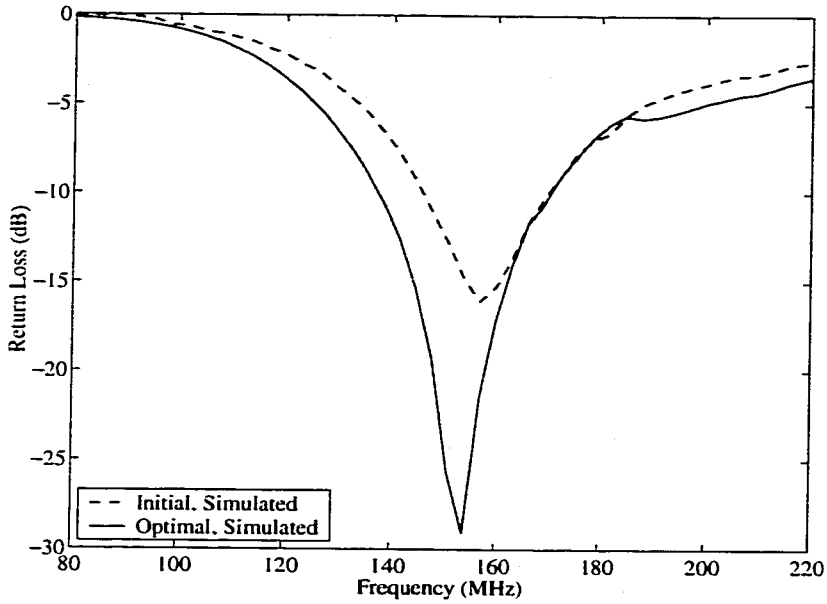

(b) Return loss

Figure 3.16: Input impedance and return loss of the initial and optimal folded-slot antennas.

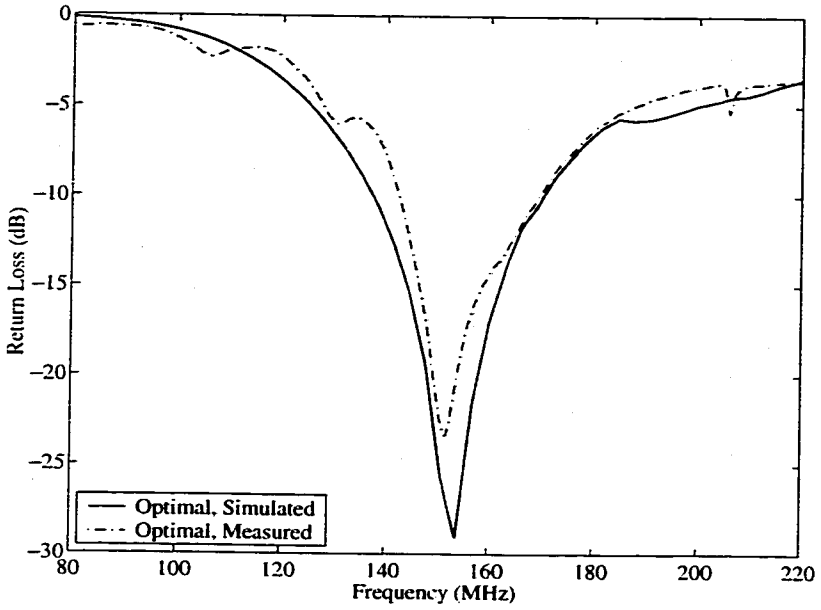

Figure 3.17: Measured and simulated return loss of the optimal folded-slot antenna.

3.3 Broadband and Dual-Frequency Antennas: Shape and Topology Design

3.3.1 Introduction

In Sections 3.1 and 3.2, we presented applications of the optimization techniques using a proportional design approach. The magnetic field strength, thickness of a substrate, and size of a slot were optimized to enhance various performance characteristics. When the design variables are not continuous, or there are a large number of design variables, gradient-based techniques may not be a good choice for solving an optimization problem. In this section, gradient-free optimization methods will be applied to obtain optimal patch configurations within a pre-specified design domain.

Problems with large number of design variables and fast objective function evaluations are suitable for global optimization methods. Global optimization techniques are largely independent of initial points and solution domain. Hence, global optima are more likely to be found, and they work extremely well for problems with discon-

tinuities and/or many local optima. However, these algorithms are generally slow with no guidance from local characteristics such as gradients, and a large amount of objective function evaluations is typically needed to achieve convergence.

Two popular global optimization methods are those based on genetic algorithm (GA) and simulated annealing (SA). The theory of GA and SA has been outlined in Chapter II. In this section, two irregular-shaped patch designs are created using both GA and SA, first a broadband patch, then a dual-resonance patch is designed for operation at GPS (global positioning system) frequencies. For each design an optimization model is established, results are then obtained based on the GA and SA optimizers.

3.3.2 Irregular-Shaped Broadband Patch

Generally, a single patch antenna has a bandwidth of only 2-4%. Our task is to find an irregular-shaped patch that could considerably improve the bandwidth (above 10%). The design space is shown in Figure 3.18, which is a 4.8 cm × 4.8 cm domain discretized into an 8 × 6 finite element grid. If the elements x_1, x_2, ..., x_{32} in Figure 3.18 are all filled with metal, a traditional square patch would be formed. The resulting antenna has a resonant frequency at around 1.86 GHz and a 10 dB bandwidth of only about 3%. To enhance the bandwidth by designing an irregular-shaped patch, the design variables x_i's are allowed to be either empty ($x_i = 0$) or filled ($x_i = 1$), where $i = 1, 2, \cdots, 32$. The two rows in the middle of the grid are set to be always filled with metal so that the feed point can be fixed and does not have to move around. The objective function for this optimization problem is given by

$$\min_{\mathbf{x}} \left(\max_{k=1,2,3} |S_{11}|_k \right). \tag{3.17}$$

Here $|S_{11}|_k$ refers to the return loss at three sample frequency points (1.85, 1.95 and 2.05 GHz in this case). $|S_{11}|$ is defined as

$$|S_{11}| = \frac{|Z_{in} - Z_0|}{|Z_{in} + Z_0|} \text{ (dB)} \tag{3.18}$$

where Z_{in} is the input impedance at the feed and $Z_0 = 50\ \Omega$. By minimizing the highest $|S_{11}|$ among the three, we could reduce the difference between the highest and lowest $|S_{11}|$'s, therefore achieving a larger bandwidth [56].

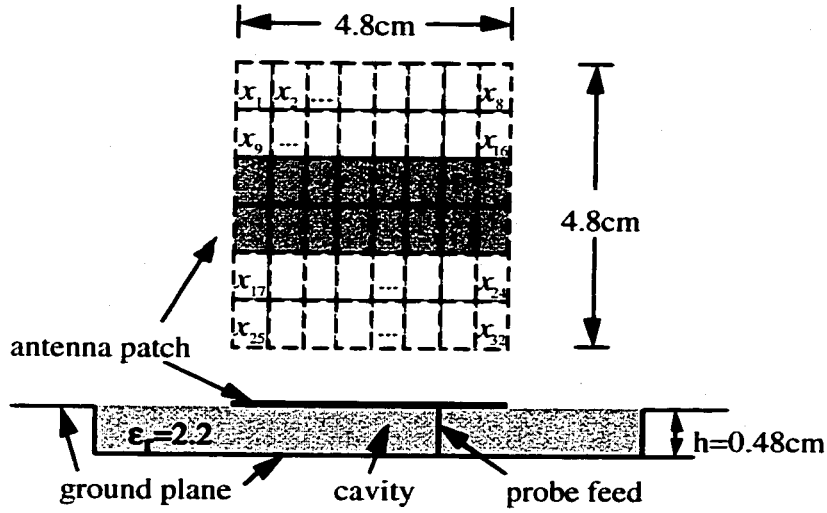

Figure 3.18: Top and side view of the broadband antenna design domain.

This problem has 32 design variables, each of which has a value of either 0 or 1. Gradient-based methods are not suitable for such discrete optimization problems. Hence global optimization algorithms, such as GA and SA, are more appropriate for this problem.

The GA code used for this task [17] is written in Fortran. The selection strategy in this GA algorithm involves a tournament selection (a widely used class of selection mechanisms that pick m members of the population at random and then select from them in a manner that depends on a fitness criterion), with a shuffling technique for

choosing random pairs for crossover. Uniform crossover with a crossover probability of 0.5 is chosen in conjunction with a mutation probability of 0.02.

For this problem, 200 generations are generated with a population size of 5 for each generation. Five initial designs are generated randomly. The impedance and $|S_{11}|$ of the antenna are computed using FE-BI method with brick elements. The number of edge unknowns is around 400, therefore each frequency response takes only less than 3 seconds to compute. The aperture configuration with the best fitness appears from the 190th generation and is plotted in Figure 3.19. The input impedance and return loss are illustrated in Figure 3.20. The 10 dB bandwidth is 10.3%, much better than the 3% bandwidth of the original square patch antenna. The best fitness and the average fitness for each iteration are both plotted in Figure 3.21.

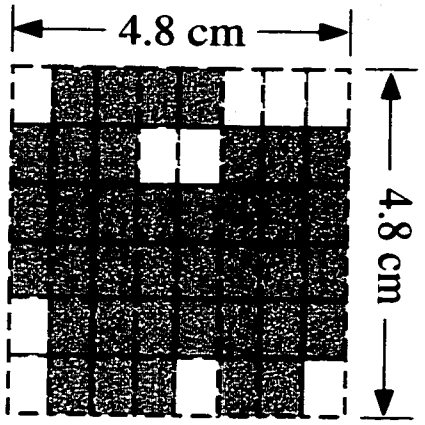

Figure 3.19: Optimal broadband patch configuration obtained by GA.

The same problem is run again with SA. In the SA algorithm, the cooling schedule starts with an initial temperature of 10 and the temperature is reduced with a factor of 0.9. 50 iterations are carried out at each temperature, hoping there is enough time spent to reach the 'equilibrium'. To compare SA with GA, it is desired to start the iteration process from the same initial design. Since our GA approach used 5 initial designs in the first generation while SA needs only one, we simply pick the one with

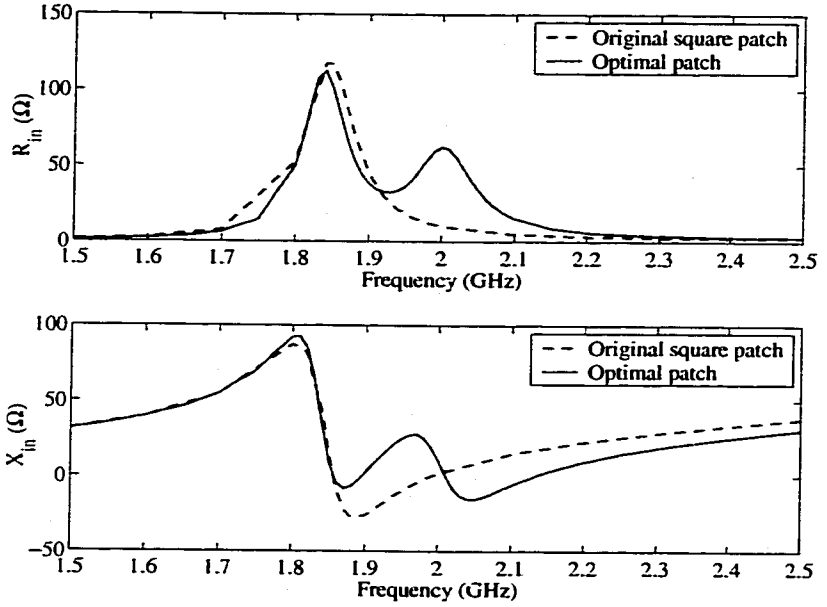

(a) Input Impedance

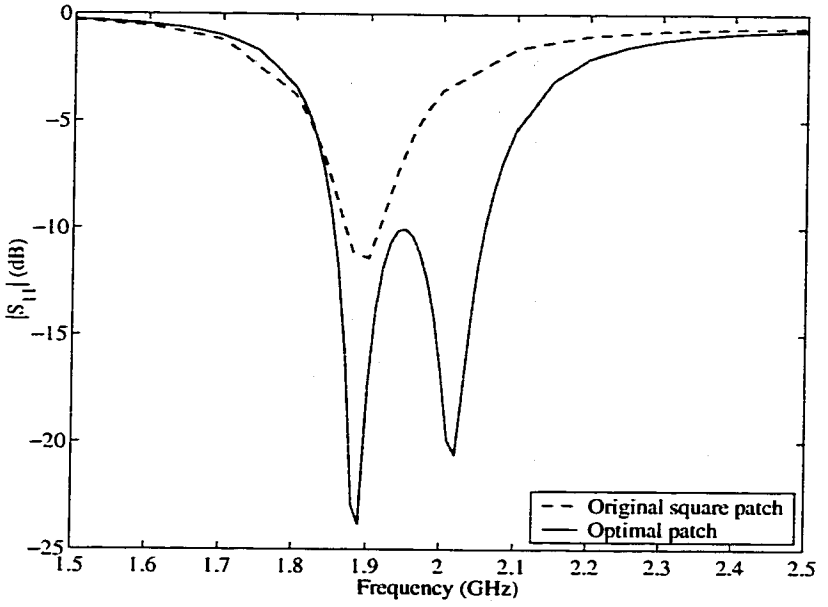

(b) Return Loss

Figure 3.20: Input impedance and impedance bandwidth of the original square patch and the optimal broadband patch obtained using GA.

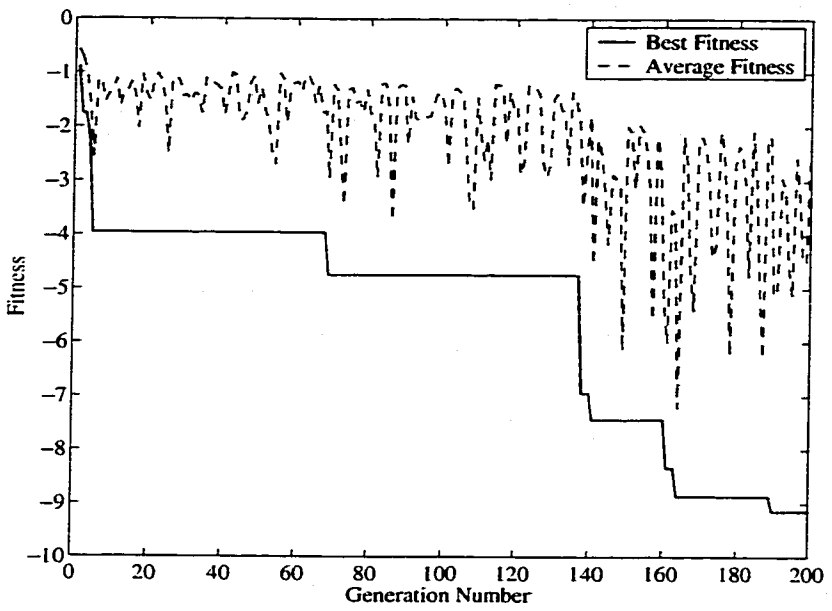

Figure 3.21: Iteration history of GA for the broadband design.

the best fitness from the 5 initial GA designs to start the SA. In each SA iteration, a new design is generated by randomly changing several bits from the previous design. When the temperature is high, more bits are flipped. As the temperature cools down, fewer and fewer bits are flipped to restrict the designs down to a more 'local' area. The probability of accepting new designs at the k-th SA iteration is

$$P_k = e^{-\frac{f_k - f_{k+1}}{T_k}} \tag{3.19}$$

where f_k and f_{k+1} are the values of objective function at the k-th and $(k+1)$-th iterations, respectively, and T_k is the temperature at the kth iteration.

The resulting optimal antenna configuration is shown in Figure 3.22. The input impedance and impedance bandwidth of both the original square patch and the optimal patch are plotted in Figure 3.23. The 10 dB bandwidth with this design is 10.8%, which is slightly better than the one obtained by GA.

The results based on GA and SA for this problem are summarized in Table 3.3. It is shown that for this specific problem, SA gives slightly better bandwidth but GA

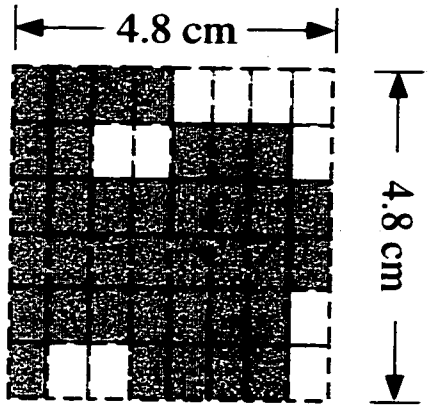

Figure 3.22: Optimal broadband patch configuration obtained by SA.

requires fewer iterations (i.e. it is faster).

	# of FEM Calls	Best Found Value of Obj. Function	Bandwidth
GA	950	-9.14	10.3%
SA	1500	-10.01	10.8%

Table 3.3: Summary of GA and SA runs for the broadband design.

We would also remark that the two broadband patches obtained by GA and SA are asymmetric. However, there is symmetry in the radiation patterns of these patches (e.g., see Figure 3.25 for the pattern of the SA-derived patch at resonant frequency $f = 1.82$ GHz and $\phi = 90°$). Nevertheless, symmetry could have been enforced.

3.3.3 Irregular-Shaped Dual-Frequency Patch

An alternative way to overcome the bandwidth limitations of patch antennas is to operate the antenna at two separate sub-bands. One of several ways to achieve such kind of dual frequency behavior is to use two stacked patches resonating at two close frequencies while operated separately [70, 109]. However, stacked patches make the

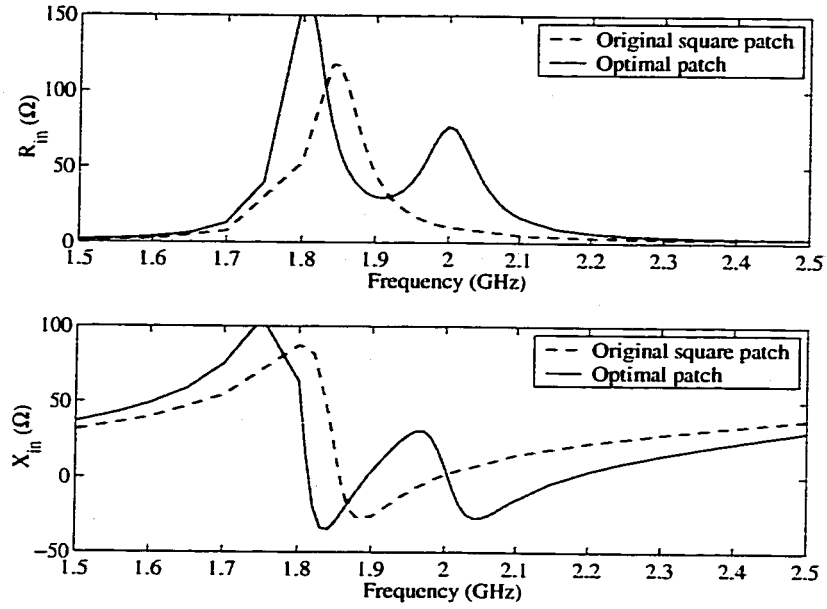

(a) Input Impedance

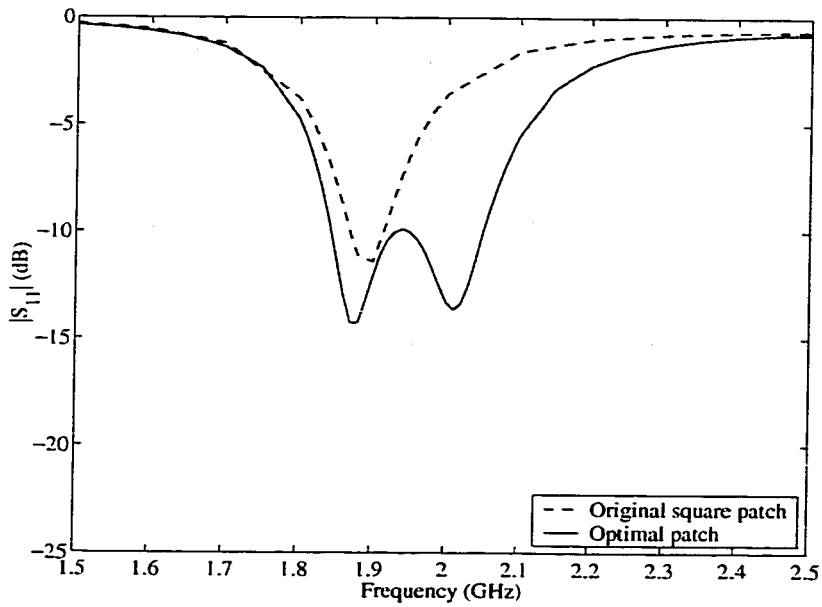

(b) Return Loss

Figure 3.23: Input impedance and impedance bandwidth of the original square patch and the optimal broadband patch obtained using SA.

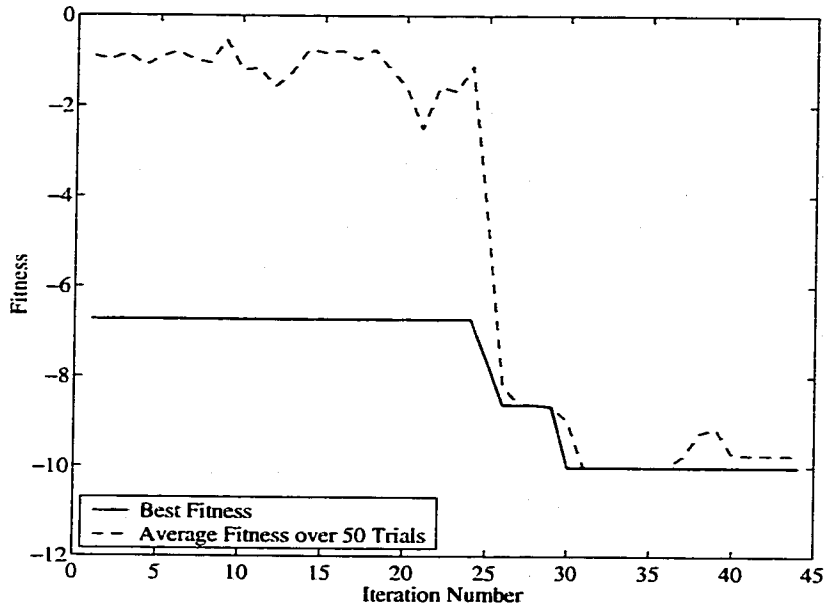

Figure 3.24: Iteration history of SA for the broadband design.

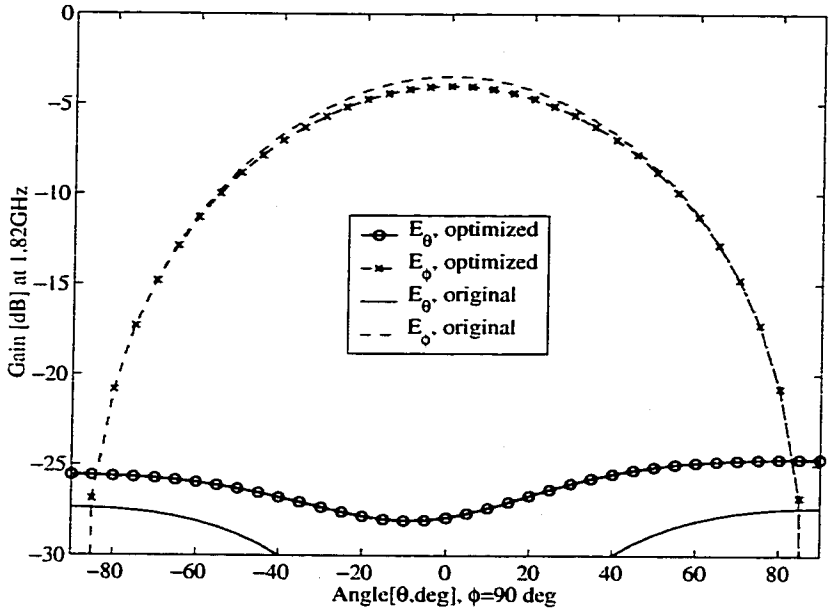

Figure 3.25: Radiation pattern of the original patch and the optimal patch obtained through SA, at $f = 1.82$ GHz.

antenna thicker and occupy more space. It is of course desirable to design a single layer patch operating over multiple frequencies. As an example, here we will design a patch operating at the two GPS frequencies: 1227 MHz and 1572 MHz. Symmetric patch configuration will be adapted. As shown in Figure 3.26, the design domain is a rectangular 6 × 6 grid of 5.36 cm × 7.02 cm, residing on top of a cavity 10.72 cm × 14.04 cm above a substrate of thickness 0.48 cm and a dielectric constant $\epsilon_r = 4.4$. Similar to the previous example, these elements are treated as design variables, which are allowed to be either filled ($x_i = 1$) or empty ($x_i = 0$). Here the 4 elements at the middle-right part of the domain are always filled with metal in order to fix the feed point. Also due to the symmetry requirement, only the upper half of the domain needs to be considered. Therefore, we have 16 design variables $x_1, x_2, ..., x_{16}$. The objective function of this problem is chosen to be:

$$\min_{\mathbf{x}} \left(|S_{11}|_1 + 0.1 * |S_{11}|_2 + |S_{11}|_3\right) \tag{3.20}$$

where $|S_{11}|_k$, for $k = 1, 2, 3$, refers to the return loss at three sample frequency points (1227, 1400 and 1573 MHz in this case). With such an objective function, more weight is placed on $|S_{11}|_1$ and $|S_{11}|_3$, and less weight is placed on $|S_{11}|_2$, therefore pushing the design to be dual-resonance. We remark that this objective function can be combined with other criteria based on polarization and pattern requirements. However, at this point our focus is restricted to the optimization of the return loss.

The GA and SA optimizers used for this task are the same as in the previous broadband design. For this design problem, both methods generate the same optimal configuration shown in Figure 3.27, whereas the corresponding impedance and return loss are shown in Figure 3.28. The radiation pattern, as depicted in Figure 3.29, is similar to a regular-shaped single patch antenna. As per design, the resonant

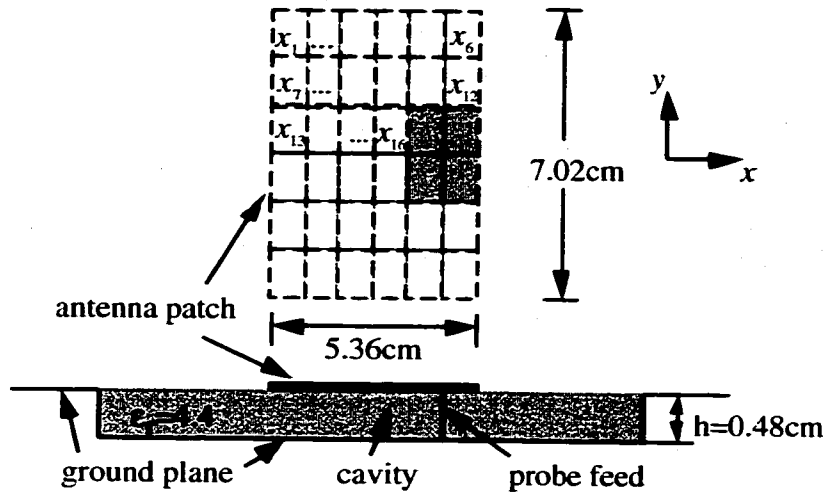

Figure 3.26: Top and side view of the dual frequency design domain.

frequencies of the optimized patch occur at both 1225 MHz and 1571 MHz. However, the iteration histories for the GA and SA runs are quite different. Although GA and SA obtained the same optimal design, Figure 3.30 shows that the GA algorithm finished at the 460th iteration (i.e., at the 92nd generation), whereas the SA took 850 iterations to reach the same design. That is, the GA algorithm converged in nearly half the number of iterations (and CPU time) as compared to the SA algorithm. Again, SA is slower for this problem. This might be due to the selection of the SA parameters such as step size, temperature decreasing rate, and the number of iterations at each temperature. If a different set of SA parameters are chosen to run this problem, the convergence speed could very well change. This is the disadvantage of SA, i.e. heavy reliance on parameters for the cooling schedule.

We close this section by noting that the proposed design was based on an objective function which only dealt with frequency tuning, but a feed must also be designed for CP radiation. The latter was not discussed since it was not included as part of the design objectives, but can be included either as a concurrent or a second step optimization.

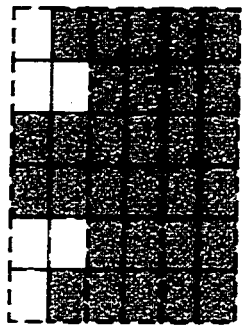

Figure 3.27: Optimal design of the patch for dual frequency operation.

3.4 Conclusions

In this chapter, we examined several methods and applications for antenna design. Among them we considered:

- Two ferrite antenna optimization problems, one on resonant frequency tuning, the other on beam steering. The SQP method was used for these designs. Both problems used the magnetic field strength as the design variable.

- Two size optimization problems involving stacked patches were proposed and solved for improved broadband performance. The substrate thickness of the probe-fed stacked rectangular patches was optimized using SQP to obtained a 21% bandwidth. For the rectangular patch stacked with folded-slot, several slot widths were optimized using GA to achieve a 22% bandwidth.

- Two irregular-shaped designs on broadband and dual-frequency patch antennas were defined and optimized using both GA and SA algorithms. For the broadband design, GA and SA yielded different designs yet both of which have a bandwidth near 10% (i.e. both satisfied the design objective). For the dual-frequency design, the GA and SA generated the same optimal design, but in general we found that GA needs fewer function evaluations.

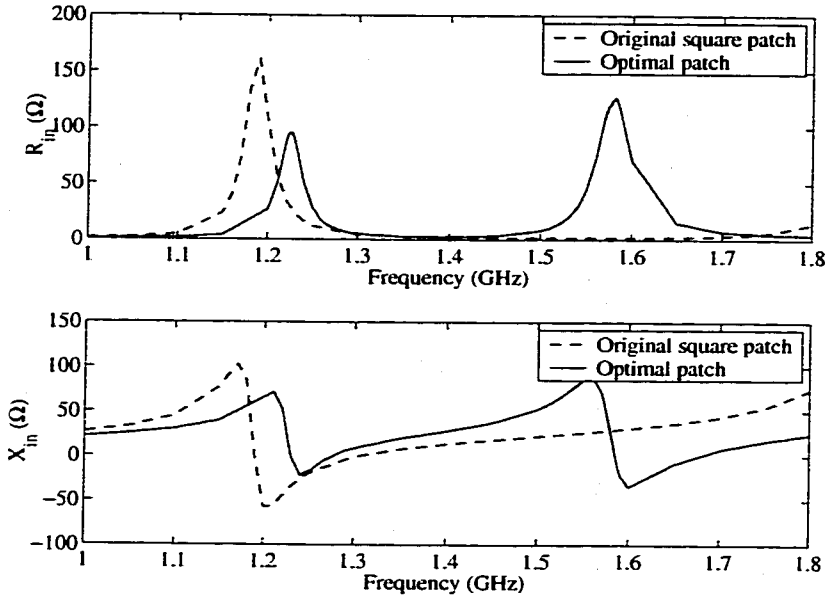

(a) Input Impedance

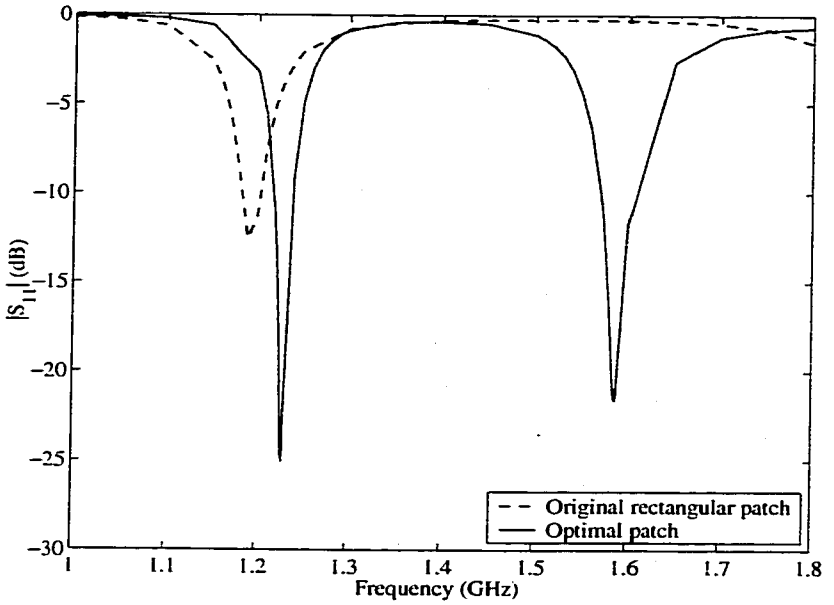

(b) Return Loss

Figure 3.28: Input impedance and impedance bandwidth of the original and optimal dual-frequency patches.

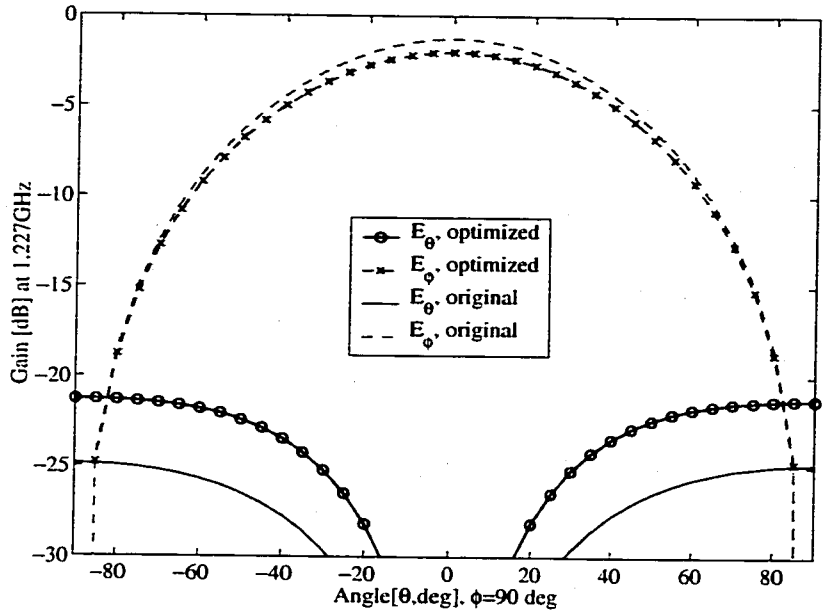

Figure 3.29: Radiation pattern of the original and optimal dual-frequency patches.

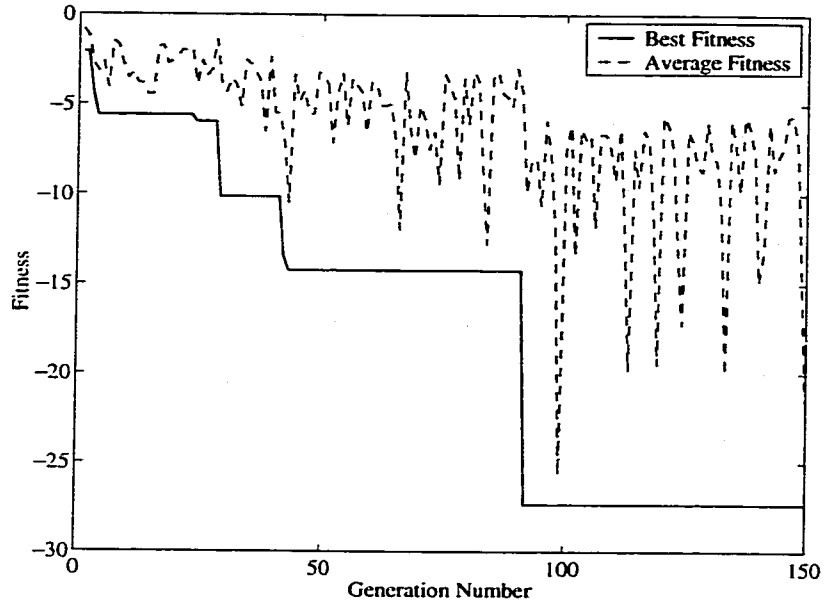

(a) GA

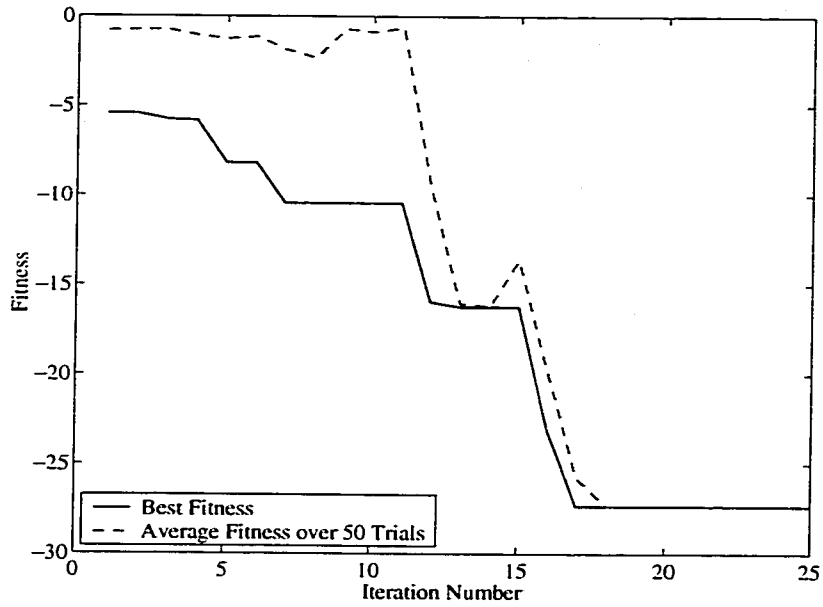

(b) SA

Figure 3.30: Iteration history of GA and SA for the dual-frequency patch design.

CHAPTER IV

FREQUENCY SELECTIVE SURFACE (FSS) ELEMENT DESIGN AND ANTENNA APPLICATIONS

4.1 Introduction

Frequency selective surfaces (FSSs) have widespread applications over much of the electromagnetic spectrum. FSSs comprise of infinite periodic arrays of patches or apertures in a conducting screen and could be either free-standing or supported by dielectric substrates, as shown in Figure 4.1. They exhibit total reflection (for patches) or transmission (for apertures) in the neighborhood of the element resonance. Typically, FSS structures are comprised of several layers of periodic elements, and are usually stacked to provide a desired frequency response. Some typical FSS element shapes are shown in Figure 4.2. FSS analysis [7, 34, 77, 85] requires rigorous techniques and to reduce CPU requirements, Floquet theory assumptions are invoked to confine the infinite computational domain within a single unit cell, also illustrated in Figure 4.1. Within the FE-model of a unit cell, the periodic boundary condition is enforced on the vertical walls of the mesh. On the boundary edges of the BI-surface, an appropriate periodic Green's function must also be used. For non-commensurate structures, special cascading methods [77] or periodic boundary conditions must be

applied, further complicating the analysis.

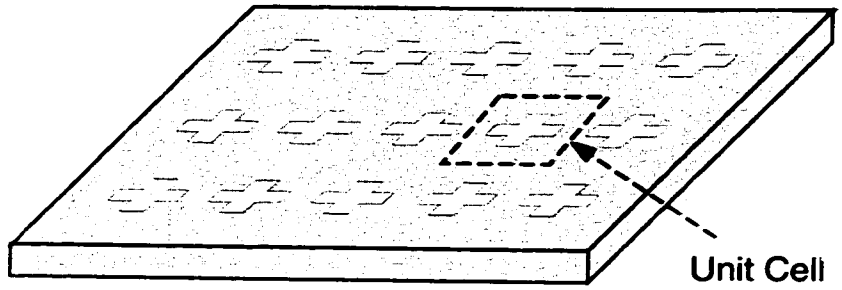

Figure 4.1: Geometry of a frequency selective surface.

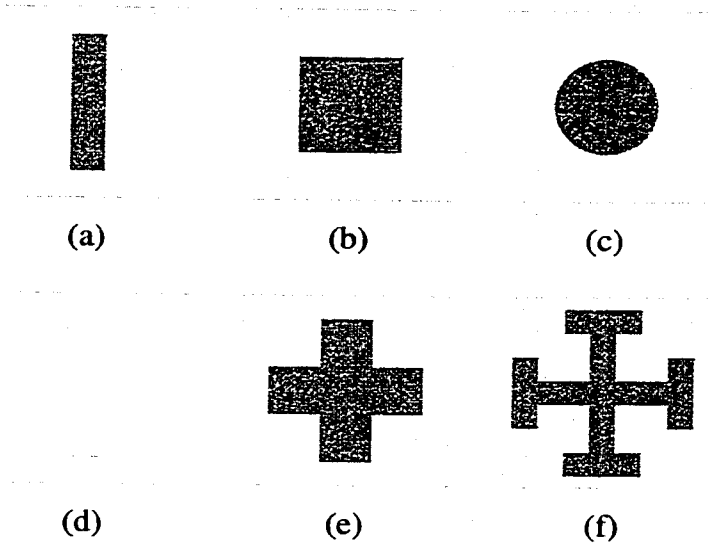

Figure 4.2: Typical FSS elements: (a) dipole; (b) square patch; (c) circular patch; (d) slot (e) cross dipole (f) erusalem cross.

Not surprisingly, the design of multilayer FSS structures is still a trial and error process due to the associated excessive CPU requirements. Automated re-gridding of the computational domain is an additional difficulty. Almost all previous design techniques on FSS structures have been heuristic or empirical. Most of the designs involve single layer or cascading pre-selected periodic elements that are known to resonate at roughly the desired frequencies, then sizes of the elements and thicknesses of the substrate layers are adjusted to tune the frequency response [28, 75, 111]. Such

techniques cannot be used as an effective synthesis method for simultaneous shape and topology design of the periodic elements.

Recently, a fast spectral domain algorithm (FSDA) was incorporated within the framework of the FE-BI approach to model FSS and printed arrays on multilayer (possibly inhomogeneous) substrates [32, 33]. This simulator also allows for automated re-gridding and modeling non-commensurate FSS layers. Use of FSDA within FE-BI results in considerable speed-ups of about two orders of magnitude and of $O(N)$ complexity.

In this chapter, we integrate this simulator with genetic algorithms (GA) to propose FSS designs subject to pre-specified performance objectives and constraints. Novel FSS elements and multilayered structures are introduced subject to given design criteria. Section 4.2 briefly introduces FSDA simulator and how it works with GA. Section 4.3 presents two free standing high-pass filters designs, one for single-layer and the other with two layers, both with a stop band below 3 GHz. Section 4.4 designs an irregular-shaped FSS element that possesses pre-specified flat phase response over a certain bandwidth. Such an FSS with nearly constant phase response is useful as a "substrate" of antenna arrays as a broadband magnetic ground plane (GP) much like the photonic bandgap (PBG) materials [99]. A printed dipole array is then placed on top of a flat-phase FSS to enhance the dipole radiation [25].

4.2 FSS Design Using GA and FSDA Combination

To synthesize an FSS element subject to a desired frequency response, one typically searches in the knowledge base through a trial-and-error process. Apart from being a tedious approach, this process does not easily lead to new and optimal designs. Therefore, optimization techniques are required to design practical FSSs that

deliver the desired filter-type response using minimal thickness. There are mainly two ways in optimizing the FSS. One is to simply optimize the dimensions and dielectric layers of a given element shape, and gradient-based techniques are best suited for this approach, although neural networks [28] have previously been employed to tune the sizes. A second approach is to cascade elementary building blocks of predefined element shapes and dielectric layers. For this approach, GA appears more attractive [75, 111].

GAs have been quite popular in many electromagnetic applications such as array synthesis, reflector antennas, microwave absorbers, etc. [55]. Recently, it has also been used with a method of moment (MoM) simulator for shape design of free standing metallic antennas [56]. However, designs conducted so far have yet to consider the integration of GAs with rigorous simulators that permit 3D designs where both shape and material is allowed to vary throughout the volume. The very few available FSS optimization processes have dealt with only size optimization [28] or fixed elements [75] without consideration of element shape, topology or material. Here we consider shape and topology optimization using GA combined with a rigorous simulator in the design loop.

FSDA was proposed for the rapid solution of planar surface integral equations in conjunction with iterative solvers. The algorithm is implemented in the BI portion of a hybrid FE-BI method, which has been described in Chapter II. Although FSDA may be applied to arbitrary integral equations with the convolutional property, it is especially advantageous for the analysis of infinite periodic arrays such as FSSs [33]. In this context, the FSDA starts with the conventional Floquet mode representation of the BI termination. However, instead of calculating the BI matrix element explicitly, at each iteration, the Fourier transforms of the basis functions, multiplied with

their actual expansion coefficients, are summed up. The spectral integral (Floquet mode series) is then computed only once for every testing function to evaluate the matrix-vector products in the iterative solver. Thus, for a fixed number of Floquet modes, the memory demand and CPU complexity are both $O(N)$. The detailed formulation of FSDA and its validation can be found in [33]. With this algorithm, multi-layer FSSs (with possibly non-commensurate periodicities) and any arbitrary printed configuration at the interface of each layer can be analyzed, including inhomogeneities within the substrate to possibly form PBG structures and defects as well as vertical posts and vias (see Figure 4.3). This capability is afforded as a result of the finite element method used for modeling the volume of the periodic cell [34].

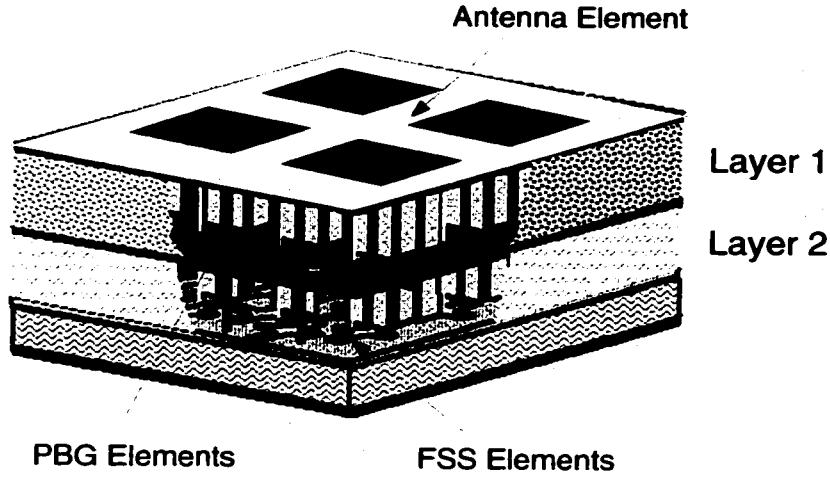

Figure 4.3: Antenna with multiple-layer PBG substrate and FSS elements.

Our goal in the next sections is to demonstrate examples where an integration of optimization algorithms with a rigorous full wave 3D electromagnetic solver can lead to practical designs in minutes of computation time using a desktop computer. We remark that the solver has been extensively validated and therefore the purpose of the work here is to demonstrate the convergence and practicality of the optimization process.

In the rest of this chapter, two different FSS designs are considered. In the first case, the FSS is designed to perform as a bandpass filter. In the second case, we design an FSS subject to a pre-specified phase of the reflection coefficient over a certain band, which is then placed under a dipole array to achieve larger bandwidth. The specific GA algorithm used here is the same as in Chapter III.

4.3 High-Pass Filter Design

4.3.1 Problem Definition

The goal in this example is to design an FSS having a stopband of < 3 GHz and no transmission above between 3 - 5 GHz. The desired frequency response is explicitly specified in a step function form instead of sharp changes at any frequency:

$$\text{magnitude}(\Gamma) = \begin{cases} 0.5 & \text{for } 0.5 - 1 \text{ GHz} \\ 1.0 & \text{for } 1 - 3 \text{ GHz} \\ 0.3 & \text{for } 3.5 - 4 \text{ GHz} \\ 0.1 & \text{for } 4.5 - 5 \text{ GHz} \end{cases} \tag{4.1}$$

where Γ denotes the field reflection coefficient at normal incidence.

In practice, the above response can be coded by satisfying Γ over a set of samples covering the band. The fitness function for this design can then be stated as follows:

$$\begin{aligned} \text{minimize} \qquad & f(\mathbf{x}) = \\ & (\textstyle\sum_{i=1}^{1} |\text{mag}(\Gamma_{f_i}) - 0.5|^2 + \sum_{i=2}^{6} |\text{mag}(\Gamma_{f_i}) - 1|^2 + \\ & \textstyle\sum_{i=7}^{8} |\text{mag}(\Gamma_{f_i}) - 0.3|^2 + \sum_{i=9}^{10} |\text{mag}(\Gamma_{f_i}) - 0.1|^2) \end{aligned} \tag{4.2}$$

where the values at $f_i, i = 1, ..., 10$ are set to 0.5, 1.0, 1.5, ..., 5.0 GHz, respectively.

with a step size of 0.5 GHz. Also $\mathbf{x} = \{x_1, x_2, ..., x_N\}$ represents the elements of the design domain.

To realize this design we may initially choose to work with a single layer FSS (free standing) whose design domain is shown in Figure 4.4. The domain is an 8.75 cm × 8.75 cm periodic cell whose lower left corner is discretized using 7 × 7 square elements. It will be further assumed that the other three quarters of the unit cell will be formed by using central or rotating symmetry. For the GA design, each of the 49 finite elements x_1, x_2, ..., x_{49} is treated as a design variable with a value of either 0 (empty) or 1 (filled metallic). A binary string of '$x_1x_2...x_{49}$' encoded using 0/1 values therefore corresponds to a certain FSS element shape/design. For example, the binary string '0000000 000000 0000001 00000001 0000001 0000001 0011111' produces a wedge shape in the lower left quarter of the unit cell, and with central symmetry it corresponds to a cross shape FSS over the whole unit cell (see Figure 4.5).

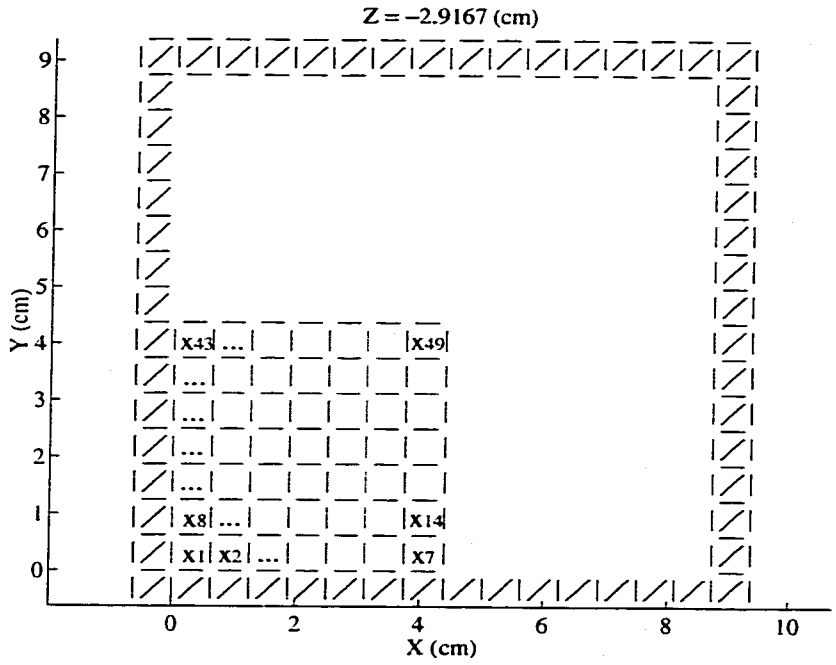

Figure 4.4: Design domain for the FSS layer: top view.

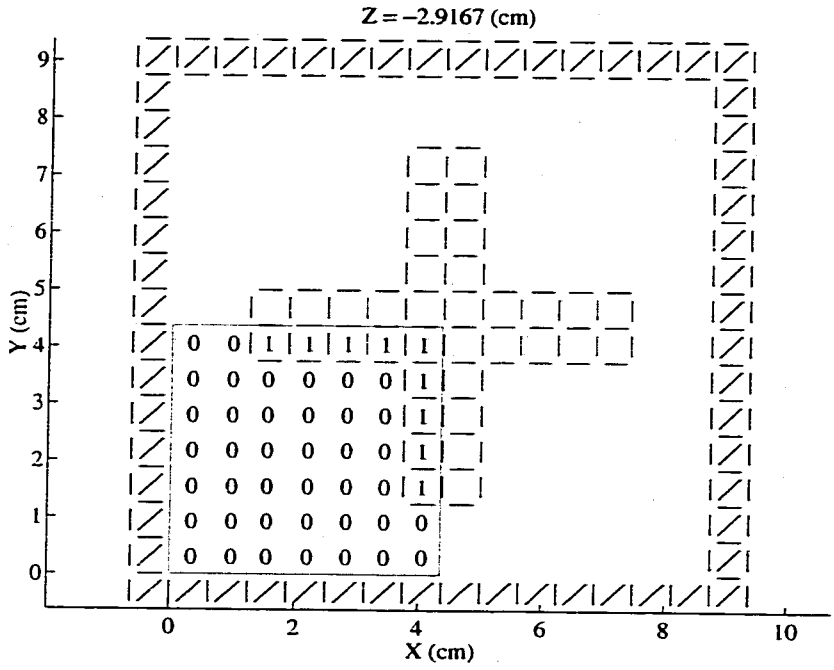

Figure 4.5: A crossed strip FSS.

4.3.2 GA Design

To begin the design, five initial element shapes were loaded to start the GA. The selection strategy in this GA algorithm involved again a tournament selection with a shuffling technique for choosing random pairs for crossover. Uniform crossover with a crossover probability of 0.5 was used in conjunction with a mutation probability of 0.02.

The cross section of the single layer FSS is depicted in Figure 4.6, and the optimized FSS layer shape is shown in Figure 4.7. The corresponding filter response is given in Figure 4.8 overlaid with the pre-specified response defined in Equation (4.1). This design was obtained in less than 50 iterations, and each iteration took about 10 minutes on a desktop SUN Ultra-30 workstation. We also remark that the solution domain involved 2644 unknowns in the finite element volume domain and 800 unknowns for the boundary integral domain which comprised the top and

bottom surfaces of the unit cell. Clearly, more design variables could be considered within the volume by allowing material variations in addition to the variations on the FSS layer.

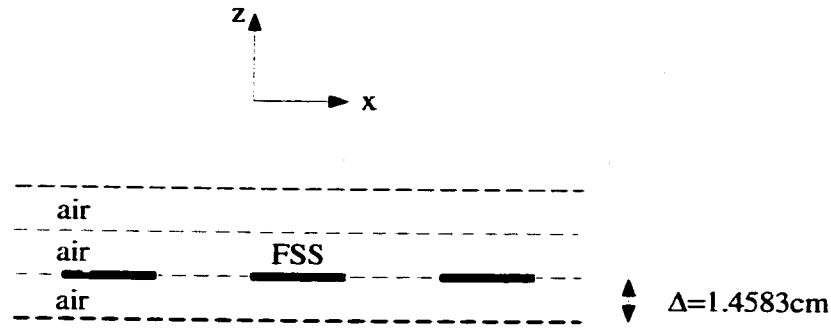

Figure 4.6: Geometry of 1-layer FSS structure: side view.

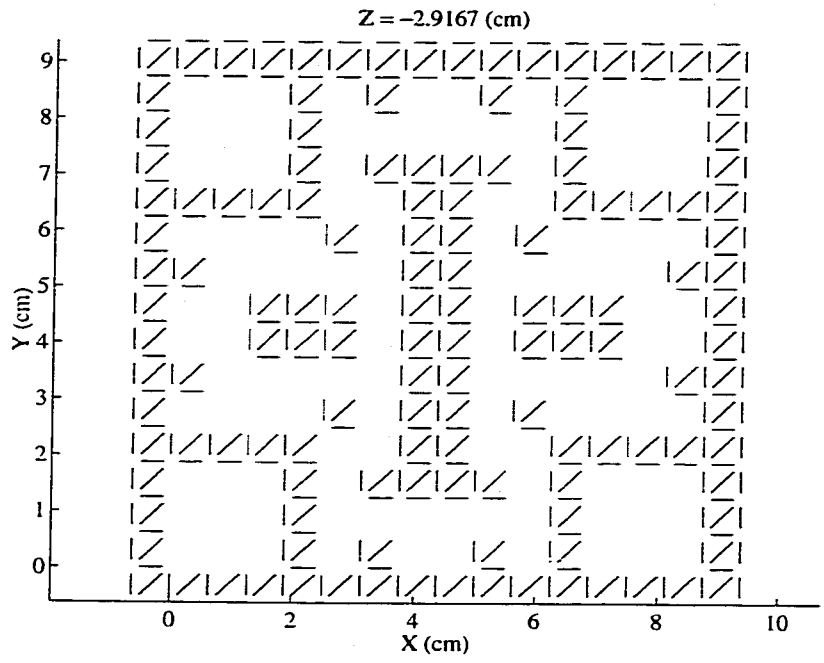

Figure 4.7: Optimized FSS element shape for the 1-layer filter design.

Although the design obtained is close to the specified response, further improvements can be achieved by adding more layers to the design. As an example, Figure 4.9 depicts a 2-layer FSS structure. In the context of the 2-layer FSS structure, our de-

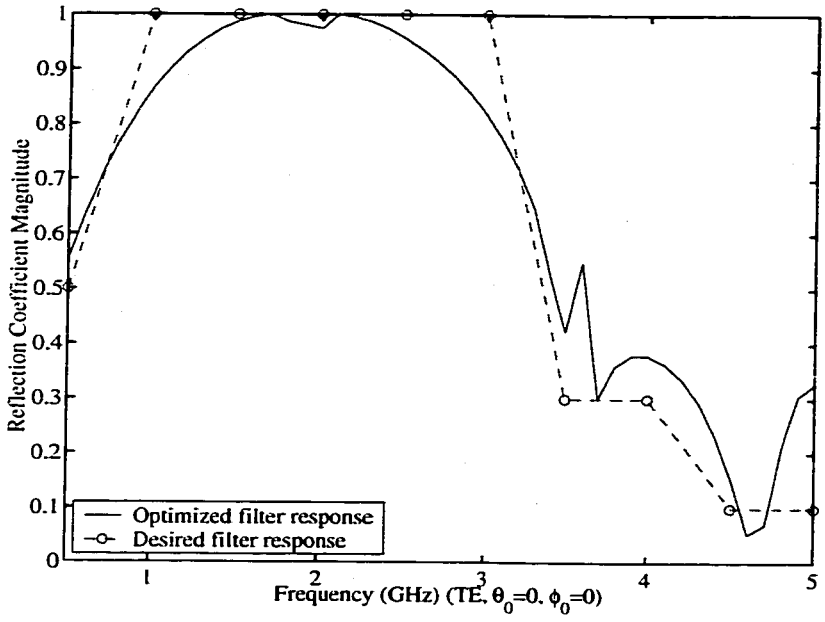

Figure 4.8: Actual and desired frequency response of the 1-layer filter.

sign approach is to select each layer to cover a different band of frequencies. The optimized shapes for the 2-layer FSS elements are depicted in Figure 4.10. The corresponding response is given in Figure 4.11 and is seen that this filter matches the pre-specified response. For this design, the solution domain involved 4806 unknowns in the finite element volume domain, and 800 unknowns for the boundary integral domain. Again less than 50 iterations were needed to arrive at the design.

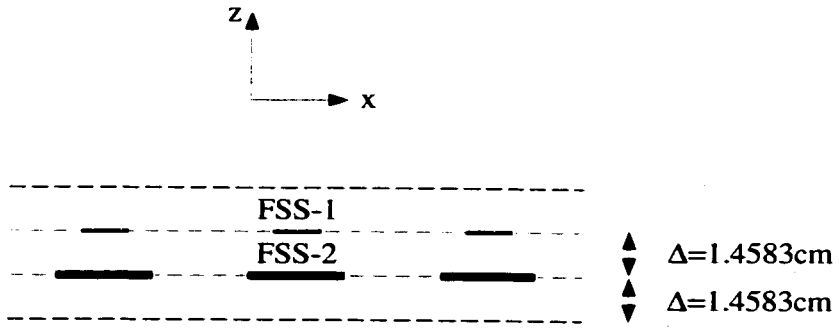

Figure 4.9: Side view of a 2-layer FSS structure.

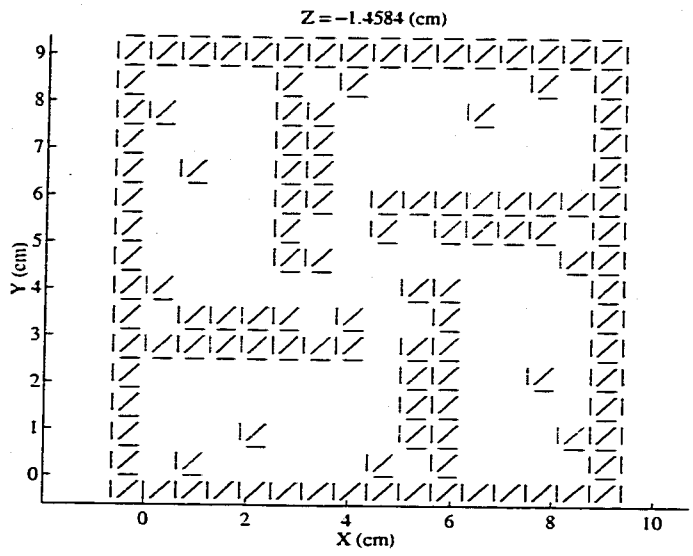

(a) Layer 1

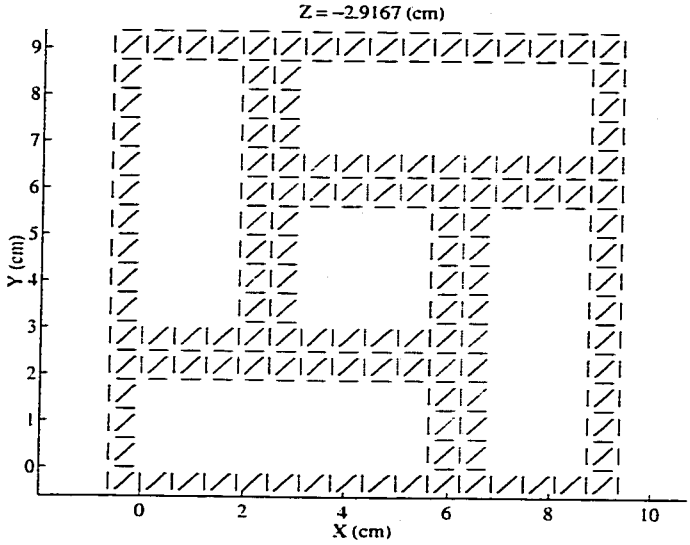

(b) Layer 2

Figure 4.10: Optimized element shape for the 2-layer filter design.

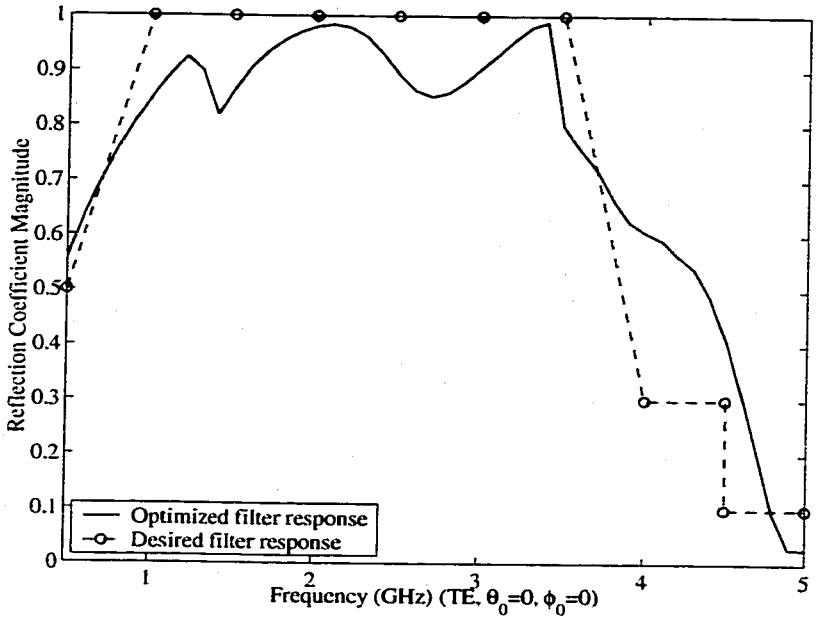

Figure 4.11: Actual and desired frequency response of the 2-layer filter.

4.4 FSS Design with Pre-specified Phase Response

For this example, the goal is to design an FSS that achieves a phase response that is within $+/-50°$ over a given band. Such designs can be used as "substrates" to printed antennas and may serve to emulate a magnetic ground plane. Paralleling circuit theory, to achieve phase control, we choose to compromise the magnitude of the FSS reflection coefficient, i.e. to prescribe an FSS having $|\Gamma| < 1$. Specifically, the design problem could be specified as follows:

$$\begin{aligned} \text{maximize} \quad & \text{Bandwidth} \\ \text{subject to} \quad & 0.4 \leq \text{magnitude}(\Gamma) \leq 1 \\ & -50° \leq \text{phase}(\Gamma) \leq 50° \\ \text{for} \quad & 0.8 \text{ GHz} \leq \text{freq} \leq 3.5 \text{ GHz}. \end{aligned} \tag{4.3}$$

To realize the design, we again define an objective function based on discrete

values of the pre-specified response. Specifically, for the above model we define the objective function as:

$$\text{minimize } f(\mathbf{x}) = \sum_{i=1}^{10} |\text{magnitude}(\Gamma_{f_i}) - 1|^2 + \sum_{i=1}^{10} |\frac{\text{phase}(\Gamma_{f_i})}{180^\circ}|^2 \qquad (4.4)$$

where Γ_{f_i} is again the reflection coefficient at frequency f_i, and $\mathbf{x}$ contains the design variables, i.e., the element metallization and possibly material constituents within each element. However, as in the previous design, only the metallization of the layer will be considered in the design. Note also that this objective function combines the magnitude and phase requirements by equally weighting them in a single function. We further chose to sample the passband reflection coefficient at 10 frequency points 0.5, 1.0, 1.5, ..., 5.0 GHz.

A GA optimization scheme similar to that described in the previous section was employed using a 8.75 cm × 8.75 cm computational domain sampled at the same rate as in the previous example with the same number of FEM volume and surface edges. The optimized FSS element shape is shown in Figure 4.12, and the achieved magnitude and phase of the reflection coefficient are depicted in Figures 4.13. It is observed that the desired amplitude response has indeed been satisfied. The phase response is also satisfied from 1.6-3.2 GHz. However, some deviation is observed between 0.8-1.6 GHz. The reflection coefficient plot also shows the necessity of using resistive elements instead of metallic ones. If metallic elements (i.e., lossless) were used, the phase would have zig-zagged throughout the band, even though the magnitude criteria could have been satisfied. This is also depicted in Figure 4.13 where the same shape metallic FSS exhibits a phase response that oscillates several times over -180° to $+180^\circ$ range within the band. For this problem, the optimal design was obtained in less than 40 iterations, and each iteration took about 20

minutes to compute 50 frequency responses. We also remark that the solution domain involved 4704 edge unknowns in the finite element volume domain and 800 unknowns for the boundary integral domain.

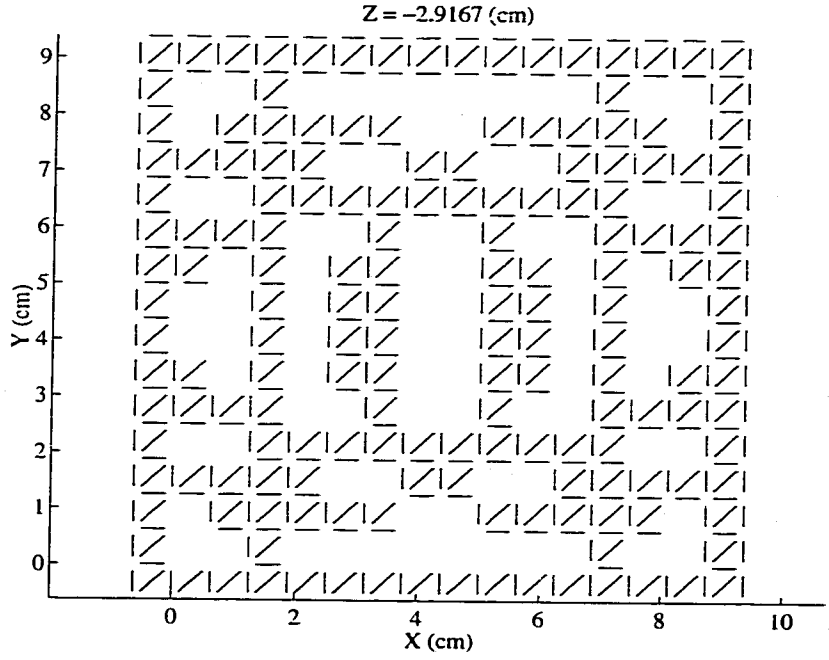

Figure 4.12: Optimized FSS element shape for the flat-phase GP design.

4.4.1 Antenna Bandwidth Improvement with Flat-Phase FSS

As noted earlier, a flat-phase FSS element is useful as a "substrate" of antenna arrays as a broadband magnetic ground plane. When placed under an antenna array, the flat-phase FSS is expected to enhance considerably the array bandwidth.

To demonstrate this, we designed a fan-shaped flat-phase FSS in order to make the element more compact than the one shown in Figure 4.12. The geometry and reflection response for this FSS are shown in Figure 4.14. The FSS is then placed under a dipole array whose size is half wavelength at 1.2 GHz. The mesh schemes of the dipole array and FSS are shown in Figure 4.15. A side view of the dipole over the fan-shaped FSS is illustrated in Figure 4.16, with a thickness of 2.34 cm for

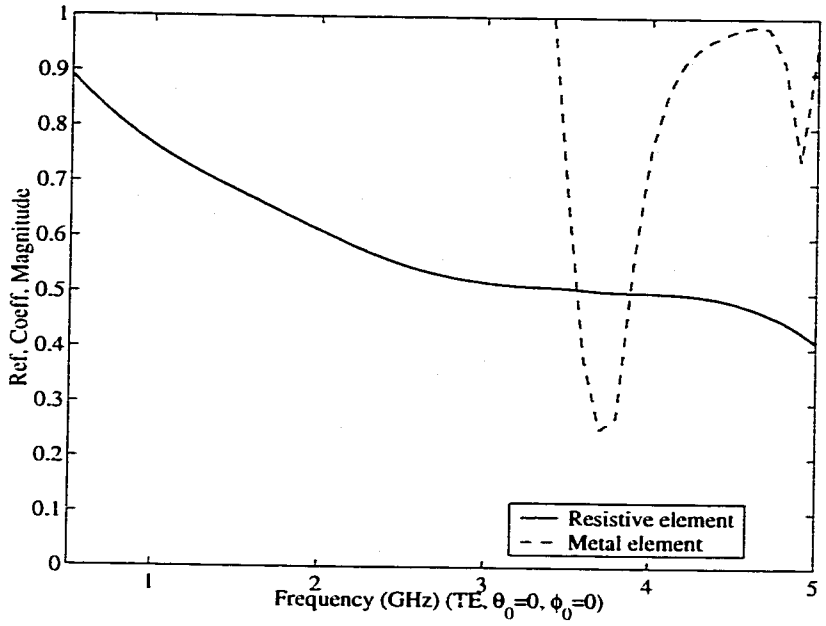

(a) Magnitude

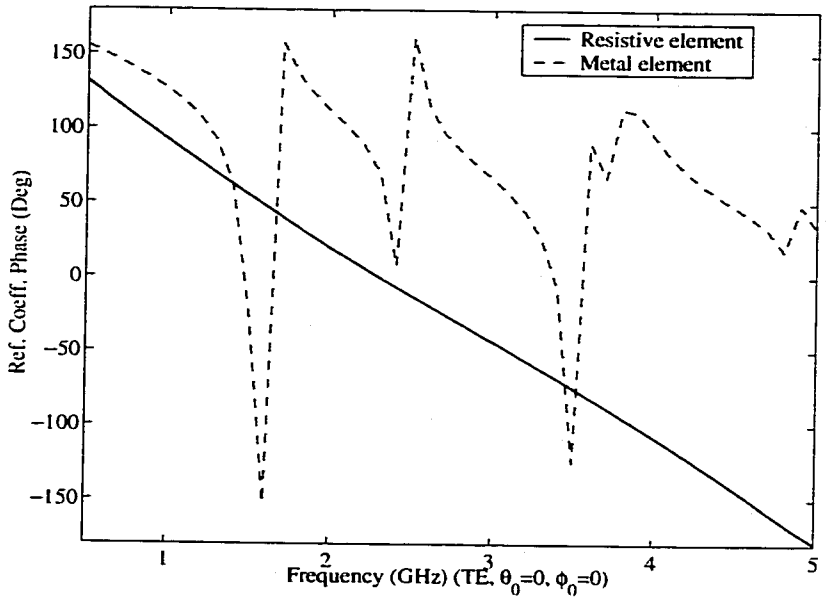

(b) Phase

Figure 4.13: Magnitude and phase of the reflection response for the optimized FSS element.

the substrate (foam with $\epsilon_r = 1.07$) between the dipole array and the FSS. From Figure 4.17 it is clearly seen that the dipole array has a much better bandwidth with the FSS below it than that without the FSS.

4.5 Conclusions

In this chapter, the concept and design of frequency selective surfaces were discussed, followed by the introduction of a fast $O(N)$ FSDA implemented within an FE-BI approach. Genetic algorithm was integrated with this simulator to allow full flexibility in geometry and layer structure decisions when designing FSSs. Example designs were demonstrated subject to pre-specified magnitude and phase criteria. Single-layer and multi-layer highpass filters were designed to meet desired frequency response. Then a flat-phase FSS element was designed subject to a phase response that is fairly constant over a given band. Such designs allow for special purpose FSS structures that can serve as "substrates" to printed antennas and have been shown to substantially enhance the bandwidth of these antennas.

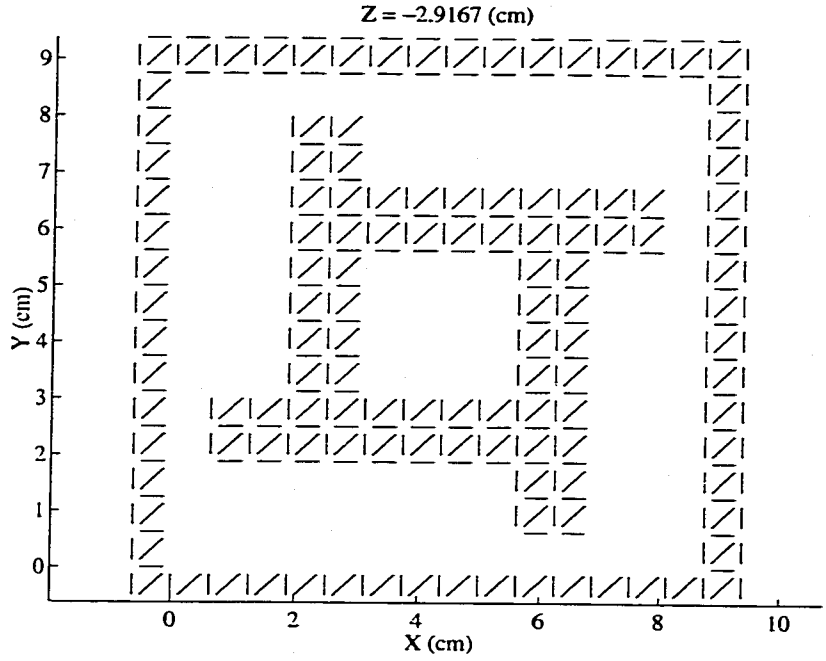

(a) Geometry

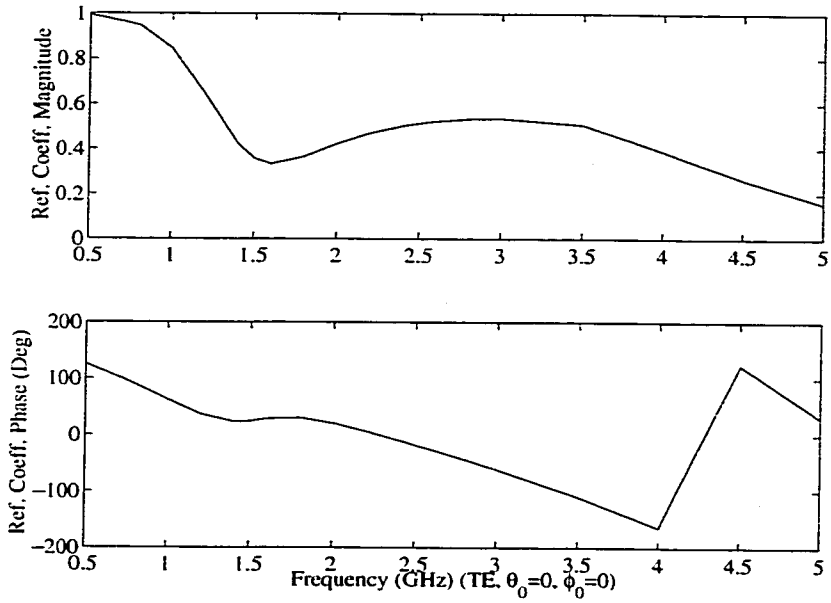

(b) Reflection Coefficient

Figure 4.14: Geometry and the reflection response for the fan-shaped flat-phase FSS element.

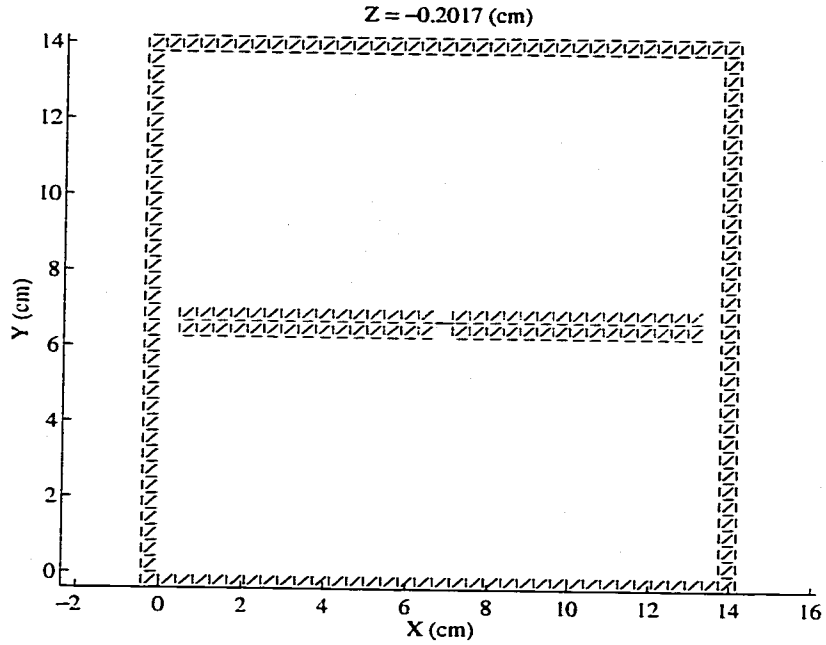

(a) Layer 1: Dipole Array

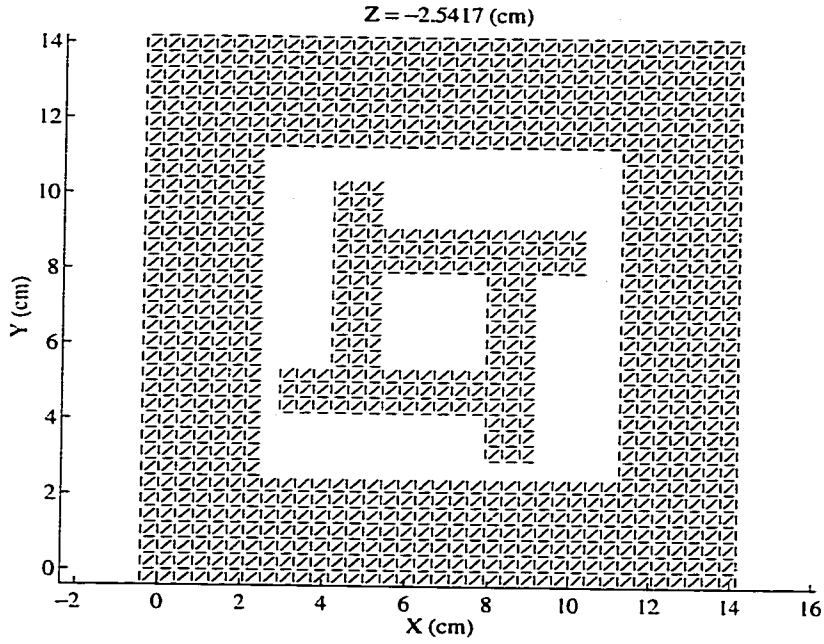

(b) Layer 2: Flat-Phase FSS

Figure 4.15: Mesh scheme for the dipole array over fan-shaped flat-phase FSS.

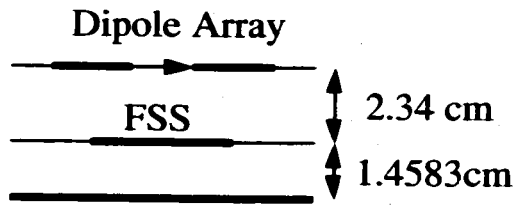

Figure 4.16: Dipole array over fan-shaped FSS: side view.

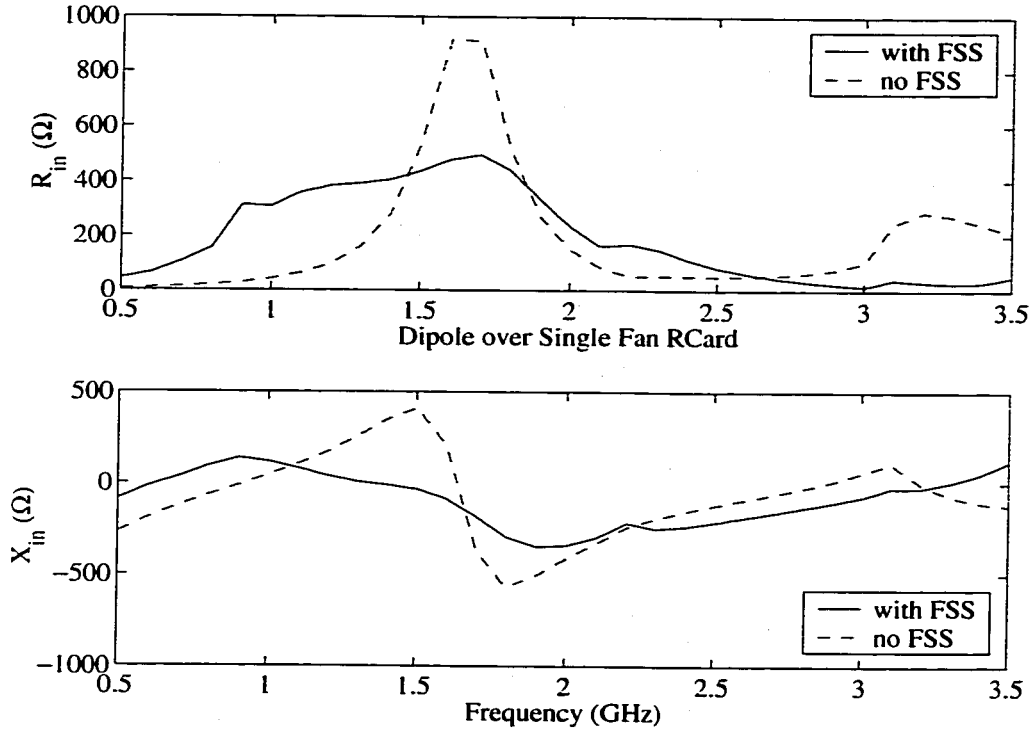

Figure 4.17: Broadband performance of the dipole array over fan-shaped FSS.

CHAPTER V

FREQUENCY SELECTIVE VOLUMES AND PHOTONIC BANDGAP STRUCTURES FOR ANTENNA APPLICATIONS

5.1 Introduction

Frequency selective volumes (FSVs) and photonic bandgap (PBG) structures have emerged as a new multidisciplinary field of study [54]. A PBG structure consists of composite materials where certain dielectric or metal sections are implanted (possibly periodically) within a background medium. In analogy to semiconductor crystals which may exhibit an electronic bandgap, in electromagnetics PBG structures are associated with a frequency band where propagation of EM waves is forbidden and may also be used to modify the reflective properties of multilayered structures. These features may be exploited in the design of EM devices. In the case of antennas, PBG substrate consists of printed elements on periodic, or more generally, on some perforated substrates which can be designed to enhance antenna properties such as bandwidth and pattern. Parameters which affect the behavior of PBGs include their periodicity, shape and spacing of the implants, and the dielectric contrast between the composite materials.

Two approaches for designing antenna substrates are proposed herein to enhance

patch antenna performance. One of the approaches involves lowering the effective dielectric constant of the substrate by introducing closely spaced small holes in the substrate within the immediate vicinity of the antenna [24, 36]. A disadvantage of this approach is that antenna dimensions may have to be enlarged for operating at a given frequency, even though efficiency may be increased. A second approach is to design a complete bandgap surrounding the patch antenna to suppress surface waves [23]. The disadvantage of this approach is that it requires considerable area around the patch antenna (on the order of at least three wavelengths [24]). Nevertheless, both approaches lead to increased antenna efficiency, gain and bandwidth as compared to antennas on uniform substrates. It is fair to state that shape (and even some topology) optimization has been extensively exploited for printed antenna design. However, designs utilizing full 3D topology and material optimization have yet to be considered.

In this chapter, both of the aforementioned approaches are considered. In Section 5.2, a patch antenna on a perforated substrate is designed using the effective dielectric constant approach. As part of our design, we develop optimal value for the size of circular air holes. In Section 5.3, we show for the first time how designs based on periodic material substrates can lead to significant increase in patch bandwidth.

5.2 Printed Antenna on Perforated Substrate

Microstrip antennas on high dielectric-constant substrates have smaller antenna size than those on low dielectric-constant substrates, but there is a sacrifice of lower efficiency and narrower bandwidth. Several methods have been proposed to solve this problem, one of which (see Figure 5.1) is to use closely spaced holes underneath and around the microstrip antenna, thus lowering the effective dielectric constant. In [36],

several patch antennas have been fabricated based on micromachining techniques and bandwidth improvement for these antennas has been observed.

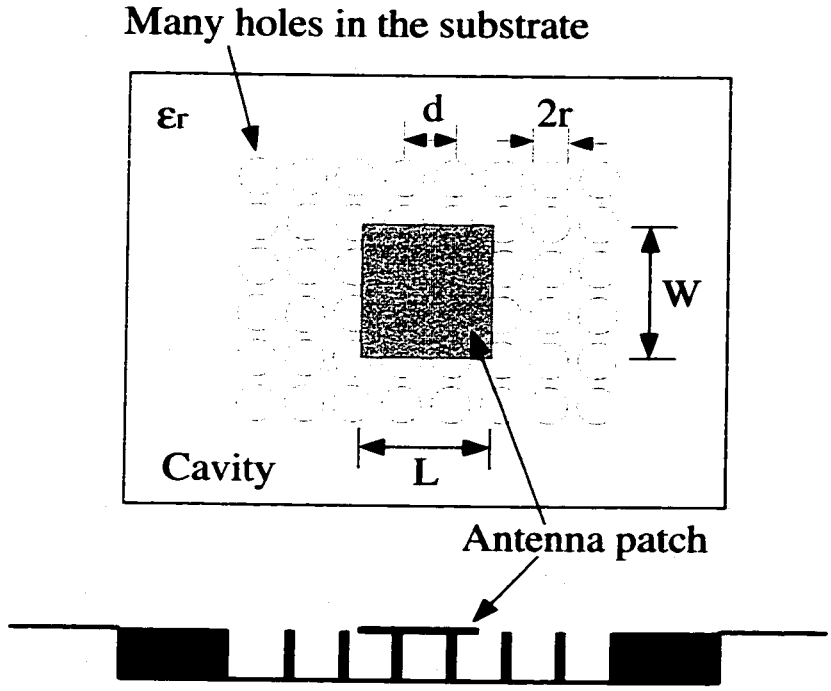

Figure 5.1: Geometry of the patch with perforated substrate: top and side view.

In a perforated substrate, the hole size is usually very small as compared to wavelength. Therefore, the hole region can be modeled as a homogeneous one using an equivalent or synthetic dielectric constant ϵ_{rsynth}. This synthetic dielectric constant can be expressed as

$$\epsilon_{rsynth} = \epsilon_r(1-x) + x \tag{5.1}$$

where

$$x = \{\text{volume removed}\}\%. \tag{5.2}$$

Here ϵ_r is the dielectric constant of the high-index material surrounding the hole region. Also, the holes are assumed to be air filled. When a certain percent of the

substrate volume is removed, the synthesized permittivity ϵ_{rsynth} can be computed using the above formula. Therefore, the substrate can be viewed as a composite of two materials with ϵ_{rsynth} as the dielectric constant for the inside (hole) region and ϵ_r being the dielectric constant for the surrounding region.

The objective of this design is to find the optimal size of the periodic holes to maximize the bandwidth but still maintaining the resonant frequency in the vicinity of 12.0 - 13.0 GHz. The length and width of the patch need to be adjusted, however, so that the resonant frequency is maintained. There is also a need to constraint the dielectric volume size, i.e., the maximum percent of volume allowed within the dielectric region. The geometries of the antennas with homogeneous substrate are similar to those in [36]. For our design we will retain the following parameters unchanged: thickness of the substrate $h = 0.0635$ cm, dimensions of the hole region 1.3 cm $\times$ 1.7 cm, dielectric constant of the substrate outside the hole region region will be set $\epsilon_r = 10.8$, and the hole spacing is chosen as $d = 0.07$ cm. Other geometrical variables such as the patch size and hole radius are subject to change.

If the volume constraint is set to be 80%, i.e., at most 80% of the dielectric volume is allowed to be removed, the obtained design has $L = 0.7$ cm and $W = 0.9$ cm residing in a cavity of 2.7 cm $\times$ 3.3 cm. Each hole of the designed substrate has a diameter of $2r = 0.06$cm and spacing of $d = 0.07$cm. The resulting ϵ_{rsynth} is about 2.3 [36]. This antenna has a resonant frequency of 12.42 GHz from the FE-BI simulation.

If we increase the volume constraint to 100%, the SQP optimizer results in a suspended patch residing over an air region of 1.6 cm $\times$ 1.8 cm (see Figure 5.2). The patch has a size of $L = 1.0$ cm and $W = 1.2$ cm residing in a cavity of 3.0 cm $\times$ 3.6 cm. In both of the above designs, the optimized patch has the maximally allowed

volume removed, implying that our optimization resulted in *boundary optima.* This is reasonable since it can be argued that as more of the volume is removed, the greater is the bandwidth.

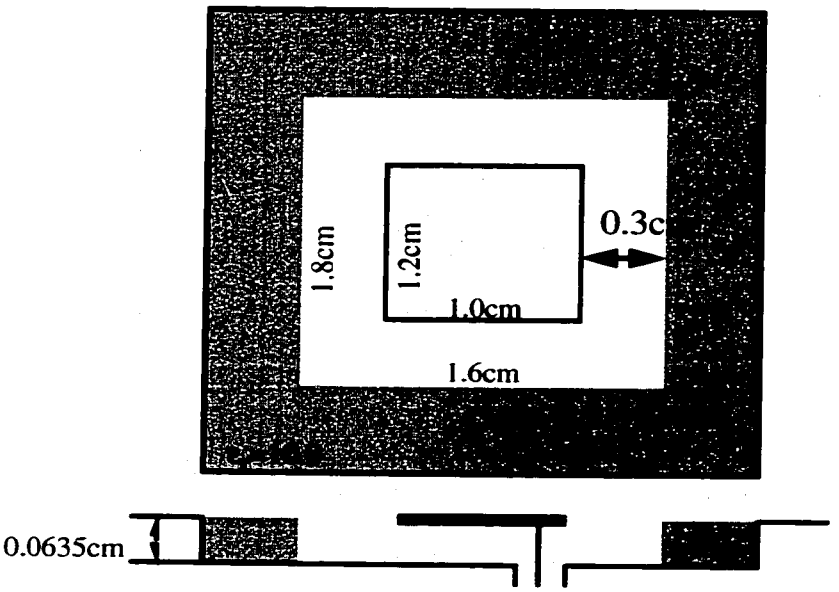

Figure 5.2: Geometry of the suspended patch.

To compare the performance of the optimized patches we modeled two other cavity-backed patch configurations with uniform substrate. The dimensions of the four antennas are shown in Table 5.1. All of them are designed to have a resonant frequency close to 12.0 GHz. The patches are fed with a single probe feed that is adjusted for impedance matching up to approximately 100 Ω.

The calculated return losses for the above four antennas are shown in Figure 5.3. It is seen that the two 'regular' patches with homogeneous $\epsilon_r = 2.2$ and $\epsilon_r = 10.8$ have a typical 10 dB bandwidth of 2.95% and 1.19%, respectively. The bandwidth of the patch with the $\epsilon_{rsynth} = 2.3$ substrate increases to 3.53%, a 200% increase over the 10 dB bandwidth of the standard patch over a uniform substrate of $\epsilon_r = 10.8$. The bandwidth of the suspended patch has a slightly wider bandwidth of 3.69%.

	Homogeneous $\epsilon_r = 2.2$	Homogeneous $\epsilon_r = 10.8$	80% removed $\epsilon_{rsynth} = 2.3$	100% removed suspended patch
Patch (cm^2)	0.74 × 0.91	0.33 × 0.47	0.7 × 0.9	1.0 × 1.2
Cavity (cm^2)	2.22 × 2.73	0.99 × 1.41	2.7 × 3.3	3.0 × 3.6
resonant freq. (GHz)	12.18	11.75	12.42	13.04

Table 5.1: Dimensions and resonant frequencies of the four patch antennas.

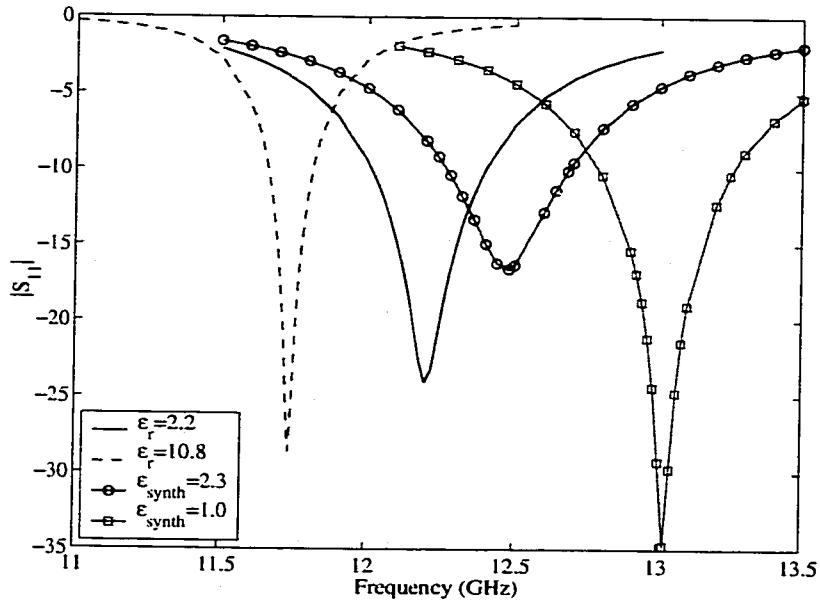

Figure 5.3: Computed return loss for the four antennas in Table 5.1.

5.3 Printed Antenna on Bandgap Substrate

When the size of periodic implants is a significant fraction of a wavelength, the whole substrate cannot be modeled with a homogeneous ϵ_r. Instead, it has to be modeled exactly with different ϵ_r's for different materials of the substrate.

We first consider a PBG layer such as that shown in Figure 5.4. This slab has a background $\epsilon_r = 4$ and a unit cell size of 2 cm $\times$ 2 cm. The embedded periodic material blocks have $\epsilon_r = 10$ and a size of 1 cm $\times$ 1 cm. We use an FE-BI simulator for the analysis of 3-D doubly periodic structures [33] to compute the reflection coefficient of plane waves incident on the PBG structure. Figure 5.5 shows the reflection coefficient curve at normal incidence ($\phi_0 = 0$ and $\theta_0 = 0$). As seen, the effective medium theory (with a homogenized $\epsilon_r = 5.5$) fails to predict the resonance at the bandgap frequency around 10-11 GHz [25]. From the field plots at three different frequencies (in band, near band and stop band) in Figure 5.6, it can be seen that the reflection coefficient exhibits resonances associated with the PBG structure.

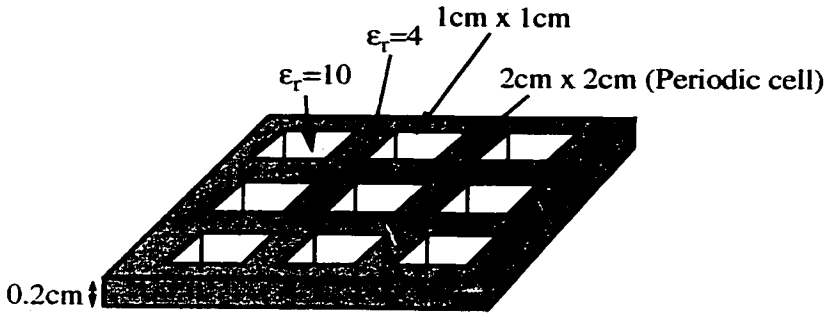

Figure 5.4: Geometry of the infinite PBG structure.

Next, we use this PBG structure as the substrate of a patch antenna (see Figure 5.7). The PBG substrate is now finite consisting of 3 $\times$ 3 unit cells. Without an air layer between the patch and PBG structure (whose thickness is Δ), this patch still exhibits a typical 10 dB bandwidth of 3%. With an air layer of 0.1 cm thickness,

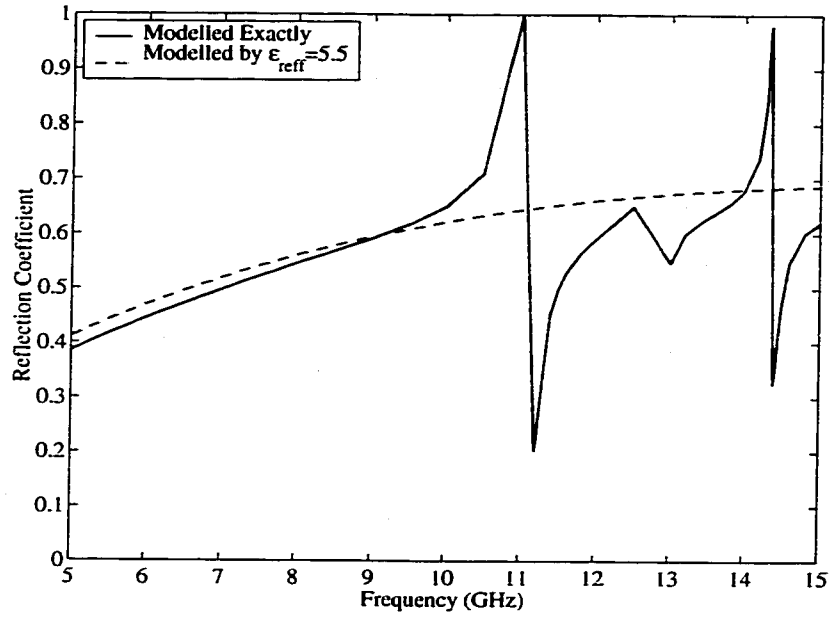

Figure 5.5: TM plane wave reflection from the PBG structure shown in Figure 5.4, using exact modeling and effective constant modeling.

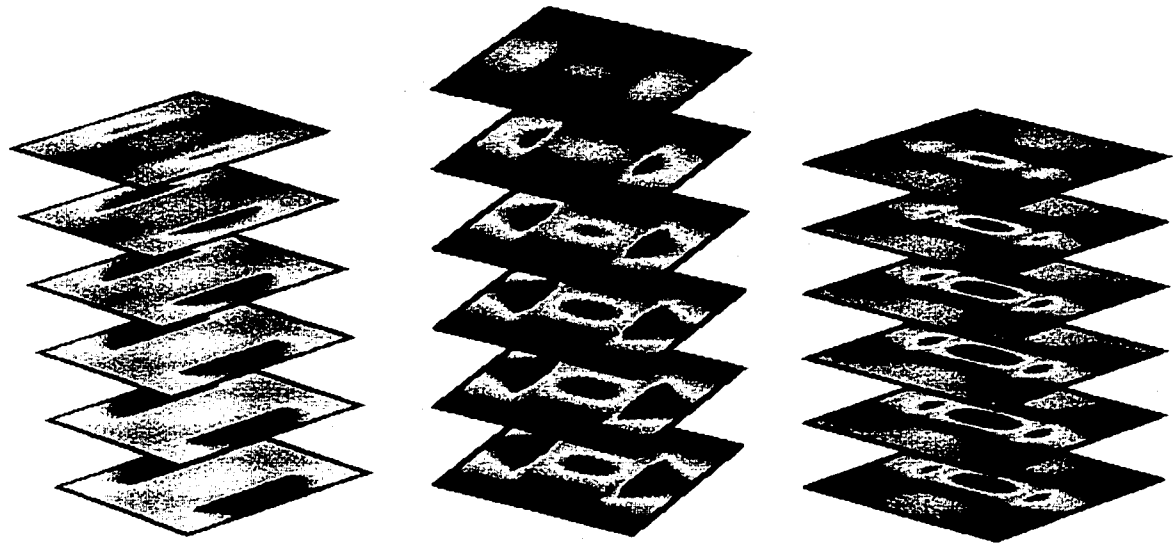

(a) 8 GHz (in band)

(b) 10 GHz (near band)

(c) 11 GHz (stop band)

Figure 5.6: Field plots at 8 GHz, 10 GHz, and 11 GHz for the PBG structure shown in Figure 5.4.

the bandwidth increases to 14.9%. The dashed line and dashdot line in Figure 5.8 illustrate the input impedance and return loss of this initial patch with and without an air layer, respectively.

The bandwidth can be further improved by optimizing the dielectric blocks within the substrate. The top view of initial square blocks is shown in Figure 5.9. By taking 1/9 of the substrate as the design domain and repeating the block shape in the rest of the substrate, the objective function can be written as

$$\min_{\mathbf{x}} \left(\max_{k=1,2,\cdots,5} |S_{11}|_k \right) \tag{5.3}$$

where $|S_{11}|_k$ refers to the return loss at five sample frequency points (10.2, 10.4, 10.6, 10.8 and 11.0 GHz in this case). This objective function is similar to the objective function for the irregular-shaped broadband antenna problem, i.e., Equation (3.17). Each GA generation consists of 5 designs, with 5 frequencies computed for each design. On an HP 900-785 workstation, each generation takes about 30 minutes to finish. The optimal block configuration for the PBG substrate is shown in Figure 5.10, separated by an air layer $\Delta = 0.1$ cm from the patch. The achieved impedance and return loss of the optimal design show a 10 dB bandwidth increase of 17.7% (see the solid line in Figure 5.8). From this, it is clear that the various material combinations such as FSVs and FSSs when used as substrates may have a significant effect on antenna bandwidth performance.

5.4 Conclusions

In this chapter, two cases of material distribution designs within PBG substrates of patch antennas were considered. When the holes inside a substrate are small as compared to the wavelength, the substrate can be modeled as a homogeneous substrate based on the equivalent effective medium theory. However, when the holes

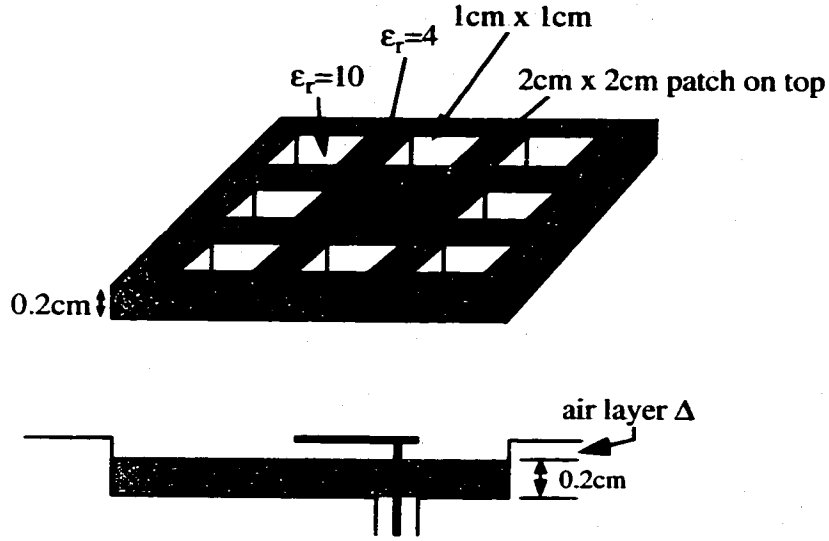

Figure 5.7: Geometry of the cavity-backed patch over finite PBG structure.

become a significant function of the wavelength, the effective medium theory fails and the structure must be modeled exactly. Antennas with both kinds of substrates were shown to obtain enhanced bandwidth. In the latter case, dielectric blocks within the substrate were optimized using GA to obtain more than 17% bandwidth for a single patch antenna. This design was the first in optimizing 3-D PBG structures in terms of their geometry and material distribution and demonstrated the full three-dimensional capability of the design approach.

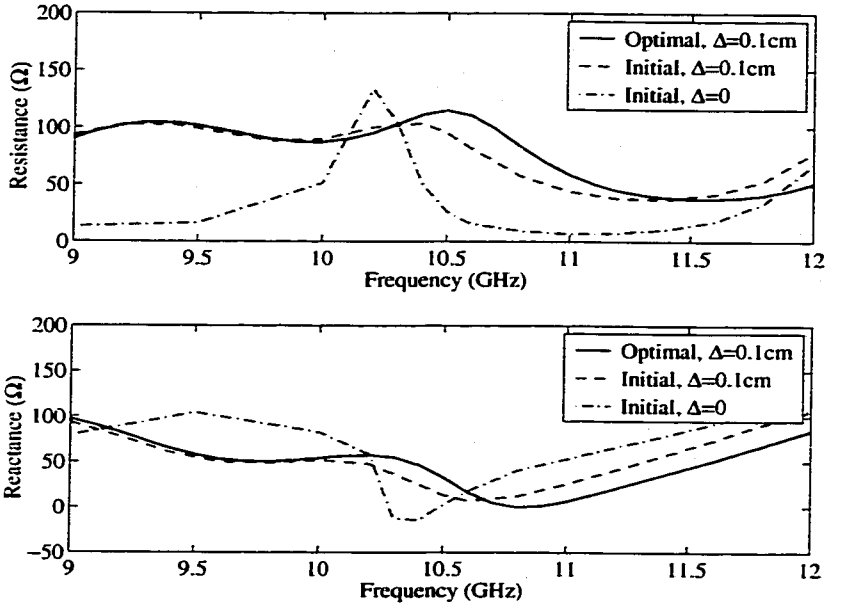

(a) Input Impedance

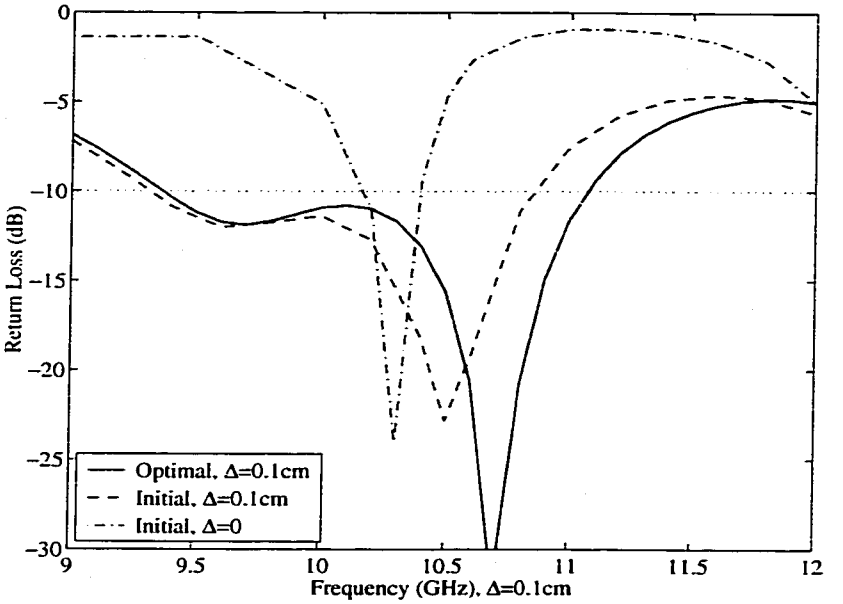

(b) Return Loss

Figure 5.8: Input impedance and return loss of the cavity-backed patch over PBG structure with and without air layer.

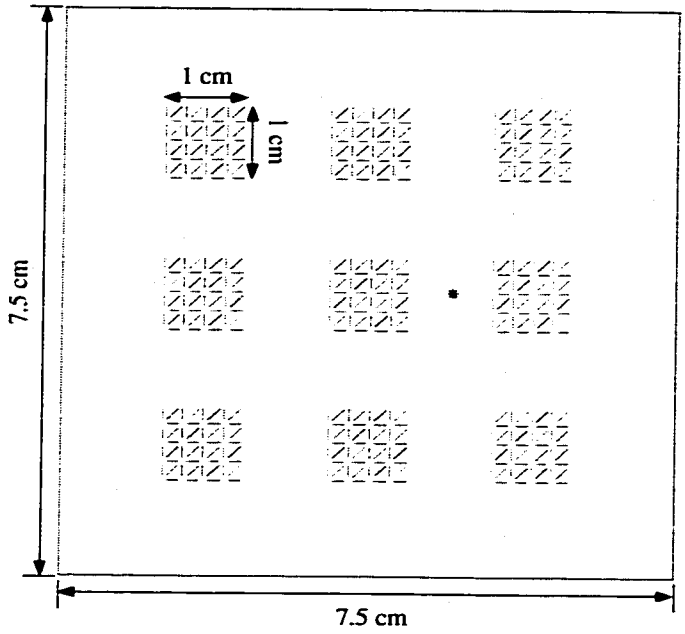

Figure 5.9: Initial 3-D block configuration for the bandgap substrate.

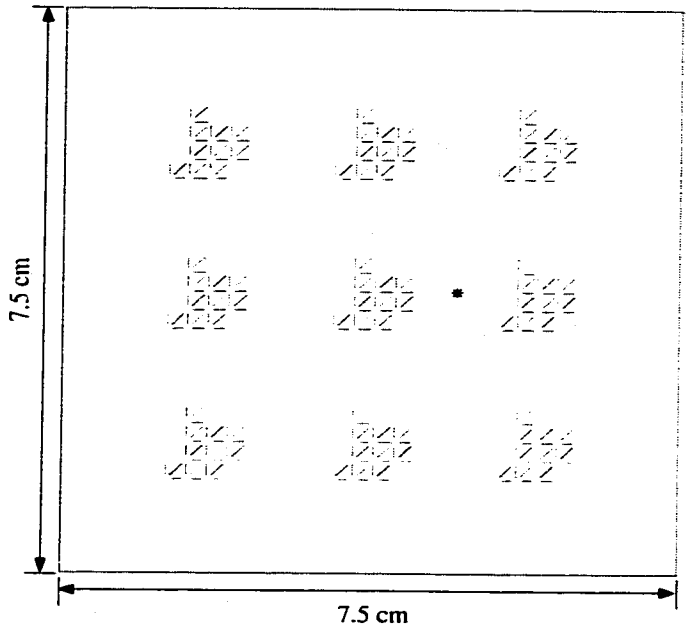

Figure 5.10: Optimal 3-D block configuration for the bandgap substrate.

CHAPTER VI

CONTRIBUTIONS AND FUTURE WORK

6.1 Contributions

In this thesis, FE-BI based optimization methodologies were investigated for the design of novel patch antennas and periodic arrays.

Optimization methods are generally classified as gradient-based techniques and gradient-free techniques, where the convergence rate and global optimality are traded. Among these the sequential quadratic programming method was considered, as a representative of gradient-based methods. Genetic algorithms and simulated annealing were those considered examples of gradient-free methods. In all cases, the analysis was carried out using the FE-BI formulation.

To validate the effectiveness of the optimization process, several antenna designs were considered in Chapter III. Most of the problems considered in Chapter III have been studied in the literature without optimization. Therefore the optimal designs obtained in Chapter III can be treated as validation of the design optimization approach. These problems include ferrite patch antennas, stacked patches, and irregular-shaped broadband and dual-band antennas.

In the design of patch antennas on ferrite substrates and superstrates, magnetic field strength was proposed as a design variable for tuning the resonant frequencies

and steering the beam to specific angles. Use of the SQP method was demonstrated for speeding up both processes to locate the resonant frequencies and obtain the necessary field strength for the beams.

Two designs involving stacked patch configurations were studied and optimized for improved broadband performance. First, the substrate thickness for probe-fed stacked rectangular patches was optimized using SQP to obtain a 21% bandwidth. A novel design of a rectangular patch stacked with a folded-slot was also proposed. For this design, several slot widths were optimized using GA to achieve a 22% bandwidth.

We further continued the study of broadband antenna designs by considering irregular shapes of single layer patch antennas. This was done by discretizing the design domain into small cells with each cell assigned an "on" or "off" state by the optimizer. A similar optimization process was conducted for finding an irregular-shaped patch having dual-band performance. Both the GA and SA algorithms were employed for the two designs. For the broadband antenna, GA and SA yielded different designs yet both of them had a bandwidth of about 10% (i.e., both satisfied the design objective). For the dual-frequency antenna, the GA and SA generated the same optimal design, but in general we found that GA needs fewer function evaluations.

In Chapters IV and V, we studied the designs of infinite and finite periodic EM structures. In Chapter IV, the concept of frequency selective surfaces (FSSs) was introduced. A fast $O(N)$ FSDA simulator was implemented within an FE-BI approach to speed up the analysis module. GA was integrated with this simulator to allow full flexibility in geometry and layer structure decisions when designing FSSs. Example designs were demonstrated subject to pre-specified magnitude and phase criteria. Single-layer and multi-layer highpass filters were designed to meet

the desired frequency response. As a new application, a flat-phase FSS element was designed subject to a phase response that is fairly constant over a given band. Such designs allow for special purpose FSS structures that can serve as "substrates" to printed antennas and was shown to substantially enhance the bandwidth of a dipole array.

In Chapter V, 3-D frequency selective volumes (FSVs) or photonic bandgap (PBG) structures were studied. FSVs/PBGs have periodic perforated substrates which can suppress surface waves within a certain frequency range, therefore improving bandwidth and gain of the patch antennas atop. Two approaches of manipulating the PBG substrates of patch antennas were discussed: when hole size in the substrate is small compared to the wavelength, the substrate can be modeled as homogeneous using the effective medium theory. When the hole size is on the order of a wavelength, the effective medium theory is no longer valid, and the structure needs to be modeled exactly. Antennas with both kinds of substrates were shown to obtain enhanced bandwidth. GA was then performed to optimize the material distributions of the dielectric implants inside the bandgap substrate and further increased the antenna bandwidth.

To summarize, the research contributions of this thesis are the following:

- The first thesis on comprehensive study of optimization combined with full wave analysis for antennas and periodic structures;
- Proposed innovative and non-intuitive antennas and FSSs for broadband applications (e.g., folded-slot antenna, irregular-shaped flat-phase FSS elements);
- First in optimizing 3-D PBG structures in terms of their geometry and material distribution.

6.2 Future Work

In this thesis, the optimal shape and topology of patches, FSS elements and FSV blocks were achieved via domain discretization and "on" / "off" state assignments for each small cell within the domain. However, such methods treat the design domain in a discrete way, and provide only an approximation to the actual continuum structures desired for most realistic applications. Therefore, it would be advantageous to use topology optimization methods to obtain the shape of the external and internal boundaries and the number of inner holes simultaneously. There are mainly two topology optimization methods available: the homogenization method [13] and the density method [12]. Both of these methods discretize the design domain into finite elements. Each finite element is viewed as one or more microstructures. A microstructure can be expressed as void, porous, or solid depending on the hole size of the microstructure. On the basis of the homogenization method, the homogenized value of the material constant for each finite element is first computed on the basis of its microstructures. For the density method, the material constants of the microstructures need not be homogenized. These methods can be used to find the shape, topology and/or the material distribution of the 2-D patches/FSSs and the 3-D FSVs/PBGs for optimal performance.

In this thesis, most of the designs treated the optimization module and the analysis module separately. That is, the analysis module (i.e., the FE-BI part) is viewed as a "black box", where design variables are the inputs and the antenna performance is the output of the module from the FE-BI simulation. Such task assignments are easy to understand and implement although possibly time-consuming. There are several ways to improve the efficiency of the design process.

A way to simplify the objective function is by modeling it using an approximate closed-form formula. As seen throughout the thesis, numerical techniques are necessary to compute the performance characteristics of patch antennas and periodic structures. Such computation consumes most of the CPU time required for the whole design optimization process. If the objective function can be simplified, considerable speedup of the process will be observed. For example, when available data are collected either from previous simulations, experiments or other empirical sources, they can be used to create an approximate (surrogate) mathematical model. This idea may be pursued via curve fitting, neural networks, or kriging [83].

Another way is to construct a simplified model, if available, for certain applications. For example, when designing a multilayer dipole FSS structure, equivalent circuit models for each layer can be established and transmission lines can be inserted between these circuits to represent layers. The geometrical variables of the FSS structure (such as lengths and widths of the dipoles and the separation between layers) can be related with the corresponding RLC (resistance, inductance, and capacitance) circuit variables. The RLC circuit model is available in an analytical form. A simple optimization method can then be employed to determine the equivalent circuit variables to achieve the desired behavior of the FSS structure. Full wave FE-BI simulation can then be carried out as a final validation step on the basis of the optimal circuit variables when their values are converted back to FSS geometry.

A third means of making the design process more efficient is to integrate the optimization algorithm into the antenna analysis directly. Consider a patch design with the GA/FE-BI method where re-meshing is not needed. An original "full" patch geometry is chosen at the beginning of optimization process for which the BI matrix is formed. During the optimization process, the GA can search for an

optimal substructure contained within the original structure, and the matrix will be modified accordingly. By doing this, the BI matrix is filled only once at the beginning of the optimization process, with no need to re-mesh and re-fill the matrices at every optimization iteration. Therefore, significant computational cost reduction can be achieved in evaluating the objective function during the iteration process.

BIBLIOGRAPHY

BIBLIOGRAPHY

[1] E. Aarts and J. Korst, *Simulated Annealing and Boltzmann Machines: A Stochastic Approach to Combinatorial Optimization and Neural Computing*, Wiley, 1989.

[2] L. Alatan, M. Aksun, K. Leblebicioglu, and M. Birand, "Use of computationally efficient method of moments in the optimization of printed antennas," *IEEE Transactions on Antennas and Propagation*, vol. 47, no. 4, pp. 725–732, April 1999.

[3] N. Alexopoulos, "Integrated-circuit structures on anisotropic substrates," *IEEE Transactions on Microwave Theory and Techniques*, vol. 33, pp. 847–881, 1985.

[4] F. Ares, S. Rengarajan, E. Villanueva, E. Skochinski, and E. Moreno, "Application of genetic algorithms and simulated annealing technique in optimising the aperture distributions of antenna array patterns," *Electronics Letters*, vol. 32, no. 3, pp. 148–149, February 1996.

[5] F. Ares-Pena, J. Rodriguez-Gonzalez, E. Villanueva-Lopez, and S. Rengarajan, "Genetic algorithms in the design and optimization of antenna array patterns," *IEEE Transactions on Antennas and Propagation*, vol. 47, no. 3, pp. 506–510, March 1999.

[6] L. Armijo, "Minimization of functions having Lipschitz continuous first partial derivatives," *Pacific Journal of Mathematics*, vol. 16, no. 1, pp. 1–3, 1966.

[7] H. Aroudaki, V. Hansen, H.-P. Gemund, and E. Kreysa, "Analysis of low-pass filters consisting of multiple stacked FSS's of different periodicities with applications in the submillimeter radioastronomy," *IEEE Transactions on Antennas and Propagation*, vol. 43, no. 12, pp. 1486–1491, December 1995.

[8] I. Bahl and P. Bhartia, *Microstrip Antennas*, Artech House, Dedham, MA, 1980.

[9] M. Bailey and M. Deshpande, "Analysis of elliptical and circular microstrip antennas using moment methods," *IEEE Transactions on Antennas and Propagation*, vol. AP-33, no. 9, pp. 854–859, September 1985.

[10] C. Balanis, *Antenna Theory: Analysis and Design*, Wiley, New York, 2nd edition, 1997.

[11] J. Batchelor and R. Langley, "Beam scanning using microstrip line on biased ferrite," *Electronics Letters*, vol. 33, no. 8, pp. 645–646, April 1997.

[12] M. Bendsøe, "Optimal shape design as a material distribution problem," *Structural Optimization*, vol. 1, no. 4, pp. 193–202, 1989.

[13] M. Bendsøe and N. Kikuchi, "Generating optimal topologies in structural design using a homogenization method," *Computer Methods in Applied Mechanics and Engineering*, vol. 71, pp. 197–224, 1988.

[14] A. Boag, A. Boag, E. Michielssen, and R. Mittra, "Design of electrically loaded wire antennas using genetic algorithms," *IEEE Transactions on Antennas and Propagation*, vol. 44, no. 5, pp. 687–695, May 1996.

[15] A. D. Brown, *Numerical Analysis and Application of Ferromagnetic Materials for Microstrip Antenna Applications*, PhD thesis, The University of Michigan, 2000.

[16] A. D. Brown, J. Volakis, L. C. Kempel, and Z. Li, "Numerical analysis of the radiation properties of ferrite patch antennas," in *Proceedings of the 1998 IEEE Antennas and Propagation Society International Symposium*, volume 1, pp. 244–247, Atlanta, GA, USA, July 1998.

[17] D. Carroll. *http://www.staff.uiuc.edu/~carroll/ga.html.* University of Illinois at Urbana Champaign.

[18] K. Carver and J. Mink, "Microstrip antenna technology," *IEEE Transactions on Antennas and Propagation*, vol. AP-29, no. 1, pp. 2–24, January 1981.

[19] P.-R. Chang, W.-H. Yang, and K.-K. Chan, "A neural network approach to MVDR beamforming problem," *IEEE Transactions on Antennas and Propagation*, vol. 40, no. 3, pp. 313–322, March 1992.

[20] D. Cheng, "Optimisation techniques for antenna arrays," *Proceedings of the IEEE*, vol. 59, pp. 1664–1674, 1971.

[21] H. Choo, A. Hutani, L. Trintinalia, and H. Ling, "Shape optimization of broadband microstrip antennas using genetic algorithm," *Electronics Letters*, vol. 36, no. 25, pp. 2057–2058, December 2000.

[22] M. Clenet, C. Ravipati, and L. Shafai, "Bandwidth enhancement of U-slot microstrip antenna using a rectangular stacked patch," *Microwave and Optical Technology Letters*, vol. 21, no. 6, pp. 393–395, June 20, 1999.

[23] R. Coccioli, W. Deal, and T. Itoh, "Radiation characteristics of a patch antenna on a thin PBG substrate," in *Proceedings of the 1998 IEEE Antennas and Propagation Society International Symposium*, pp. 656–659, Atlanta, GA, 1998.

[24] J. Colburn and Y. Rahmat-Samii, "Patch antennas on externally perforated high dielectric constant substrates," *IEEE Transactions on Antennas and Propagation*, vol. 47, no. 12, pp. 1785–1794, December 1999.

[25] H. Contopanagos, L. Zhang, and N. Alexopoulos, "Thin frequency-selective lattices integrated in novel compact MIC, MMIC, and PCA architectures," *IEEE Transactions on Microwave Theory and Techniques*, vol. 46, no. 11, pp. 1936–1948, November 1998.

[26] N. Das and S. Chowdhury, "Rectangular microstrip antennas on a ferrite substrate," *IEEE Transactions on Antennas and Propagation*, vol. AP-30, pp. 499–502, 1982.

[27] N. Das, S. Chowdhury, and J. Chatterjee, "Circular microstrip antenna on ferrimagnetic substrate," *IEEE Transactions on Antennas and Propagation*, vol. AP-31, no. 1, pp. 188–190, January 1983.

[28] D. Davis, C. Chan, and J. Hwang, "Frequency selective surface design using neural networks inversion based on parameterized representations," in *Proceedings of the IEEE 1991 International Symposium Digest of Antennas and Propagation Society*, pp. 200–203, 1991.

[29] L. Davis, editor, *Genetic Algorithms and Simulated Annealing*, Pitman, London, 1987.

[30] C. Delabie, M. Villegas, and O. Picon, "Creation of new shapes for resonant microstrip structures by means of genetic algorithms," *Electronics Letters*, vol. 33, no. 18, pp. 1509–1510, August 1997.

[31] G. A. Deschamps, "Microstrip microwave antennas," Presented at the Third USAF Symp. on Antennas, 1953.

[32] T. Eibert and J. Volakis, "Fast spectral domain algorithm for rapid solution of integral equations," *Electronics Letters*, vol. 34, no. 13, pp. 1297–1299, June 1998.

[33] T. Eibert and J. Volakis, "Fast spectral domain algorithm for hybrid finite element/boundary integral modelling of doubly periodic structures," *IEE Proceedings: Microwaves, Antennas and Propagation*, vol. 147, no. 5, pp. 329–334, October 2000.

[34] T. Eibert, J. Volakis, D. Wilton, and D. Jackson, "Hybrid FE-BI modeling of 3-D doubly periodic structures utilizing triangular prismatic elements and an MPIE formulation accelerated by the Ewald transformation," *IEEE Transactions on Antennas and Propagation*, vol. 47, no. 5, pp. 843–850, May 1999.

[35] M. Fujita and K. Takao, "Asymptotic feature of an adaptive array and its application to array pattern synthesis," *Trans. Inst. Electron. Commun. Eng., Japan*, vol. E61, pp. 599–604, 1978.

[36] G. Gauthier, A. Courtay, and G. Rebeiz, "Microstrip antennas on synthesized low dielectric-constant substrates," *IEEE Transactions on Antennas and Propagation*, vol. 45, no. 8, pp. 1310–1314, August 1997.

[37] D. Goldberg, *Genetic Algorithms in Search, Optimization, and Machine Learning*, Addison-Wesley, 1989.

[38] A. Goldstein, "On steepest descent," *SIAM J. on Control*, vol. 3, pp. 147–151, 1965.

[39] R. Haupt, "Adaptive nulling in monopulse antennas," *IEEE Transactions on Antennas and Propagation*, vol. 36, no. 2, pp. 202–208, February 1988.

[40] R. Haupt, "Thinned arrays using genetic algorithms," *IEEE Transactions on Antennas and Propagation*, vol. 42, no. 7, pp. 993–999, July 1994.

[41] R. Haupt, "Phase-only adaptive nulling with a genetic algorithm," *IEEE Transactions on Antennas and Propagation*, vol. 45, no. 6, pp. 1009–1015, June 1997.

[42] A. Henderson, J. James, and A. Fray, "Magnetised microstrip antenna with pattern control," *Electronics Letters*, vol. 24, no. 1, pp. 45–47, January 1988.

[43] K. Hirasawa, "The application of a biquadratic programming method to phase only optimization of antenna arrays," *IEEE Transactions on Antennas and Propagation*, vol. 36, no. 11, pp. 1545–1550, November 1988.

[44] J. Holland, *Adaptation in Natural and Artificial Systems*, University of Michigan Press, Ann Arbor, 1975.

[45] A. Hoorfar and Y. Liu, "Antenna optimization using an evolutionary programming algorithm with a hybrid mutation operator," in *IEEE Antennas and Propagation Society International Symposium*, volume 2, pp. 1026–1029, Salt Lake City, UT, 2000.

[46] R. Horst, P. Pardalos, and N. Thoai, *Introduction to Global Optimization*, volume 3 of *Nonconvex Optimization and Its Applications*, Kluwer Academic Publishers, Dordrecht, 1995.

[47] H. How, T.-M. Fang, D.-X. Guan, and C. Vittoria, "Magnetic steerable ferrite patch antenna array," *IEEE Transactions on Magnetics*, vol. 30, no. 6, pp. 4551–4553, November 1994.

[48] J.-N. Hwang, C.-H. Chan, and R. Marks II, "Frequency selective surface design based on iterative inversion of neural networks," in *Proceedings of International Joint Conference on Neural Networks*, pp. 39–44, San Diego, June 1990.

[49] J. James and P. Hall, *Handbook of Microstrip Antennas*, IEE Electromagnetics Waves, Series 28, Peter Peregrinus, London, U.K., 1989.

[50] J. James, P. Hall, and C. Wood, *Microstrip Antenna Theory and Design*, Peter Peregrinus, London, U.K., 1981.

[51] J. Jin, *The Finite Element Method in Electromagnetics*, John Wiley & Sons, Inc., 1993.

[52] J. Jin and J. Volakis, "A hybrid finite element method for scattering and radiation by microstrip patch antennas and arrays residing in a cavity," *IEEE Transactions on Antennas and Propagation*, vol. 39, no. 11, pp. 1598–1604, November 1991.

[53] J. Jin, J. Volakis, and J. Collins, "A finite element-boundary integral method for scattering and radiation by two- and three-dimensional structures," *IEEE Antennas and Propagation Magazine*, vol. 33, no. 3, pp. 22–32, June 1991.

[54] J. Joannopoulus, R. Meade, and J. Winn, *Photonic Crystals: Molding the Flow of Light*, Princeton University Press, Princeton, N.J., 1995.

[55] J. Johnson and Y. Rahmat-Samii, "Genetic algorithms in engineering electromagnetics," *IEEE Antennas and Propagation Magazine*, pp. 7–25, August 1997.

[56] J. Johnson and Y. Rahmat-Samii, "Genetic algorithms and method of moments (GA/MoM) for the design of integrated antennas," *IEEE Transactions on Antennas and Propagation*, vol. 47, no. 10, pp. 1606–1614, October 1999.

[57] A. Jones and G. Forbes, "An adaptive simulated annealing algorithm for global optimization over continuous variables," *Journal of Global Optimization*, vol. 6, no. 1, pp. 1–37, January 1995.

[58] E. Jones and W. Joines, "Design of Yagi-Uda antennas using genetic algorithms," *IEEE Transactions on Antennas and Propagation*, vol. 45, no. 9, pp. 1386–1392, September 1997.

[59] S. Kirkpatrick, C. Gelatt Jr., and M. Vecchi, "Optimization by simulated annealing," *Science*, vol. 220, no. 4598, pp. 671–680, 1983.

[60] D. Kokotoff, *Full-Wave Analysis of a Ferrite-Tuned Cavity-Backed Slot Antenna*, PhD thesis, Arizona State University, 1995.

[61] K. Kunz and R. Luebbers, *The Finite Difference Time Domain Method for Electromagnetics*, CRC Press, Boca Raton, 1993.

[62] P. Kwok and P. Brandon, "Maximisation of signal/noise ratio in antenna array subject to constraints," *Proceedings of the Institution of Electrical Engineers*, vol. 126, no. 12, pp. 1241–1244, December 1979.

[63] B. Lax and K. Button, *Microwave Ferrites and Ferrimagnetics*, McGraw-Hill, New York, 1962.

[64] Z. Li, P. Papalambros, and J. Volakis, "Designing broad-band patch antennas using the sequential quadratic programming method," *IEEE Transactions on Antennas and Propagation*, vol. 45, no. 11, pp. 1689–1692, November 1997.

[65] Z. Li, P. Papalambros, and J. Volakis, "Frequency selective surface design by integrating optimization algorithms with fast full wave numerical methods," submitted to *IEE Proceedings on Microwaves, Antennas and Propagation*, 2001.

[66] Z. Li, J. Volakis, and P. Papalambros, "Optimization of patch antennas on ferrite substrate using the finite element method," in *Proceedings of the 1999 IEEE International Antennas and Propagation Symposium*, volume 2, pp. 1026–1029, Orlando, FL., July 1999.

[67] Z. Li, J. Volakis, and P. Papalambros, "Antenna design on periodic and aperiodic structures," in *Proceedings of the 2000 IEEE International Antennas and Propagation Symposium*, Salt Lake City, Utah, July 2000.

[68] D. Linden and E. Altschuler, "The design of Yagi antennas using a genetic algorithm," in *Proceedings of USNC/URSI Radio Science Meeting*, p. 283, Baltimore, MD, 1996.

[69] Y. Lo, S. Lee, and Q. Lee, "Optimisation of directivity and signal/noise ratio of an arbitrary antenna array," *Proceedings of the IEEE*, vol. 54, pp. 1033–1045, 1966.

[70] S. Maci and G. Gentili, "Dual-frequency patch antennas," *IEEE Antennas and Propagation Magazine*, vol. 39, no. 6, pp. 13–20, December 1997.

[71] J. Maloney, G. Smith, and W. Schott Jr., "Accurate computation of the radiation from simple antennas using the finite-difference time-domain method," *IEEE Transactions on Antennas and Propagation*, vol. 38, no. 7, pp. 1059–1068, July 1990.

[72] J. Mayhan, "Nulling limitations for a multiple-beam antenna," *IEEE Transactions on Antennas and Propagation*, vol. AP-24, pp. 769–779, 1976.

[73] N. Metropolis, A. Rosenbluth, M. Rosenbluth, A. Teller, and E. Teller, "Equation of state calculations by fast computing machines," *Journal of Chemical Physics*, vol. 21, no. 6, pp. 1087–1092, 1953.

[74] E. Michielssen, S. Ranjithan, and R. Mittra, "Optimal multilayer filter design using real coded genetic algorithms," *IEE Proceedings - J*, vol. 139, no. 6, pp. 413–420, December 1992.

[75] E. Michielssen, J. Sajer, and R. Mittra, "Design of multilayered FSS and waveguide filters using genetic algorithms," in *Proceedings of the IEEE 1993 International Symposium Digest of Antennas and Propagation Society*, volume 3, pp. 1936–1939, 1993.

[76] E. Michielssen, J. Sajer, S. Ranjithan, and R. Mittra, "Design of lightweight, broad-band microwave absorbers using genetic algorithms," *IEEE Transactions on Microwave Theory and Techniques*, vol. 41, pp. 1024–1031, June/July 1993.

[77] R. Mittra, C. Chan, and T. Cwik, "Techniques for analyzing frequency selective surfaces - a review," *Proceedings of the IEEE*, vol. 72, no. 12, pp. 1593–1615, December 1988.

[78] P. Moosbrugger, Z. Lo, L. Carpenter, and R. Barton, "Experimental design of a two-layer electromagnetically coupled rectangular patch with a global response surface modeling technique," *IEEE Transactions on Antennas and Propagation*, vol. 45, no. 5, pp. 781–787, May 1997.

[79] R. Myers, *Response Surface Methodology: Process and Product in Optimization Using Designed Experiments*, Wiley, New York, 1995.

[80] E. Newman and P. Tulyathan, "Analysis of microstrip antennas using moment methods," *IEEE Transactions on Antennas and Propagation*, vol. AP-29, no. 1, pp. 47–53, January 1981.

[81] B. Ng, M. Er, and C. Kot, "A flexible array synthesis method using quadratic programming," *IEEE Transactions on Antennas and Propagation*, vol. 41, no. 11, pp. 1541–1550, November 1993.

[82] B. Ooi and C. Lee, "Broadband air-filled stacked U-slot patch antenna," *Electronics Letters*, vol. 35, no. 7, pp. 515–517, April 1999.

[83] P. Papalambros and D. Wilde, *Principles of Optimal Design: Modeling and Computation*, Cambridge University Press, New York, 2nd edition, 2000.

[84] T. Peters, "A conjugate gradient-based algorithm to minimize the sidelobe level of planar arrays with element failures," *IEEE Transactions on Antennas and Propagation*, vol. 39, no. 10, pp. 1497–1504, October 1991.

[85] R. Pous and D. Pozar, "A frequency-selective surface using aperture-coupled microstrip patches," *IEEE Transactions on Antennas and Propagation*, vol. 39, no. 12, pp. 1763–1769, December 1991.

[86] M. Powell, "A fast algorithm for nonlinearly constrained optimization calculations," in *Numerical Analysis*, G. Watson, editor, volume 630 of *Lecture Notes in Mathematics*, Springer, 1978.

[87] D. Pozar, "Microstrip antennas," *Proceedings of the IEEE*, vol. 80, no. 1, pp. 79–91, January 1992.

[88] D. Pozar, "Radiation and scattering characteristics of microstrip antennas on normally biased ferrite substrates," *IEEE Transactions on Antennas and Propagation*, vol. 40, no. 9, pp. 1084–1092, September 1992.

[89] D. Pozar, "RCS reduction for a microstrip antenna using a normally biased ferrite substrate," *IEEE Microwave Guided Wave Letters*, vol. 2, no. 5, pp. 196–198, 1992.

[90] D. Pozar, "A review of bandwidth enhancement techniques for microstrip antennas," in *Microstrip Antennas: The Analysis and Design of Microstrip Antennas and Arrays*, D. Pozar and D. Schaubert, editors, pp. 157–166, IEEE Press, New York, 1995.

[91] D. Pozar, *Microwave Engineering*, Wiley, New York, 2nd edition, 1998.

[92] D. Pozar and V. Sanchez, "Magnetic tuning of a microstrip antenna on a ferrite substrate," *Electronics Letters*, vol. 24, pp. 729–731, 1988.

[93] S. Rao, *Engineering Optimization: Theory and Practice*, Wiley, New York, 3rd edition, 1996.

[94] C. Ravipati and L. Shafai, "A wide bandwidth circularly polarized microstrip antenna using a single feed," in *Proceedings of the 1999 IEEE Antennas and Propagation Society International Symposium*, volume 1, pp. 244–247, Orlando, Florida, July 1999.

[95] C. Ruf, "Numerical annealing of low-redundancy linear arrays," *IEEE Transactions on Antennas and Propagation*, vol. 41, no. 1, pp. 85–90, January 1993.

[96] B. Saka and E. Yazgan, "Pattern optimization of a reflector antenna with planar-array feeds and cluster feeds," *IEEE Transactions on Antennas and Propagation*, vol. 45, no. 1, pp. 93–97, January 1997.

[97] T. Sarkar and N. Sangruji, "An adaptive nulling system for a narrow-band signal with a look-direction constraint utilizing the conjugate gradient method," *IEEE Transactions on Antennas and Propagation*, vol. 37, no. 7, pp. 940–944, July 1989.

[98] K. Schittkowski, "On the convergence of a sequential quadratic programming method with an augmented lagrangian line search function," *Optimization, Methematische Operationsforschung und Statistik*, vol. 14, pp. 197–216, 1983.

[99] D. Sievenpiper, L. Zhang, R. Broas, and E. Yablonovitch, "High-impedance electromagnetic surfaces in a forbidden frequency band," *IEEE Transactions on Microwave Theory and Techniques*, vol. 47, no. 11, pp. 2059–2074, November 1999.

[100] P. Silvester and R. Ferrari, *Finite Elements for Electrical Engineers*, Cambridge University Press, Cambridge, U.K., 3rd edition, 1996.

[101] R. Stern, R. Babbitt, and J. Borowick, "A mm-wave homogeneous ferrite phase scan antenna," *Microwave Journal*, pp. 101–108, April 1987.

[102] A. Tennant and B. Chambers, "Adaptive optimization techniques for the design of microwave absorbers," in *Proc. Conf. Adaptive Computing Eng. Design Contr.*, pp. 44–49. University of Plymouth, U.K., September 1994.

[103] A. Trucco and V. Murino, "Stochastic optimization of linear sparse arrays," *IEEE Journal of Oceanic Engineering*, vol. 24, no. 3, pp. 291–299, July 1999.

[104] H. Tsai, M. Rodwell, and R. York, "Planar amplifier array with improved bandwidth using folded-slots," *IEEE Microwave and Guided Wave Letters*, vol. 4, no. 4, pp. 112–114, April 1994.

[105] H. Tsai and R. York, "Applications of planar multiple-slot antennas for impedance control, and analysis using FDTD with Berenger's PML method," in *Proceedings of the 1995 IEEE Antennas and Propagation Society International Symposium*, volume 1, pp. 370–373, 1995.

[106] J. Volakis, A. Chatterjee, and L. Kempel, *Finite Element Method for Electromagnetics : Antennas, Microwave Circuits, and Scattering Applications*, IEEE Press, New York, 1998.

[107] J. Volakis, J. Gong, and T. Özdemir, "Application of the FEM to conformal antennas," in *Finite Element Software for Microwave Engineering*, Itoh, *et al.*, editor, pp. 313–345, Wiley, New York, 1996.

[108] J. Volakis, T. Özdemir, and J. Gong, "Hybrid finite-element methodologies for antennas and scattering," *IEEE Transactions on Antennas and Propagation*, vol. 45, no. 3, pp. 493–507, March 1997.

[109] J. Wang, R. Fralich, C. Wu, and J. Litva, "Multifunctional aperture coupled stack antenna," *Electronics Letters*, vol. 26, no. 25, pp. 2067–2068, December 1990.

[110] R. Waterhouse, "Stacked patches using high and low dielectric constant material combinations," *IEEE Transactions on Antennas and Propagation*, vol. 47, no. 12, pp. 1767–1771, December 1999.

[111] D. Weile and E. Michielssen, "Design of doubly periodic filter and polarizer structures using a hybridized genetic algorithm," *Radio Science*, vol. 34, no. 1, pp. 51–63, Jan-Feb 1999.

[112] H.-Y. Yang, "Characteristics of switchable ferrite microstrip antennas," *IEEE Transactions on Antennas and Propagation*, vol. 44, no. 8, pp. 1127–1132, August 1996.

[113] H.-Y. Yang and N. Alexopoulos, "Gain enhancement methods for printed circuit antennas through multiple superstrates," *IEEE Transactions on Antennas and Propagation*, vol. AP-35, no. 7, pp. 860–863, July 1987.